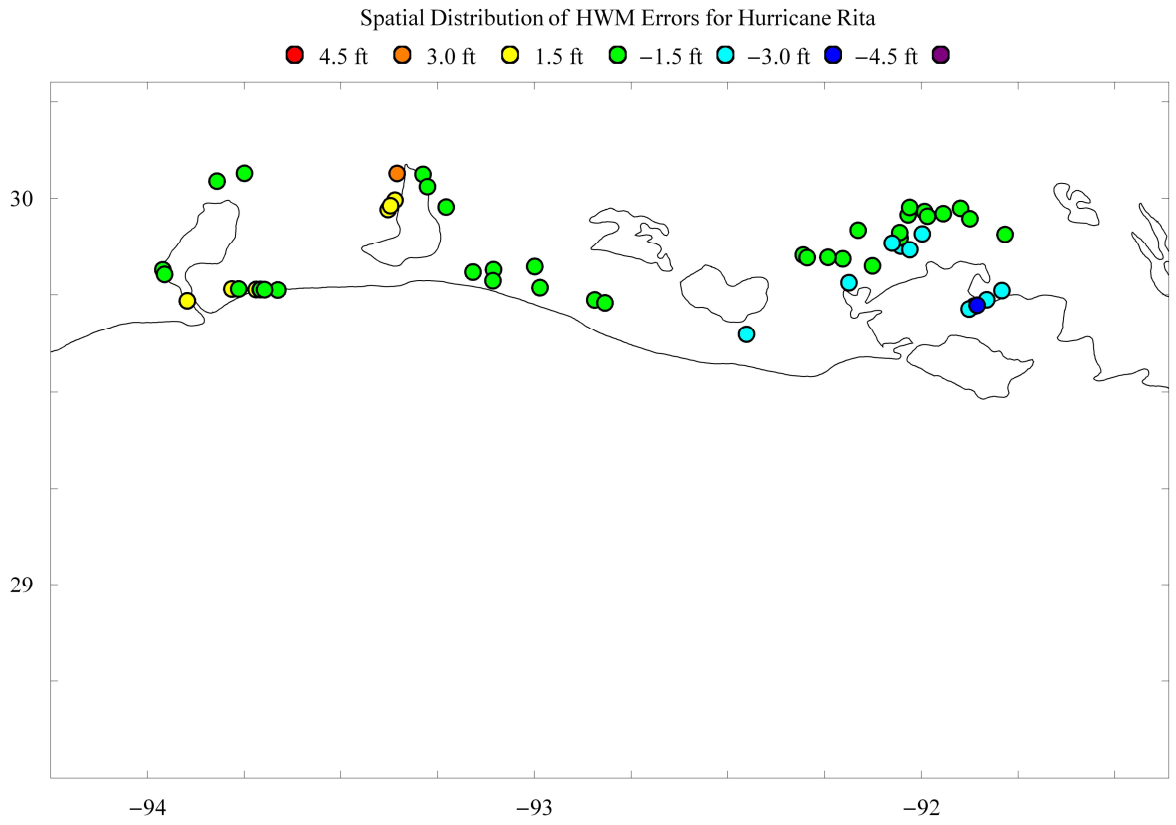

Figure 374: Distribution of errors between measured high-water marks and temporal maximums of the ADCIRC Rita hindcast solution, for Southwestern Louisiana.

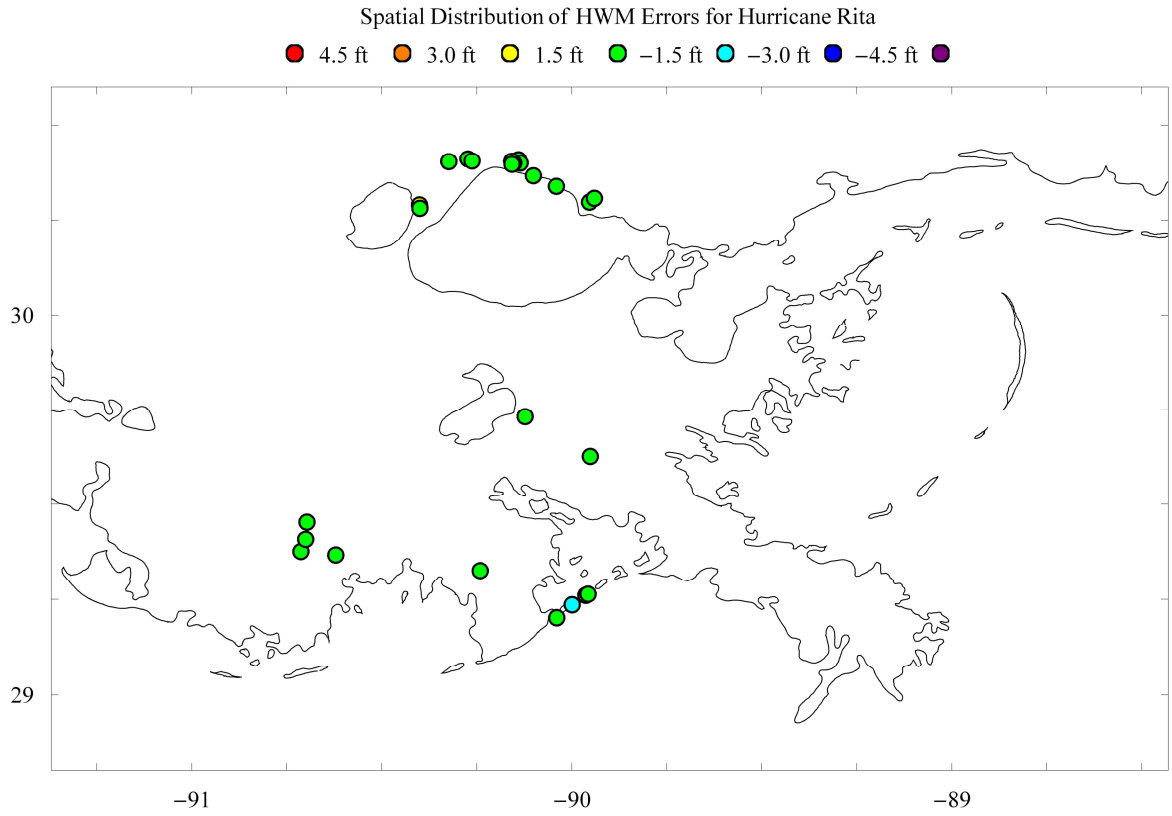

Figure 375: Distribution of errors between measured high-water marks and temporal maximums of the ADCIRC Rita hindcast solution, for Southeastern Louisiana.

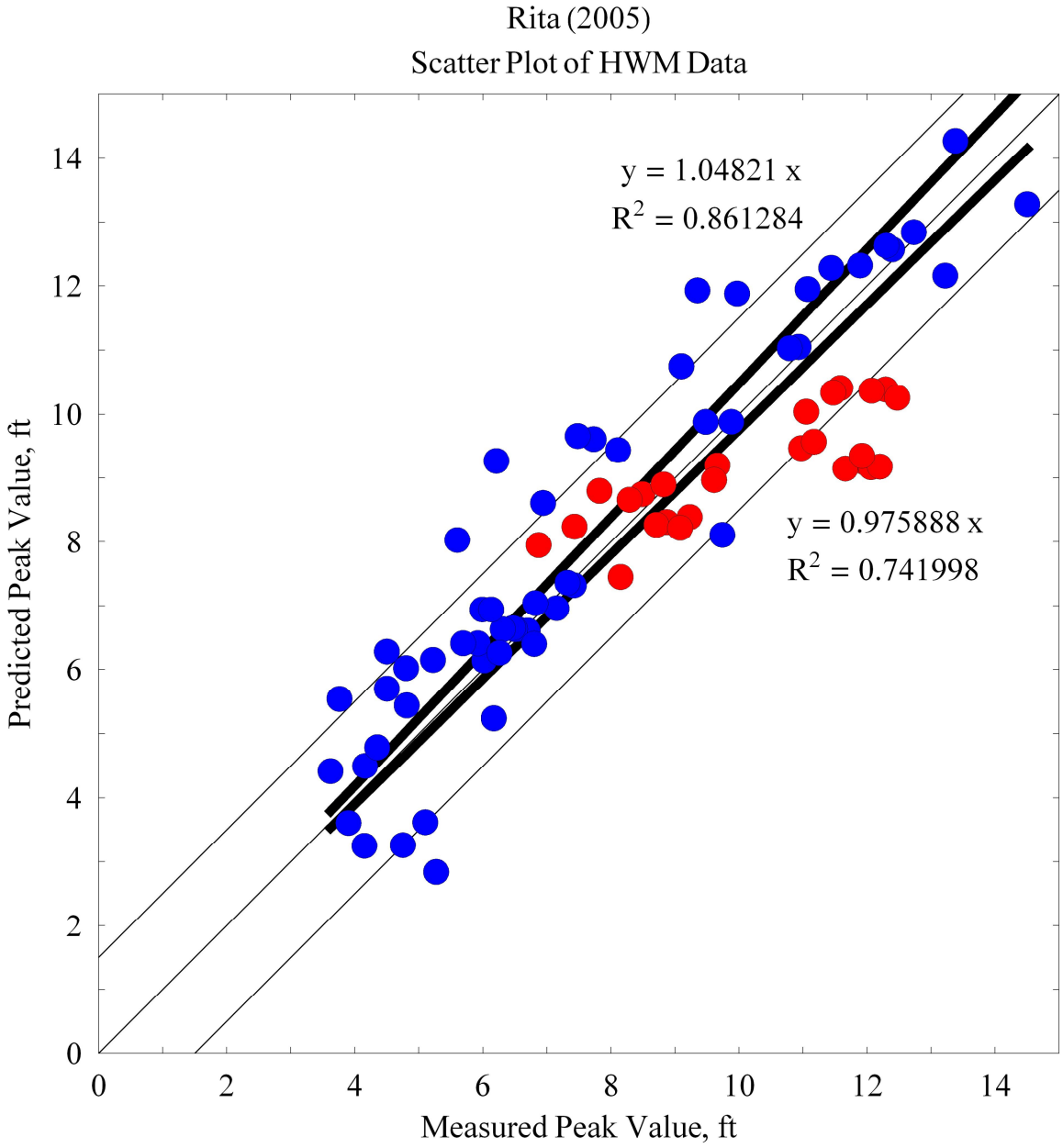

Figure 376: Scatter plot of high-water marks for Hurricane Rita. The high-water marks near Vermilion Bay are shown in red. Note that high-water marks that fall below the one-to-one line are under-predicted by the ADCIRC SL15 model.

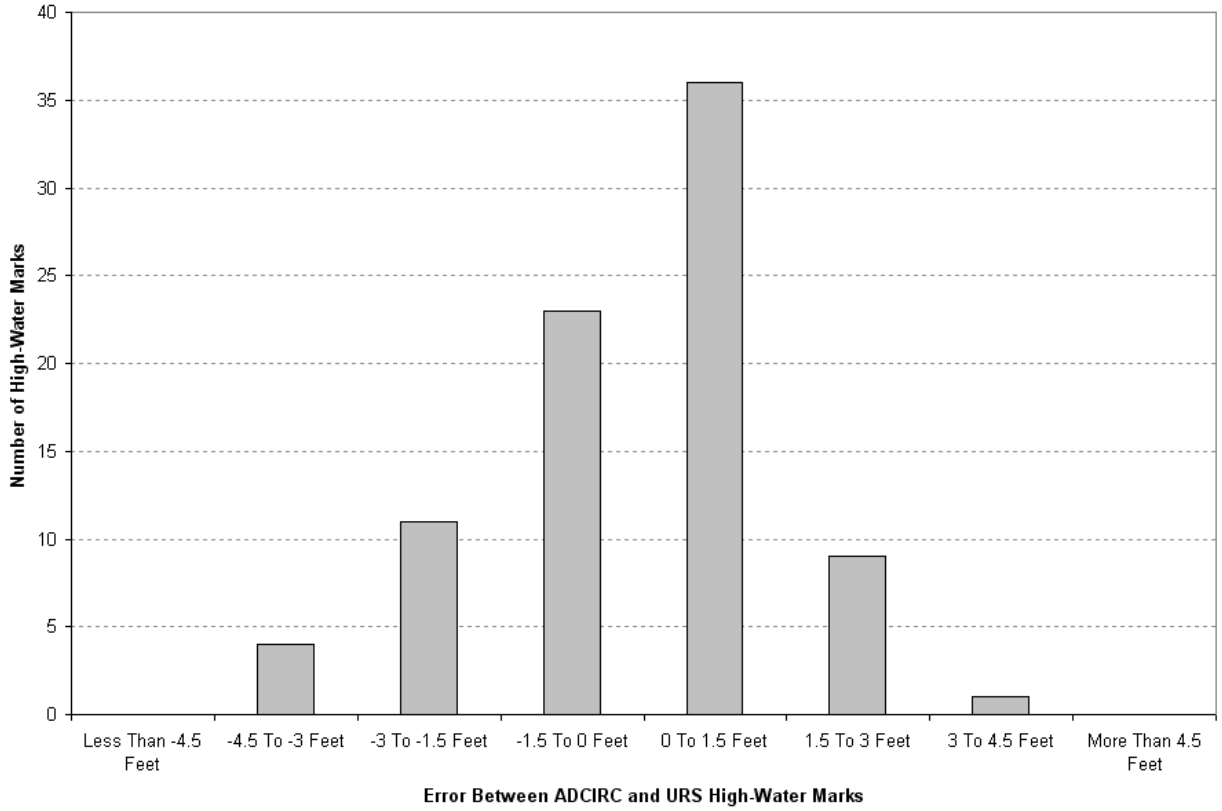

Figure 377: Bar graph of errors between measured and predicted peak values.

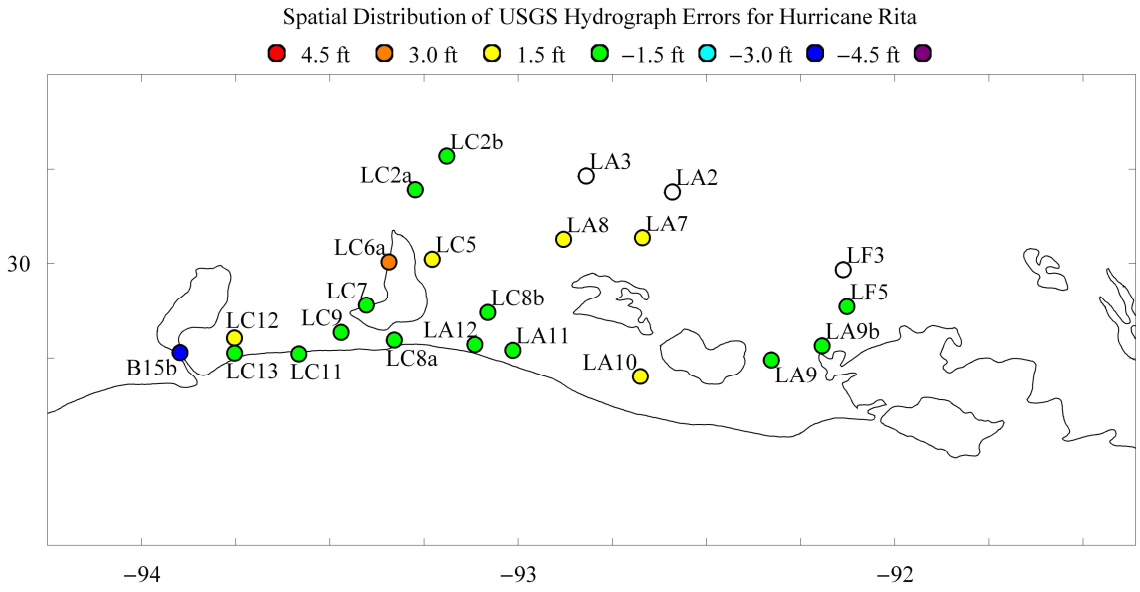

Figure 378: Locations of the 23 USGS stations in Southwestern Louisiana.

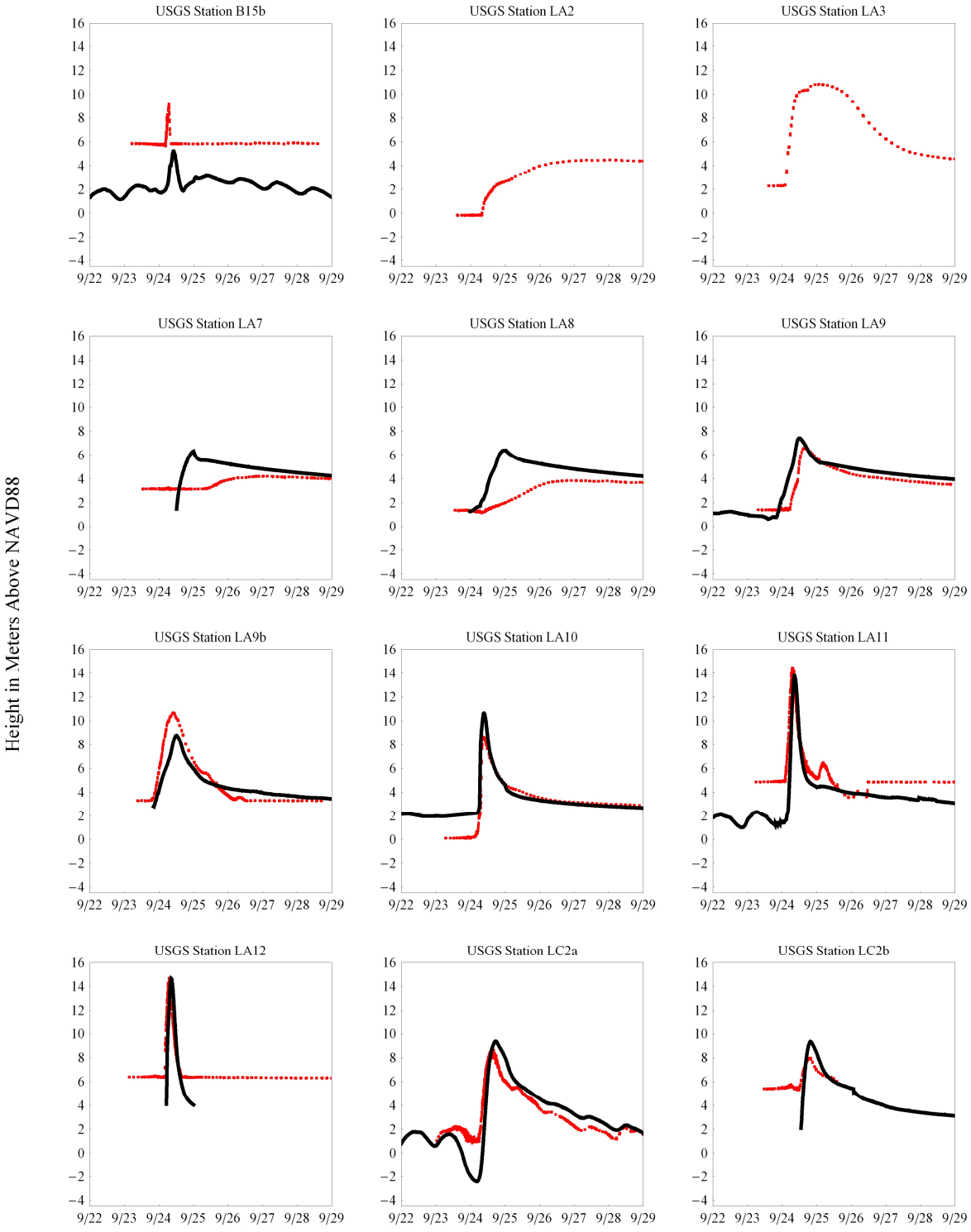

Figure 379: Hydrographs for Hurricane Rita at the first 12 USGS stations.

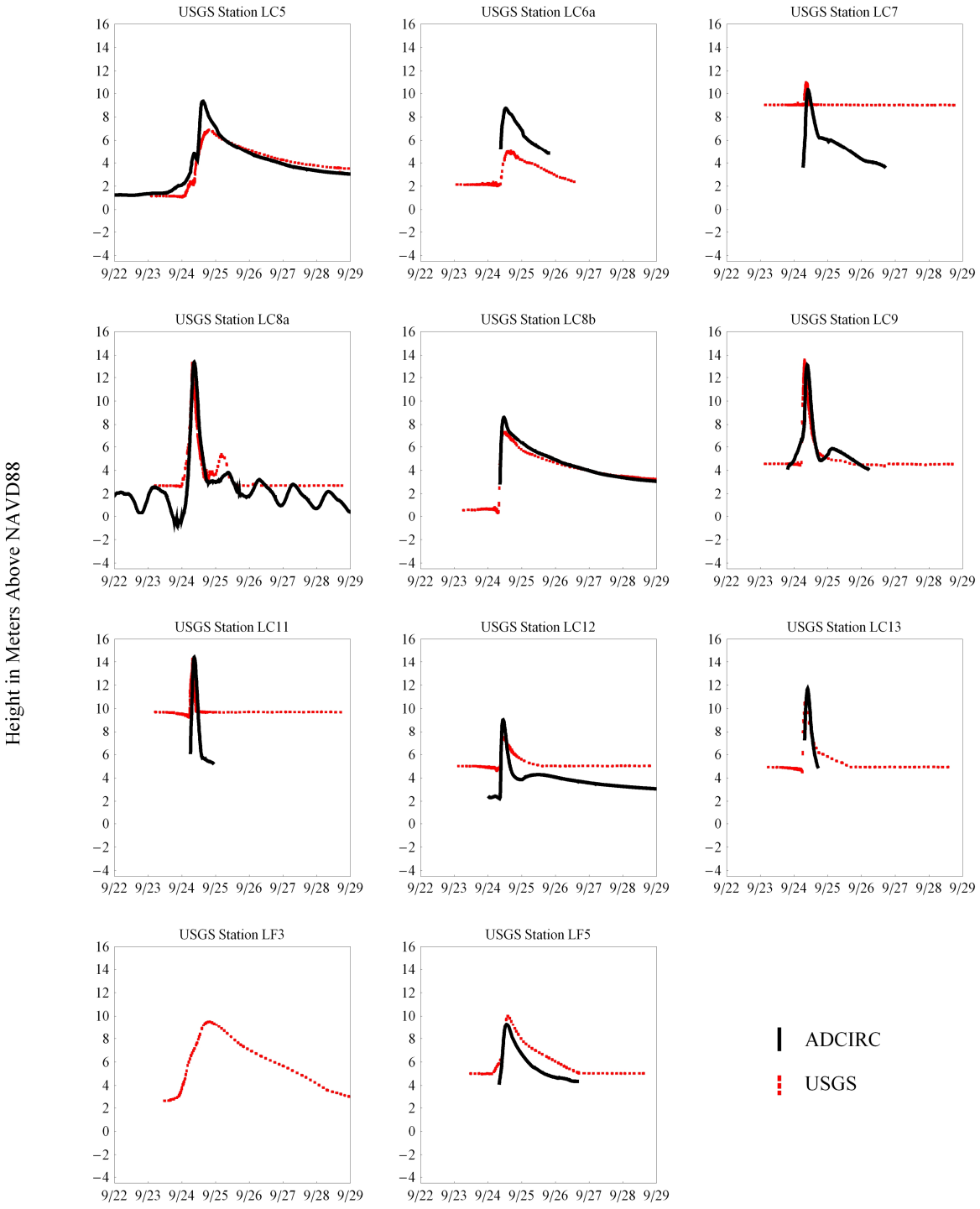

Figure 380: Hydrographs for Hurricane Rita at the last 11 USGS stations.

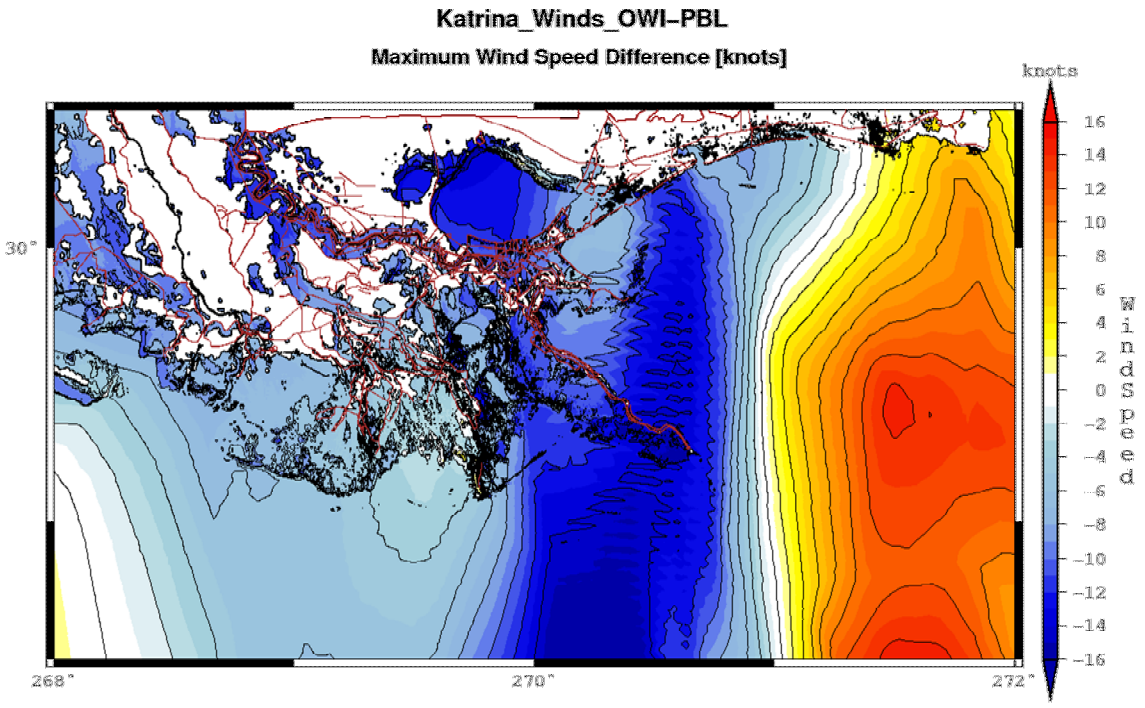

Figure 381: Maximum wind speed differences from H*WIND/IOKA wind generated results less PBL wind generated results for Hurricane Katrina in Southeastern Louisiana. Brown lines delineate interior boundaries. Black lines are contours denoting every 2 knots of difference.

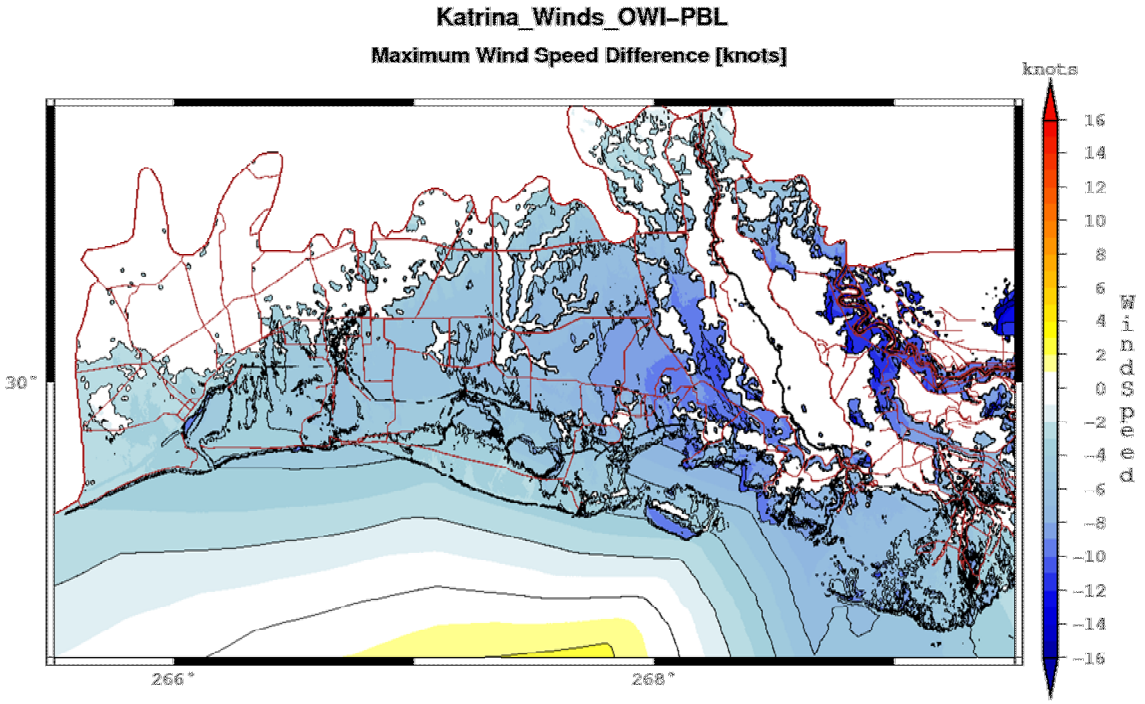

Figure 382: Maximum wind speed differences from H*WIND/IOKA wind generated results less PBL wind generated results for Hurricane Katrina in Southwestern Louisiana. Brown lines delineate interior boundaries. Black lines are contours denoting every 2 knots of difference.

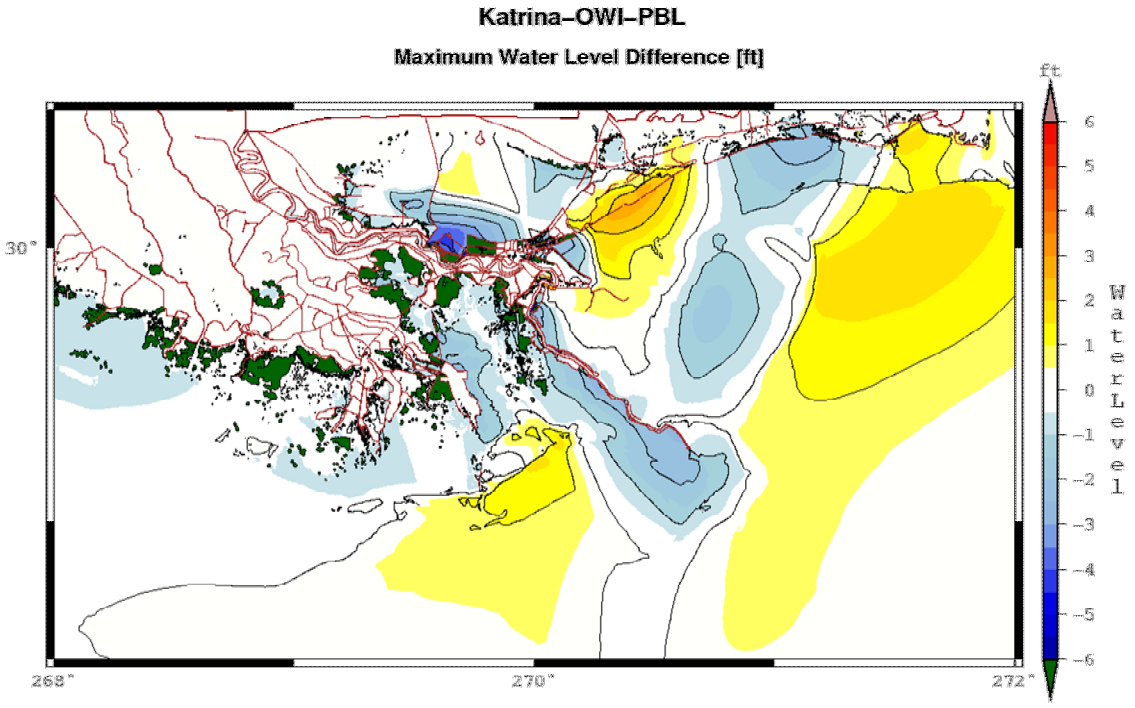

Figure 383: Maximum water level differences from H*WIND/IOKA wind generated results less PBL wind generated results for Hurricane Katrina in Southeastern Louisiana. Brown lines delineate interior boundaries. Black lines are contours denoting every foot of difference in surge. Dark green and light purple illustrate difference is inundation limits for the two wind fields.

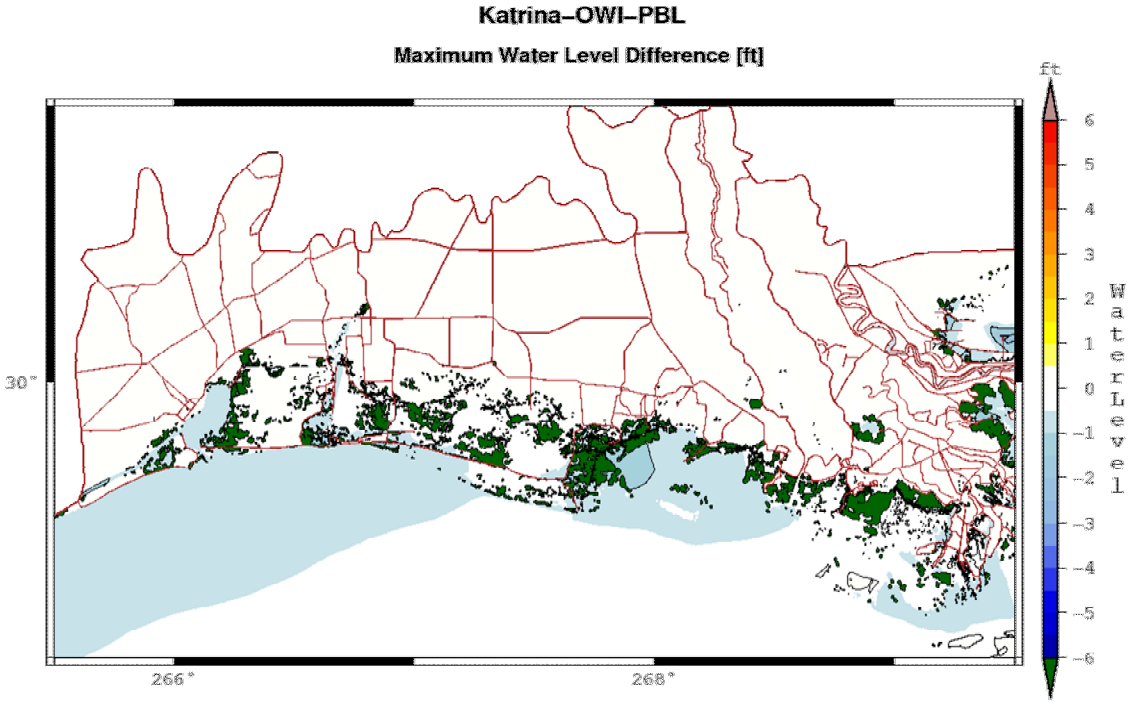

Figure 384: Maximum water level differences from H*WIND/IOKA wind generated results less PBL wind generated results for Hurricane Katrina in Southwestern Louisiana. Brown lines delineate interior boundaries. Black lines are contours denoting every foot of difference in surge. Dark green and light purple illustrate difference is inundation limits for the two wind fields.

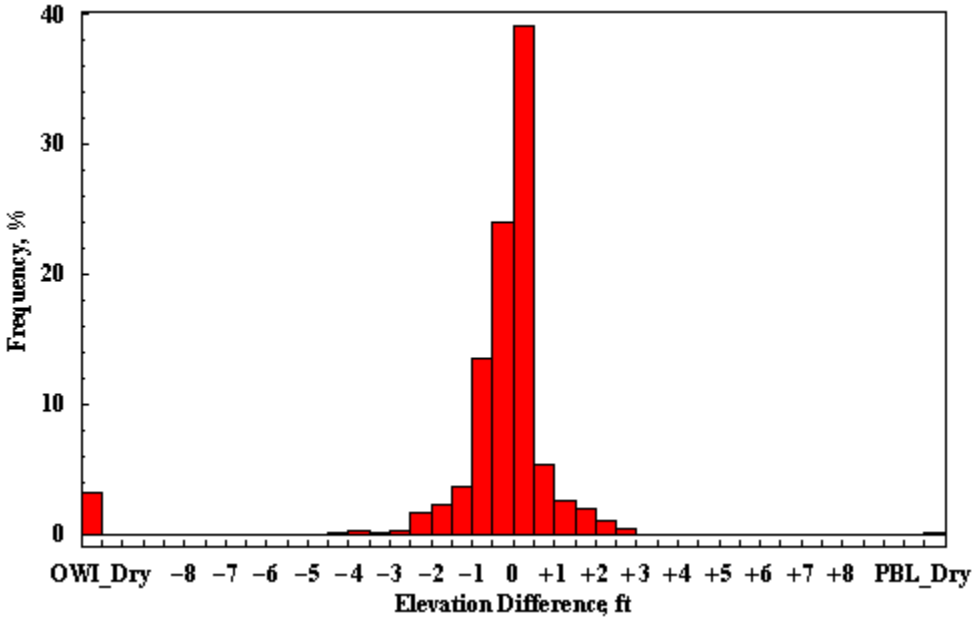

Figure 385: Histogram of water level surfaces differences for H*WIND/IOKA wind generated results less PBL wind generated results for Hurricane Katrina. Bins are every 0.5 foot.

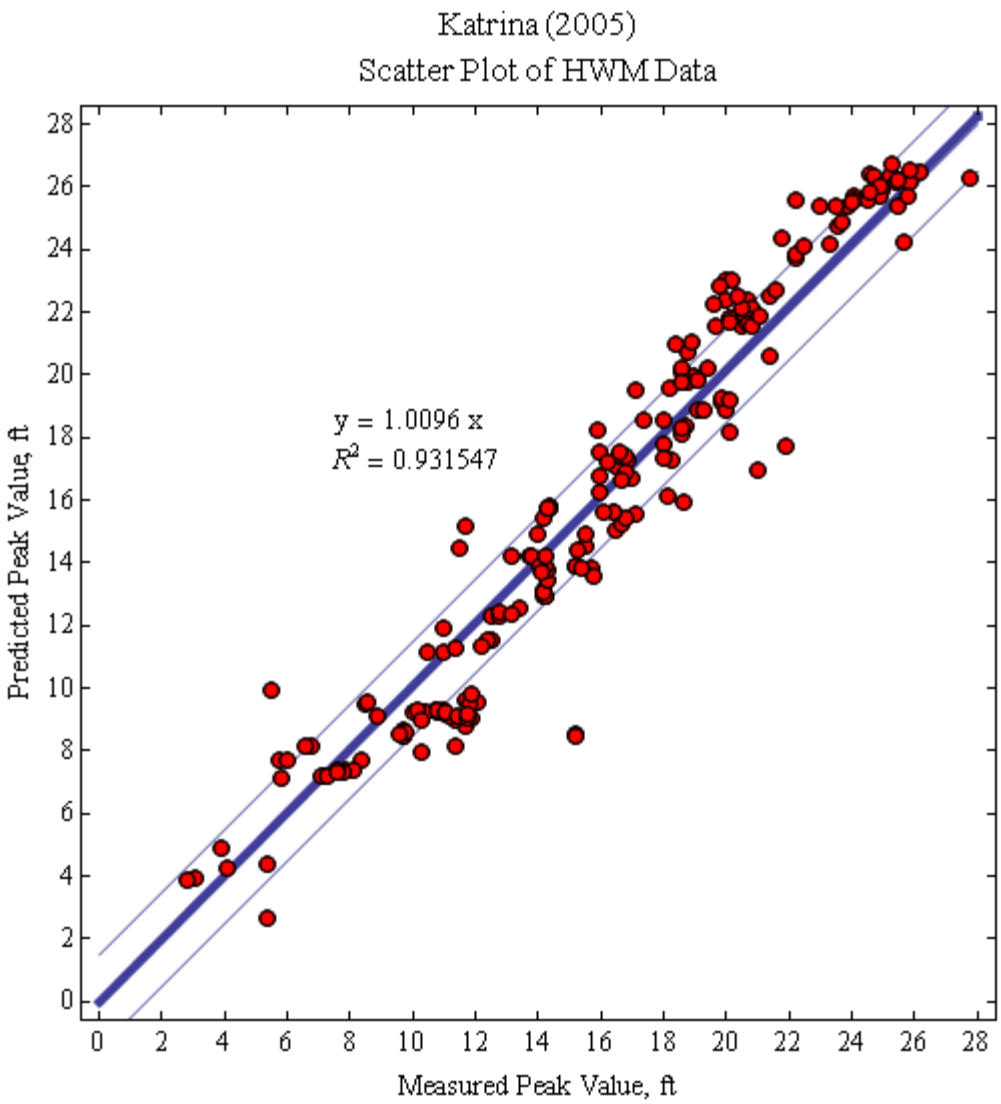

Figure 386: Comparison of observed USACE High-Water Marks (HWMs) for Hurricane Katrina and the simulation using the H*WIND/IOKA wind fields. The red points are the values at the recorded USACE HWMs. Thin blue lines display a 1:1 correlation as well as a 1.5-foot variance on each side.

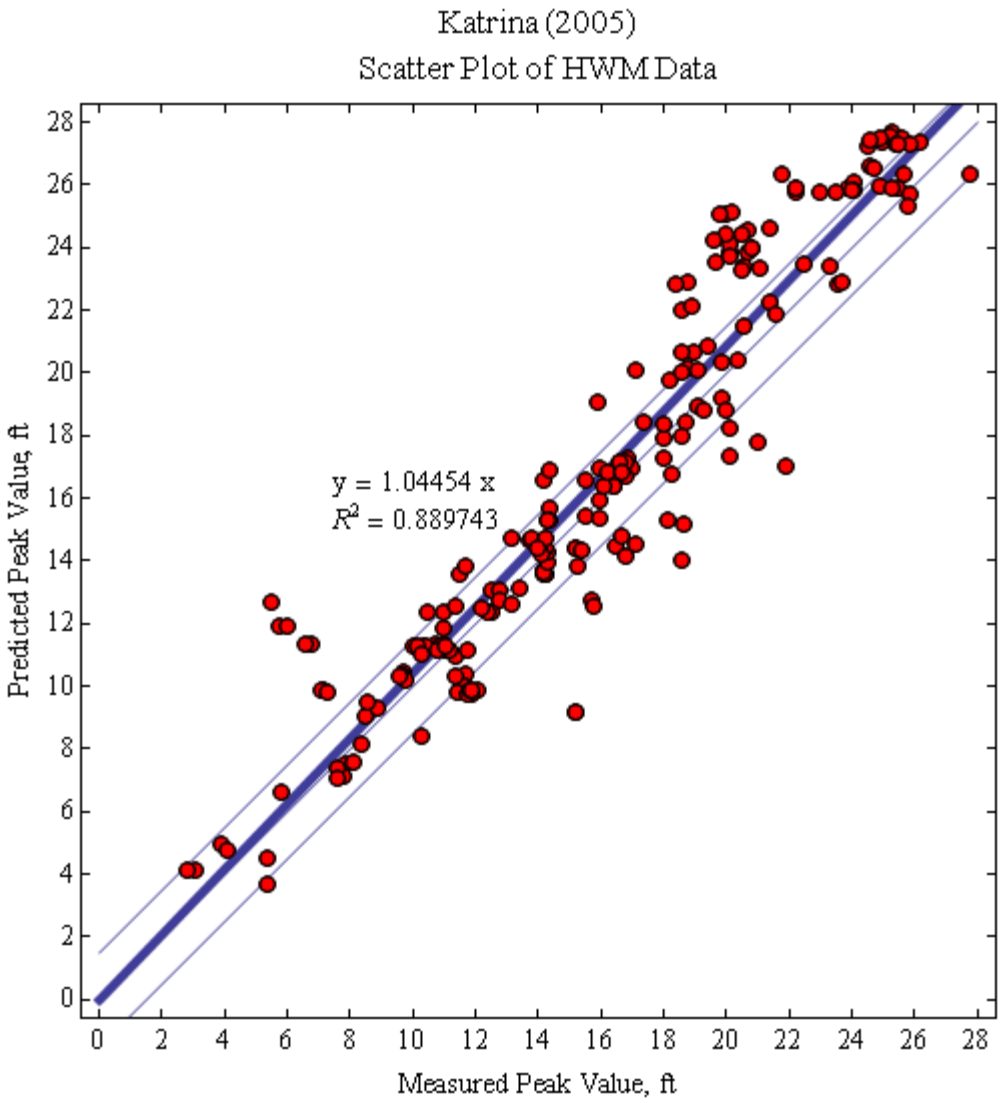

Figure 387: Comparison of observed USACE High-Water Marks (HWMs) for Hurricane Katrina and the simulation using the PBL wind fields. The red points are the values at the recorded USACE HWMs. Thin blue lines display a 1:1 correlation as well as a 1.5-foot variance on each side.

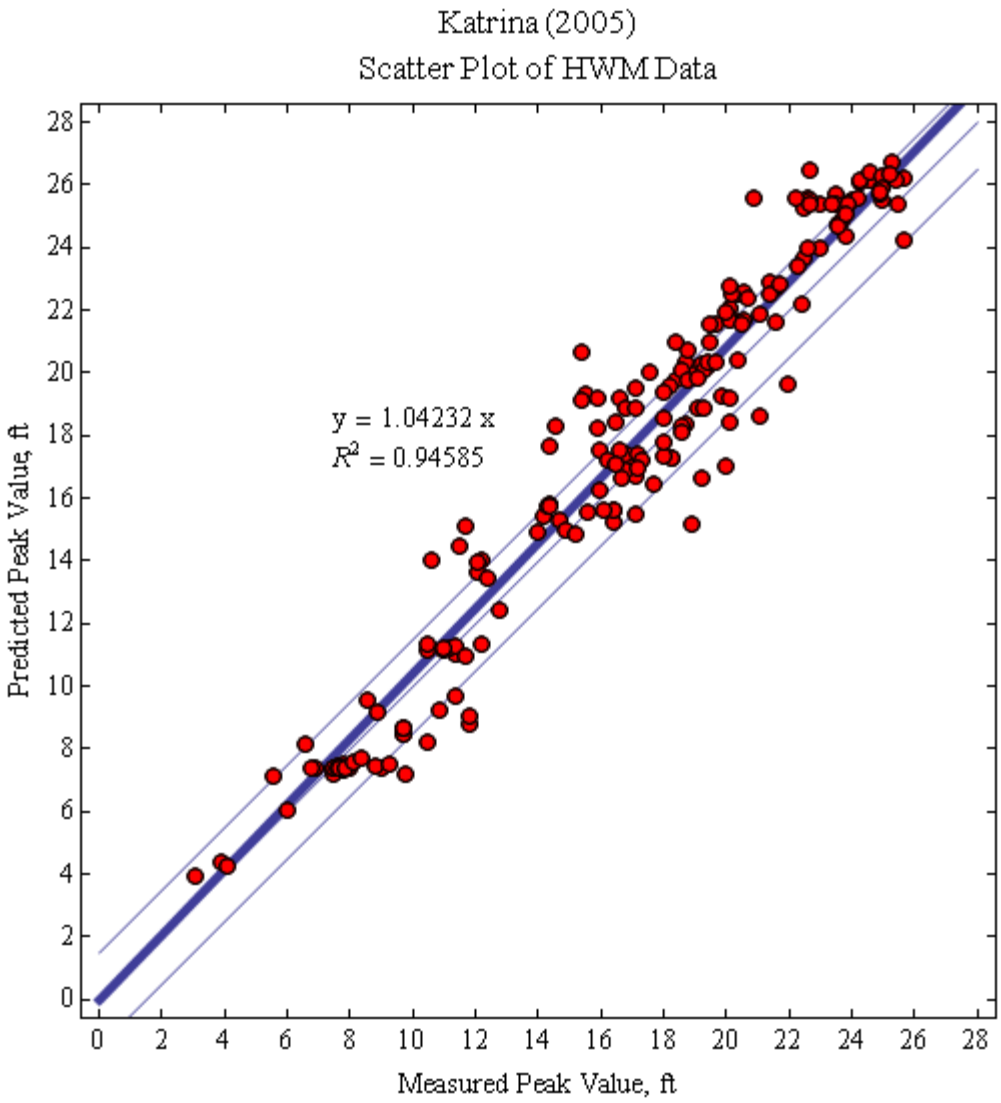

Figure 388: Comparison of observed URS High-Water Marks (HWMs) for Hurricane Katrina and the simulation using the H*WIND/IOKA wind fields. The red points are the values at the recorded URS HWMs. Thin blue lines display a 1:1 correlation as well as a 1.5-foot variance on each side.

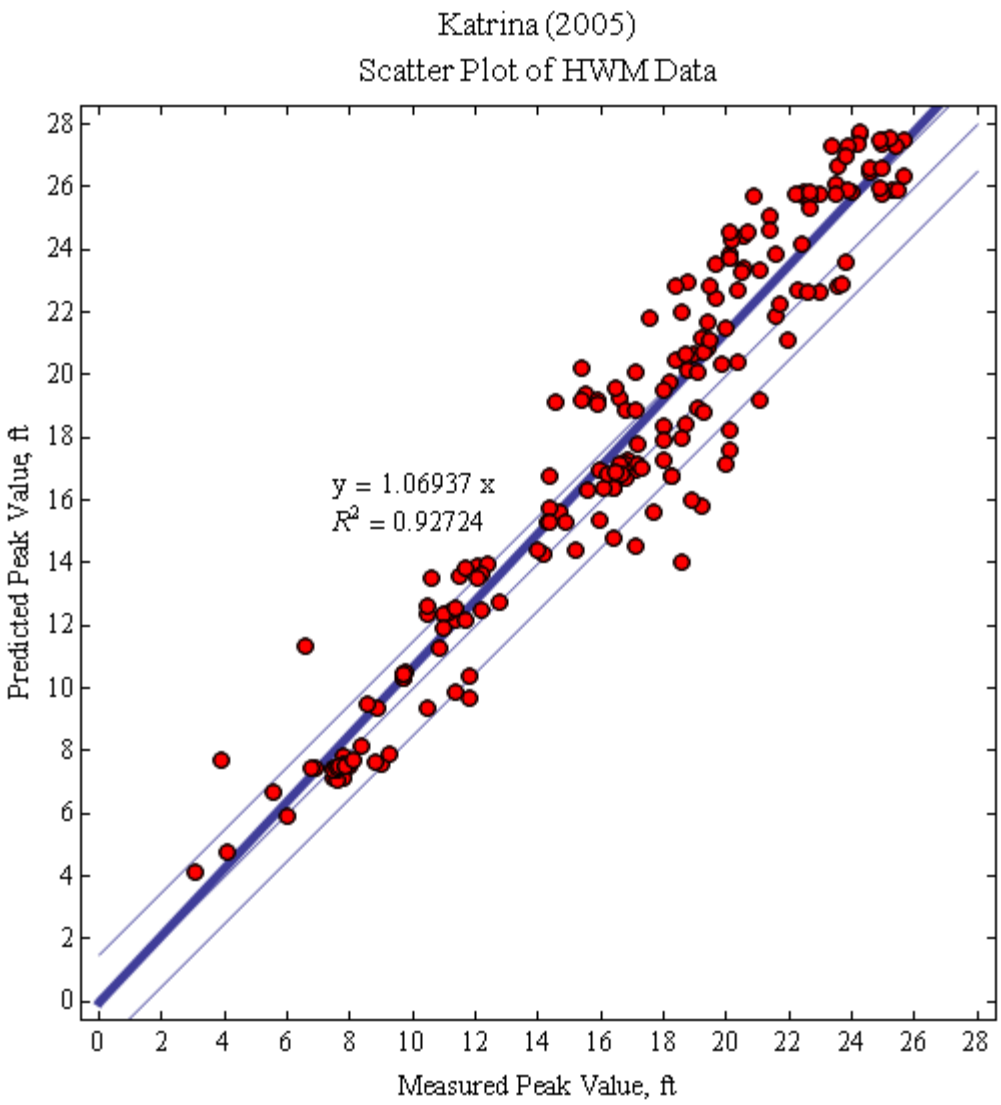

Figure 389: Comparison of observed URS High-Water Marks (HWMs) for Hurricane Katrina and the simulation using the PBL wind fields. The red points are the values at the recorded URS HWMs. Thin blue lines display a 1:1 correlation as well as a 1.5-foot variance on each side.

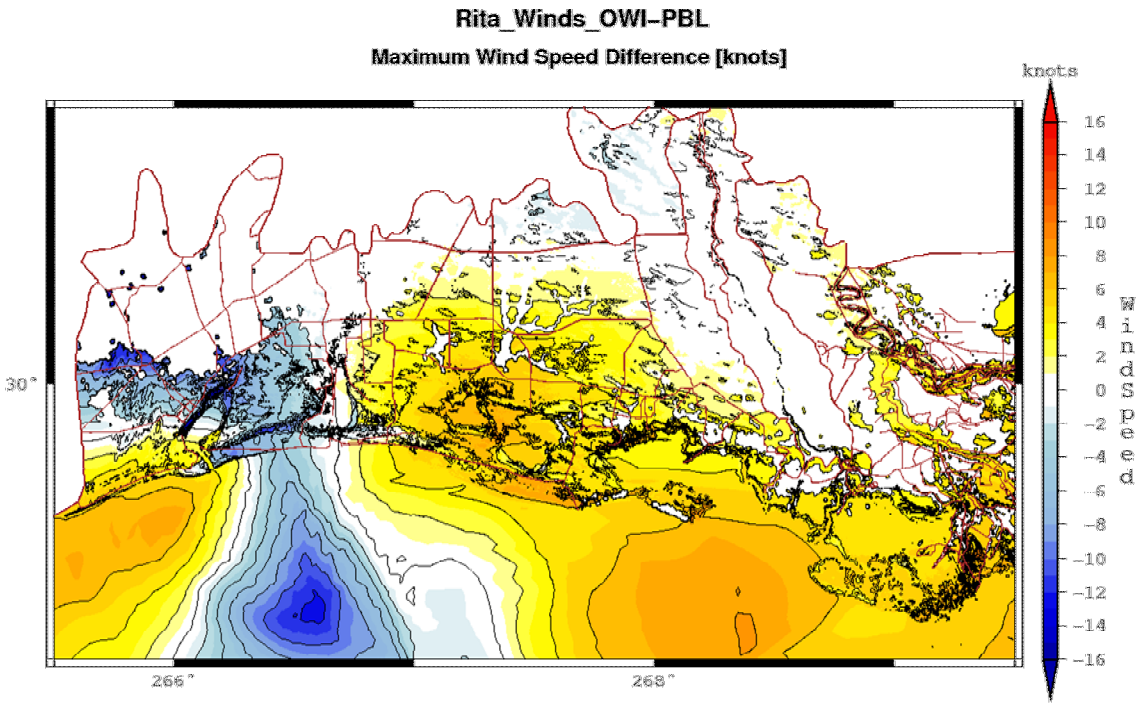

Figure 390: Maximum wind speed differences from H*WIND/IOKA wind generated results less PBL wind generated results for Hurricane Rita in Southwestern Louisiana. Brown lines delineate interior boundaries. Black lines are contours denoting every 2 knots of difference.

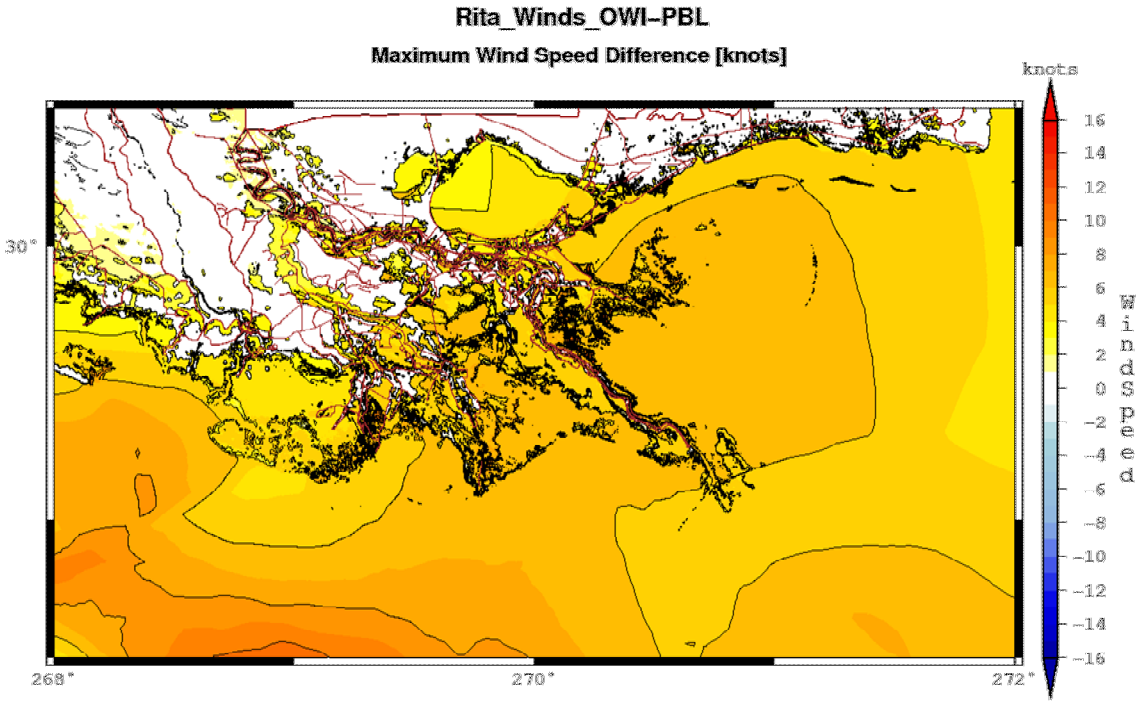

Figure 391: Maximum wind speed differences from H*WIND/IOKA wind generated results less PBL wind generated results for Hurricane Rita in Southeastern Louisiana. Brown lines delineate interior boundaries. Black lines are contours denoting every 2 knots of difference.

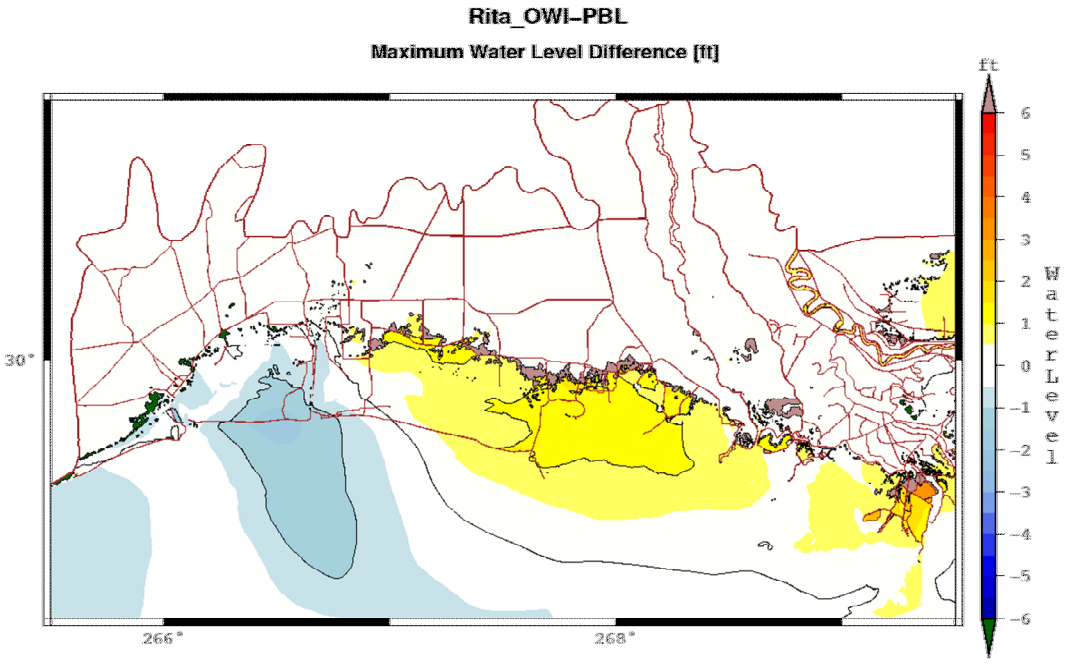

Figure 392: Maximum water level differences from H*WIND/IOKA wind generated results less PBL wind generated results for Hurricane Rita in Southwestern Louisiana. Brown lines delineate interior boundaries. Black lines are contours denoting every foot of difference in surge. Dark green and light purple illustrate difference is inundation limits for the two wind fields.

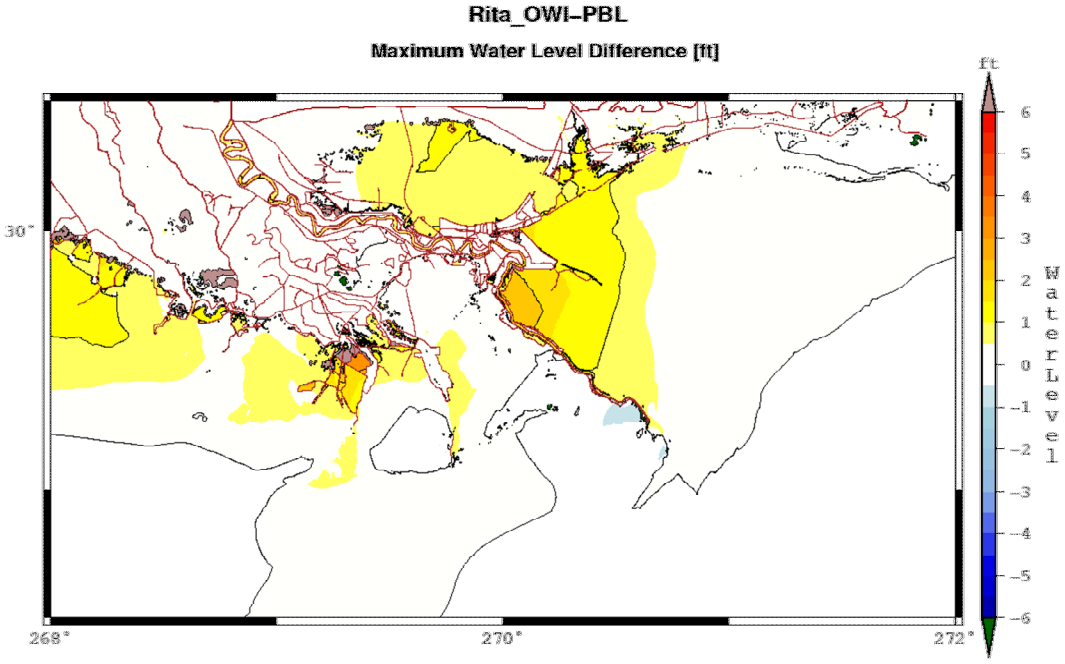

Figure 393: Maximum water level differences from H*WIND/IOKA wind generated results less PBL wind generated results for Hurricane Rita in Southeastern Louisiana. Brown lines delineate interior boundaries. Black lines are contours denoting every foot of difference in surge. Dark green and light purple illustrate difference is inundation limits for the two wind fields.

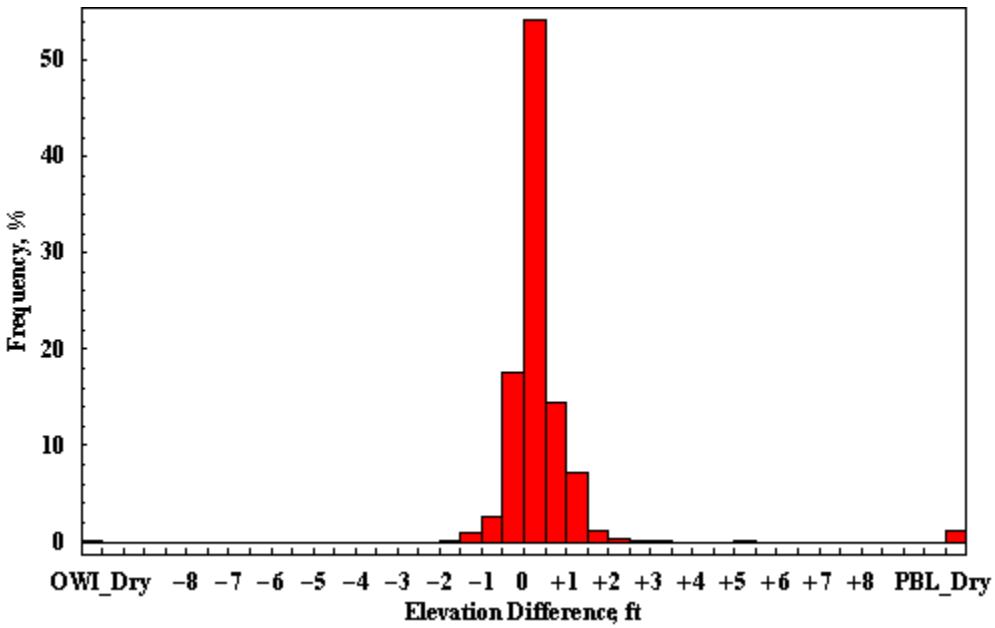

Figure 394: Histogram of water level surfaces differences for H*WIND/IOKA wind generated results less PBL wind generated results for Hurricane Rita. Bins are every 0.5 foot.

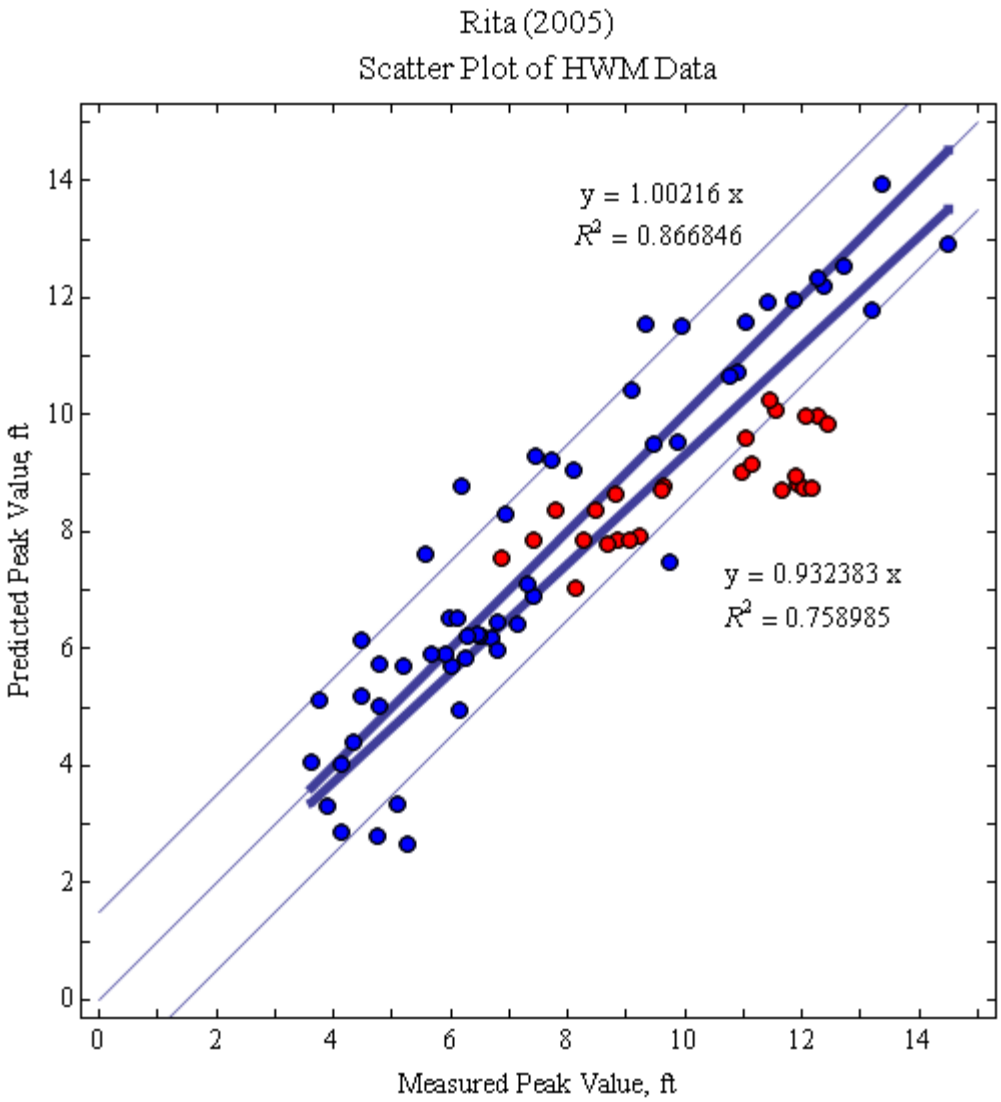

Figure 395: Comparison of observed High-Water Marks (HWMs) for Hurricane Rita and the simulation using the H*WIND/IOKA wind fields. The blue and red points are the values at the recorded FEMA HWMs. Red points denote those in Vermilion Bay. Thin blue lines display a 1:1 correlation as well as a 1.5-foot variance on each side.

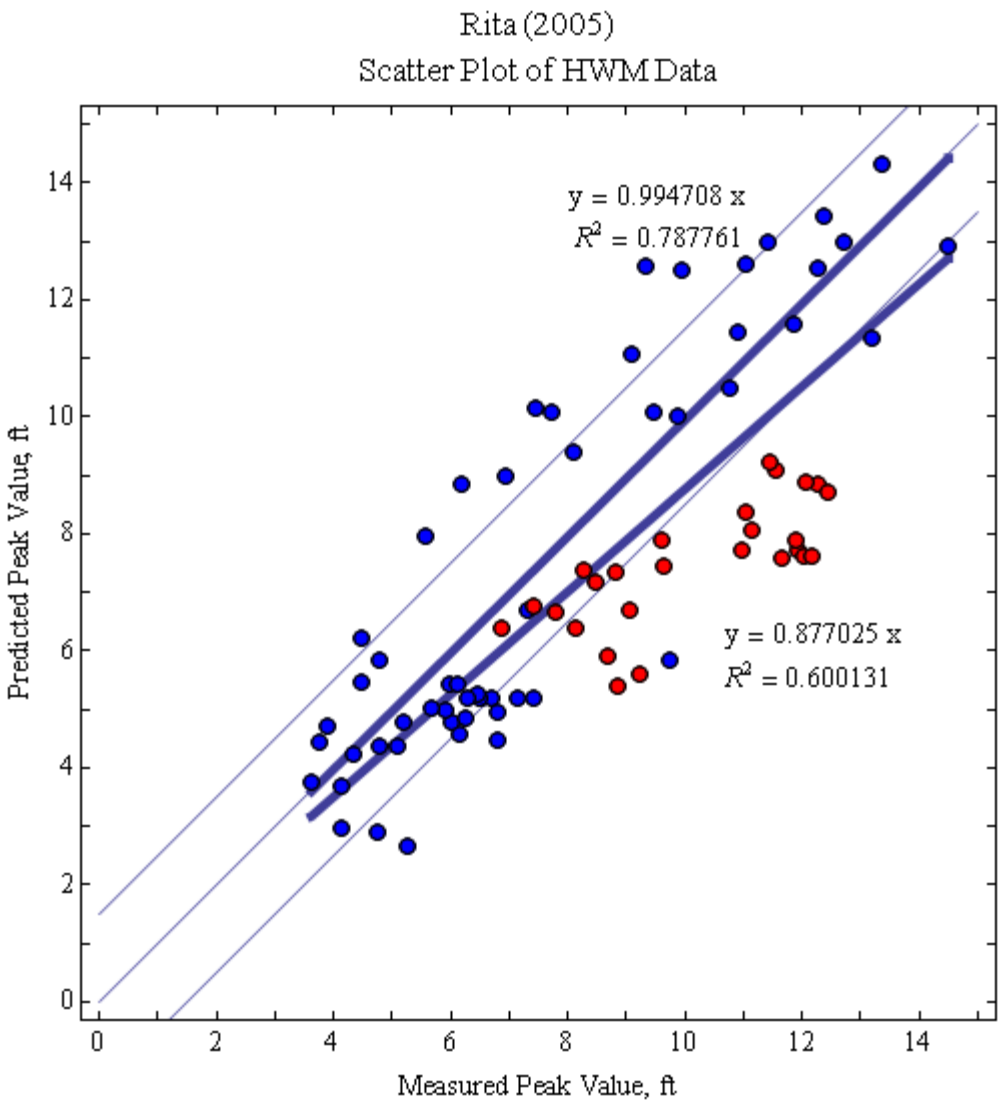

Figure 396: Comparison of observed High-Water Marks (HWMs) for Hurricane Rita and the simulation using the PBL wind fields. The blue and red points are the values at the recorded FEMA HWMs. Red points denote those in Vermilion Bay. Thin blue lines display a 1:1 correlation as well as a 1.5-foot variance on each side.

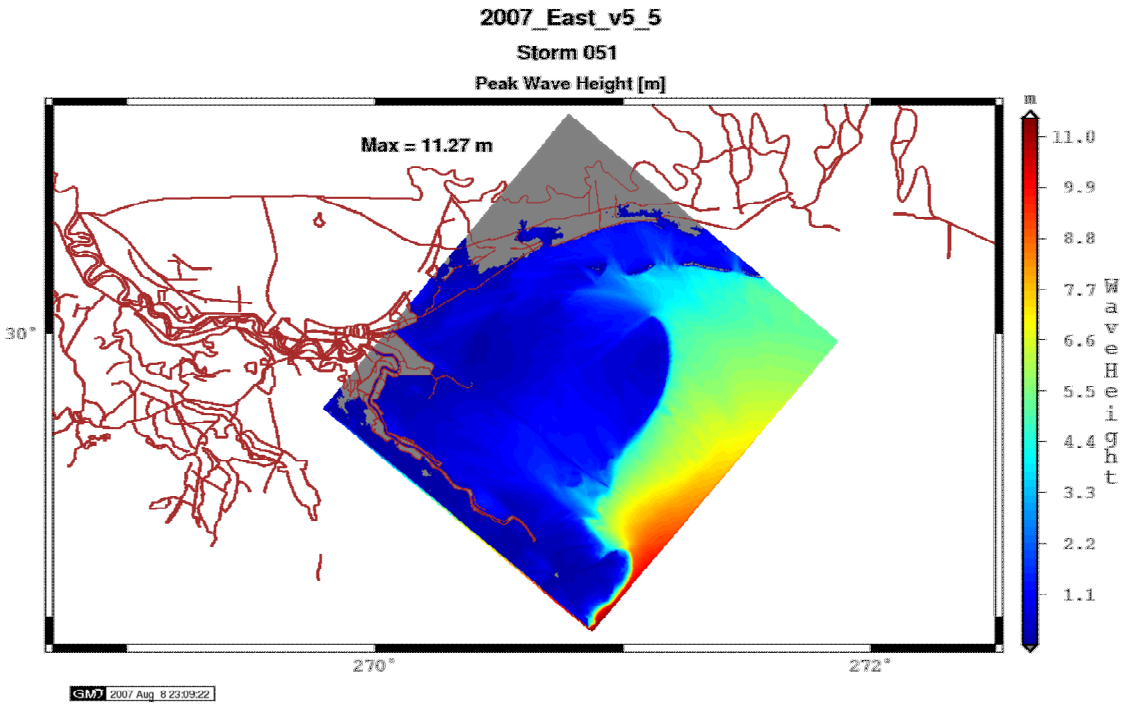

Figure 397: Plot of maximum wave heights on the SE STWAVE grid for storm 051.

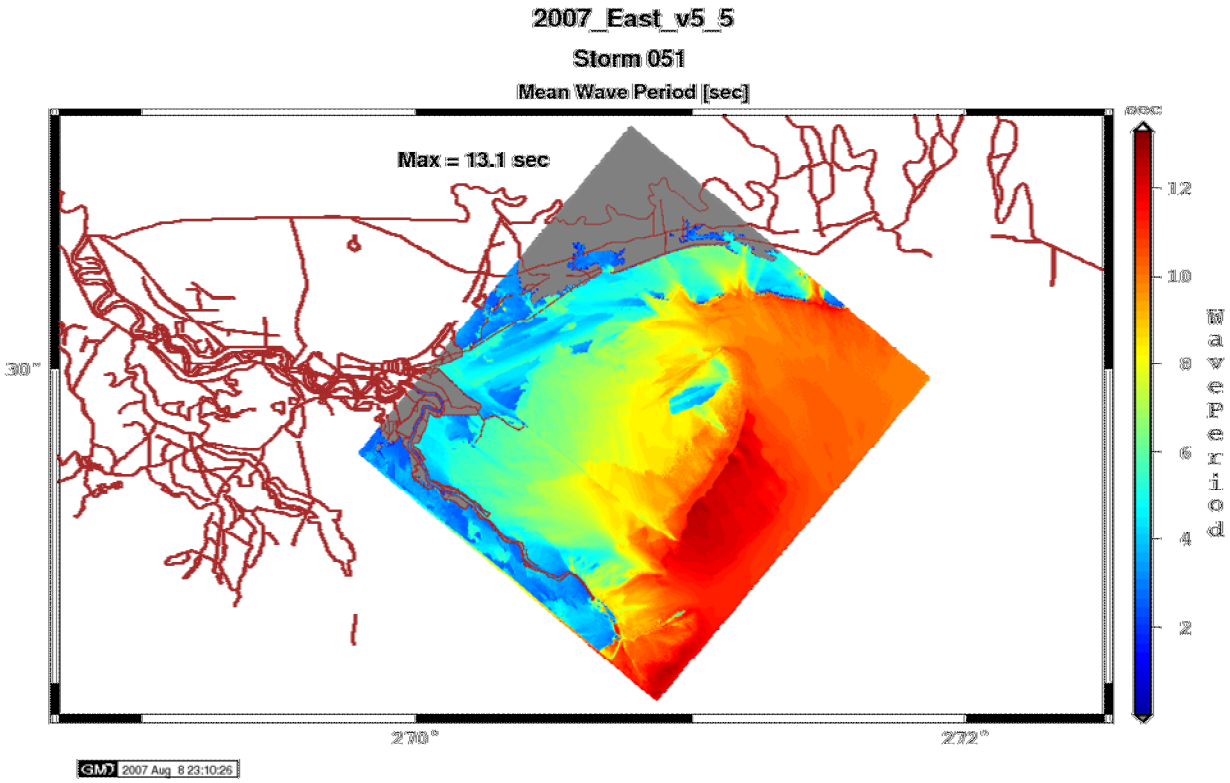

Figure 398: Plot of mean wave period on the SE STWAVE grid for storm 051.

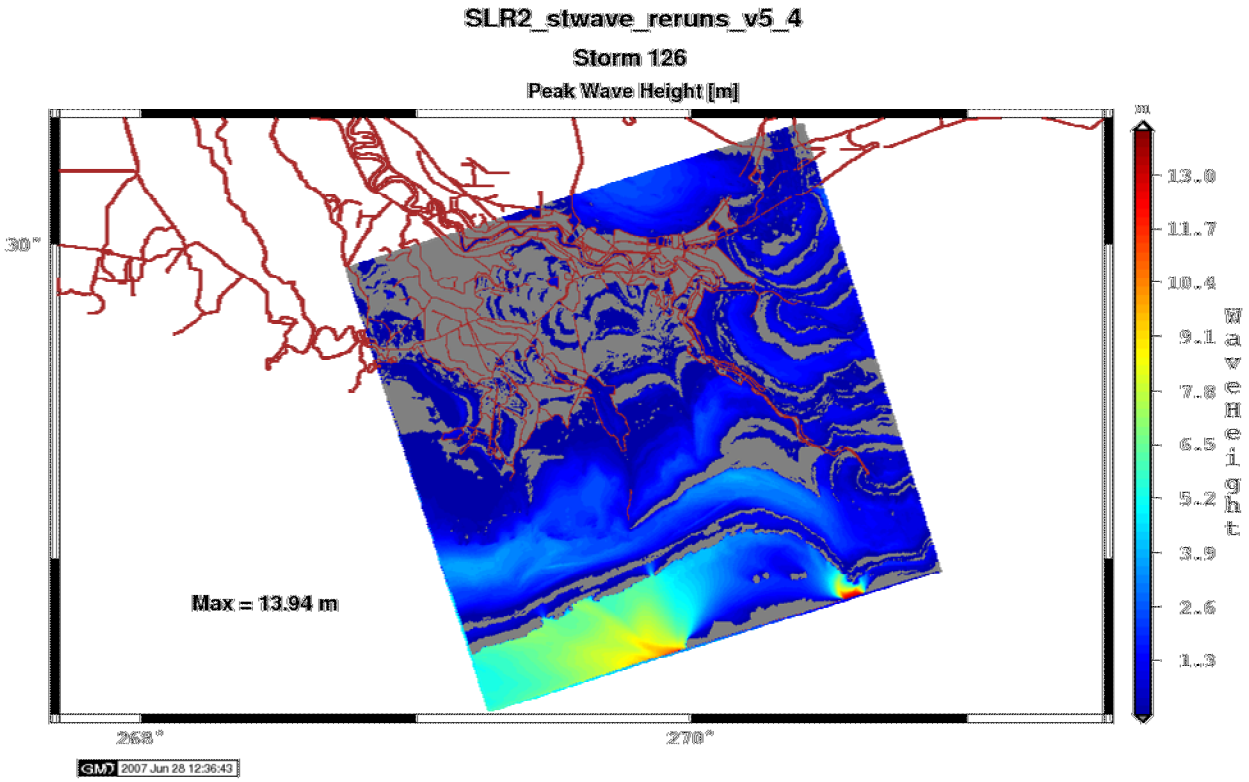

Figure 399: Results for storm 126 on the SE STWAVE grid; note the physically unrealistic striping that resulted from using a bad interpolation file; the correct behavior should be similar to Figure 397.

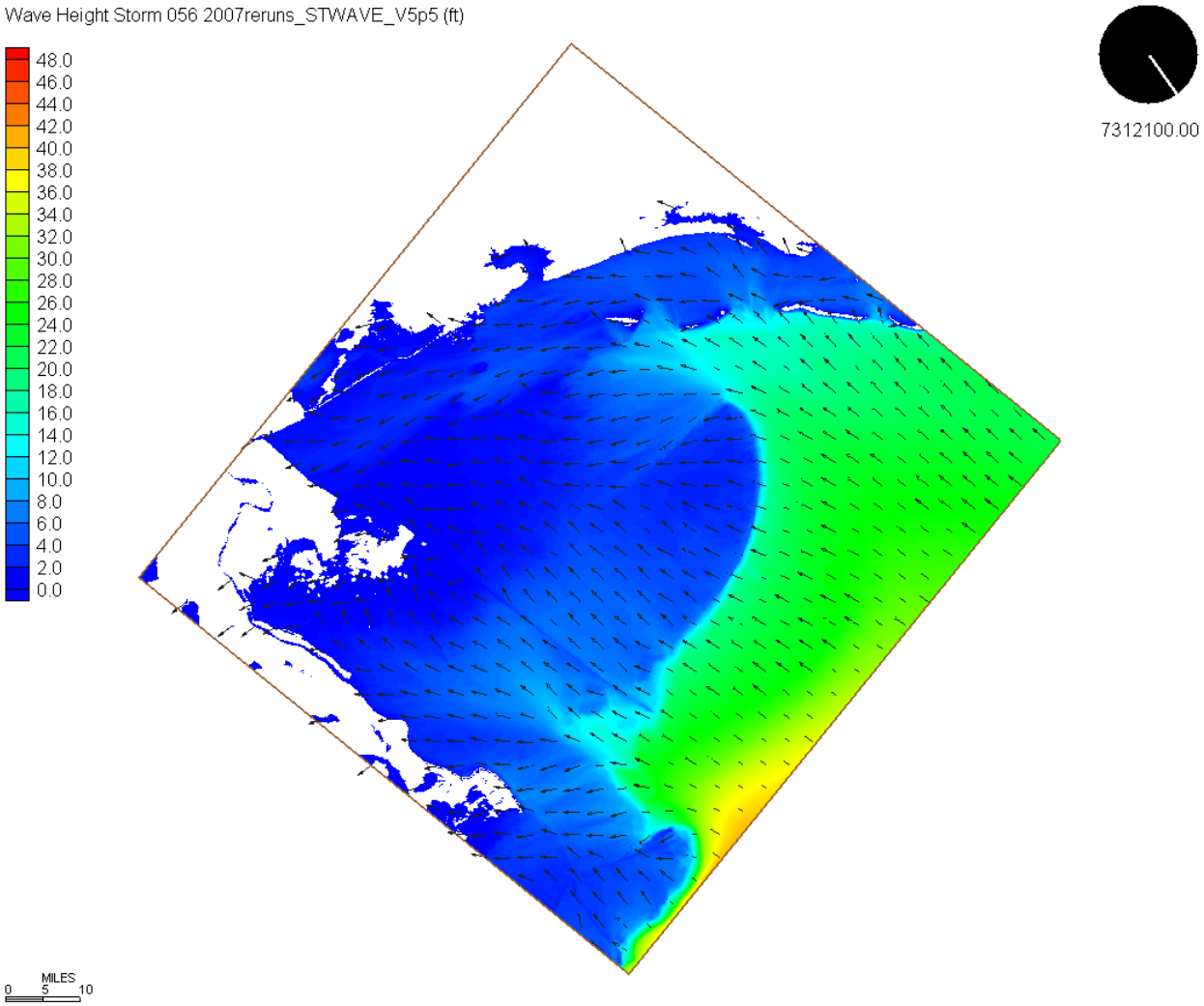

Figure 400: Snapshot from a quality assurance/quality control movie product that animates wave height (color contours) and wind field (black vectors) for storm 056.

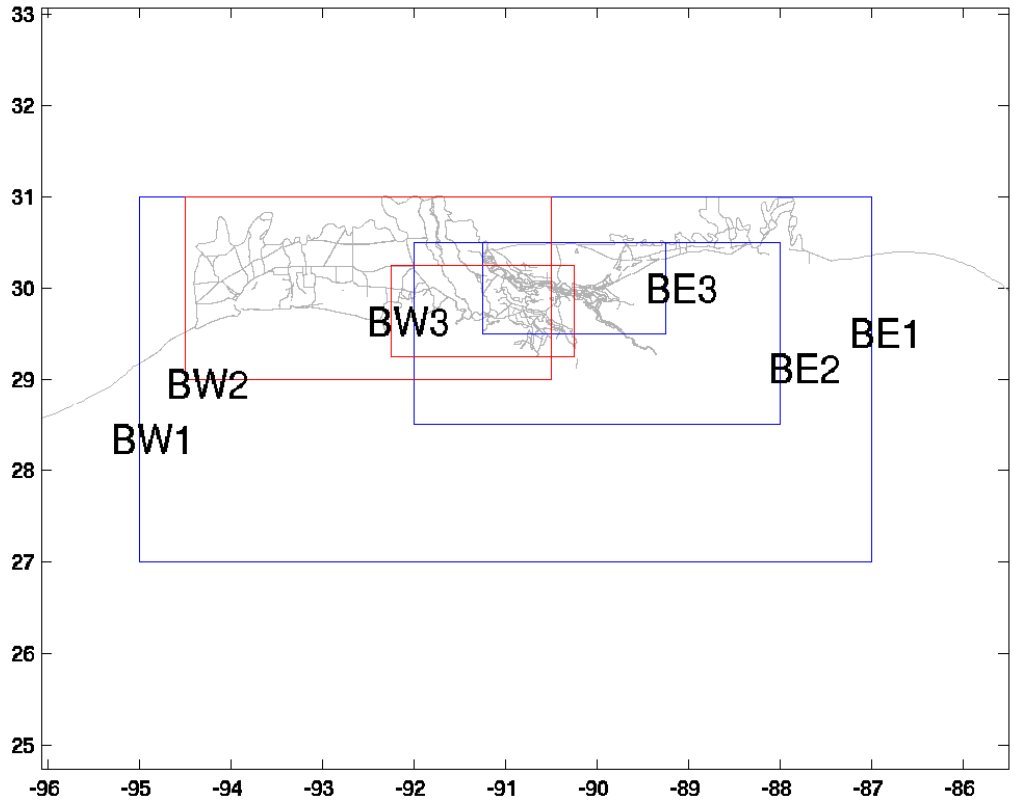

Figure 401: Skeleton view of Southern Louisiana showing the box outlines for the ADCIRC zooms used in the post-production process; only east (“E”) results reported herein.

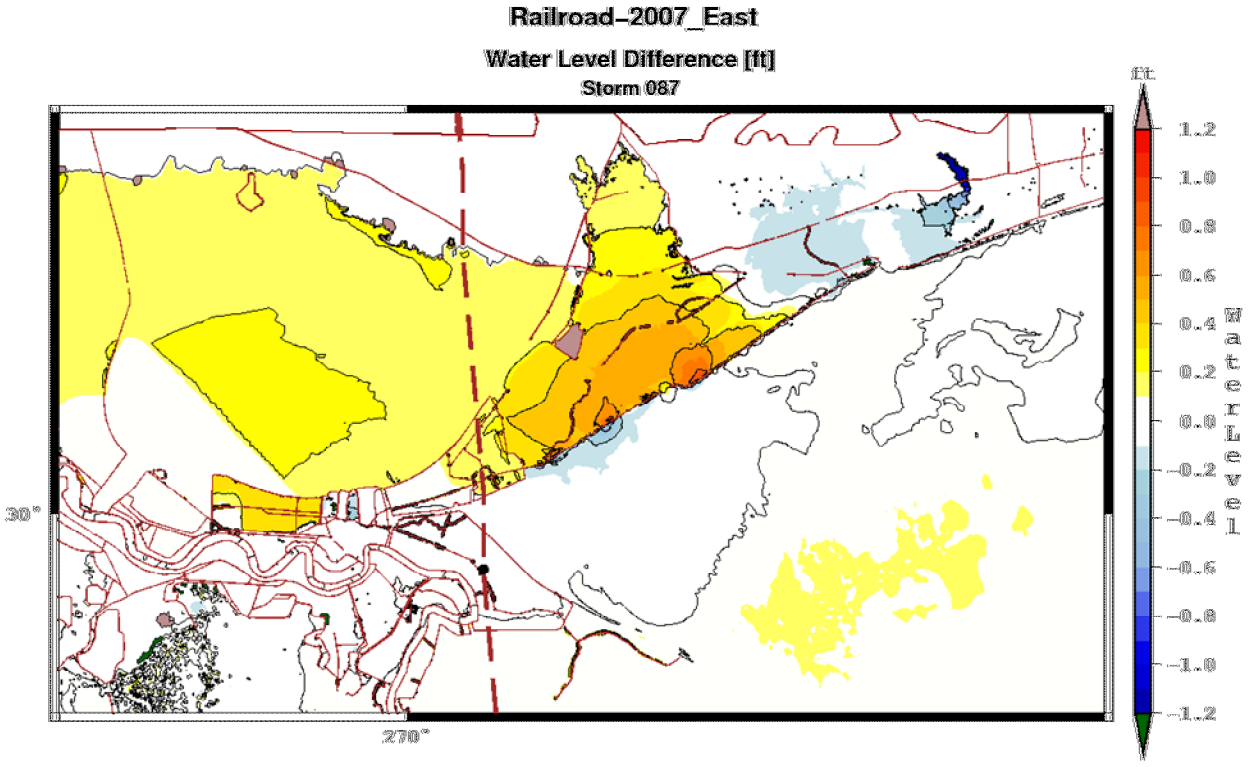

Figure 402: Plot of differences between the maximum elevations for the case of the railroad treated as a submerged levee versus the railroad gridded over and treated as a bathymetric rise; storm 087 is a high-intensity storm.

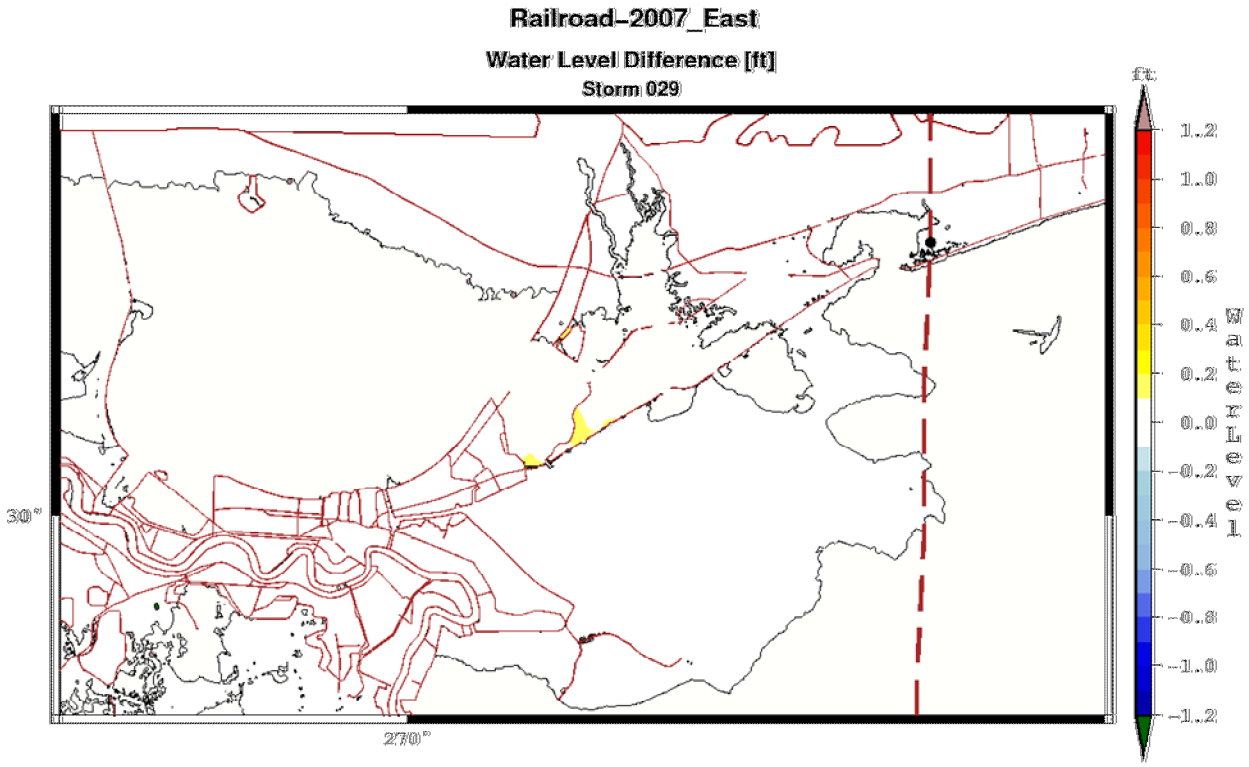

Figure 403: Plot of differences between the maximum elevations for the case of the railroad treated as a submerged levee versus the railroad gridded over and treated as a bathymetric rise; storm 029 is a low-intensity storm.

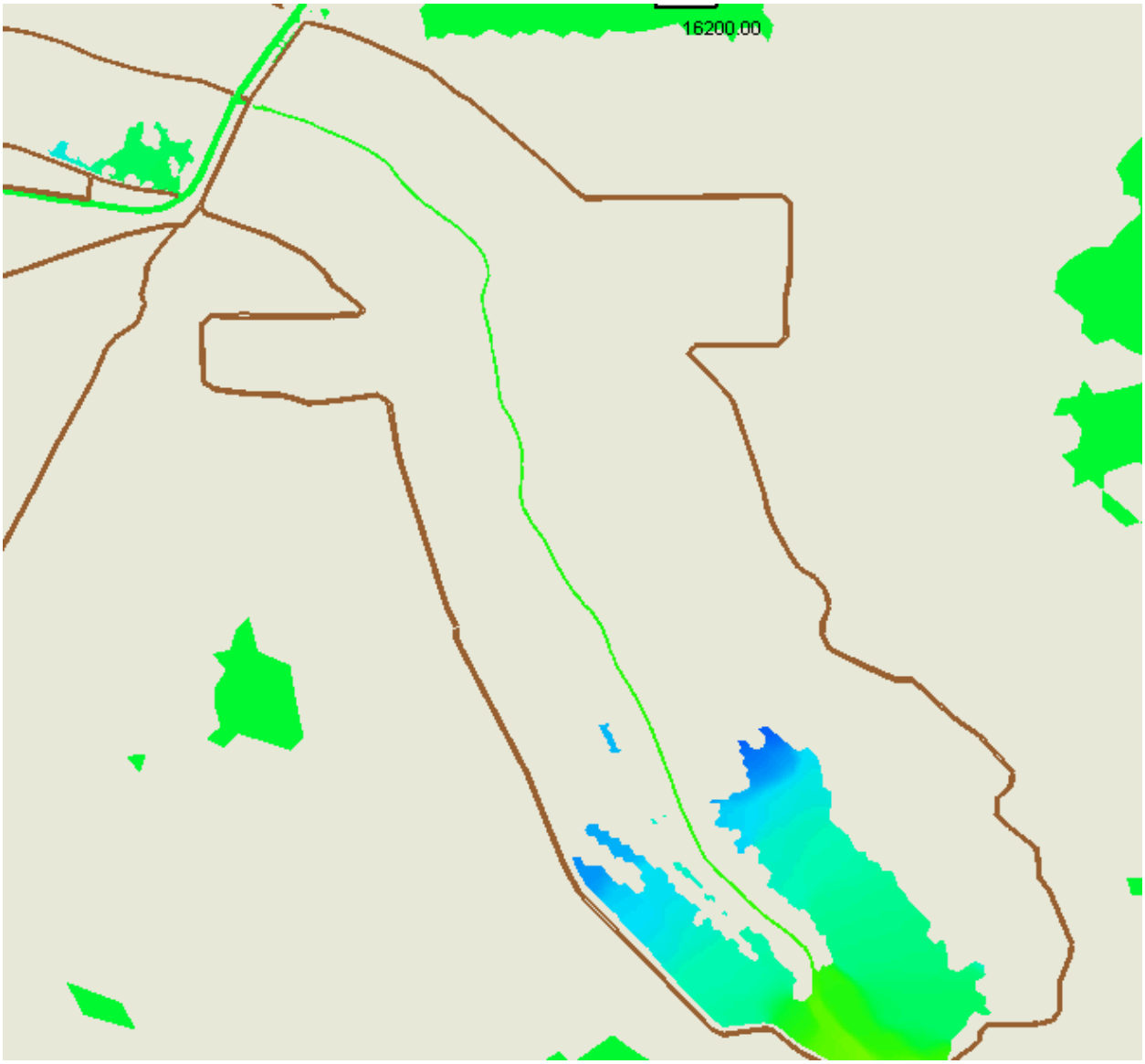

Figure 404: Zoom of the Golden Meadow region that illustrates the artificial flooding that can occur if the natural levees along canals are not properly resolved by the grid (note flooding in lower right).

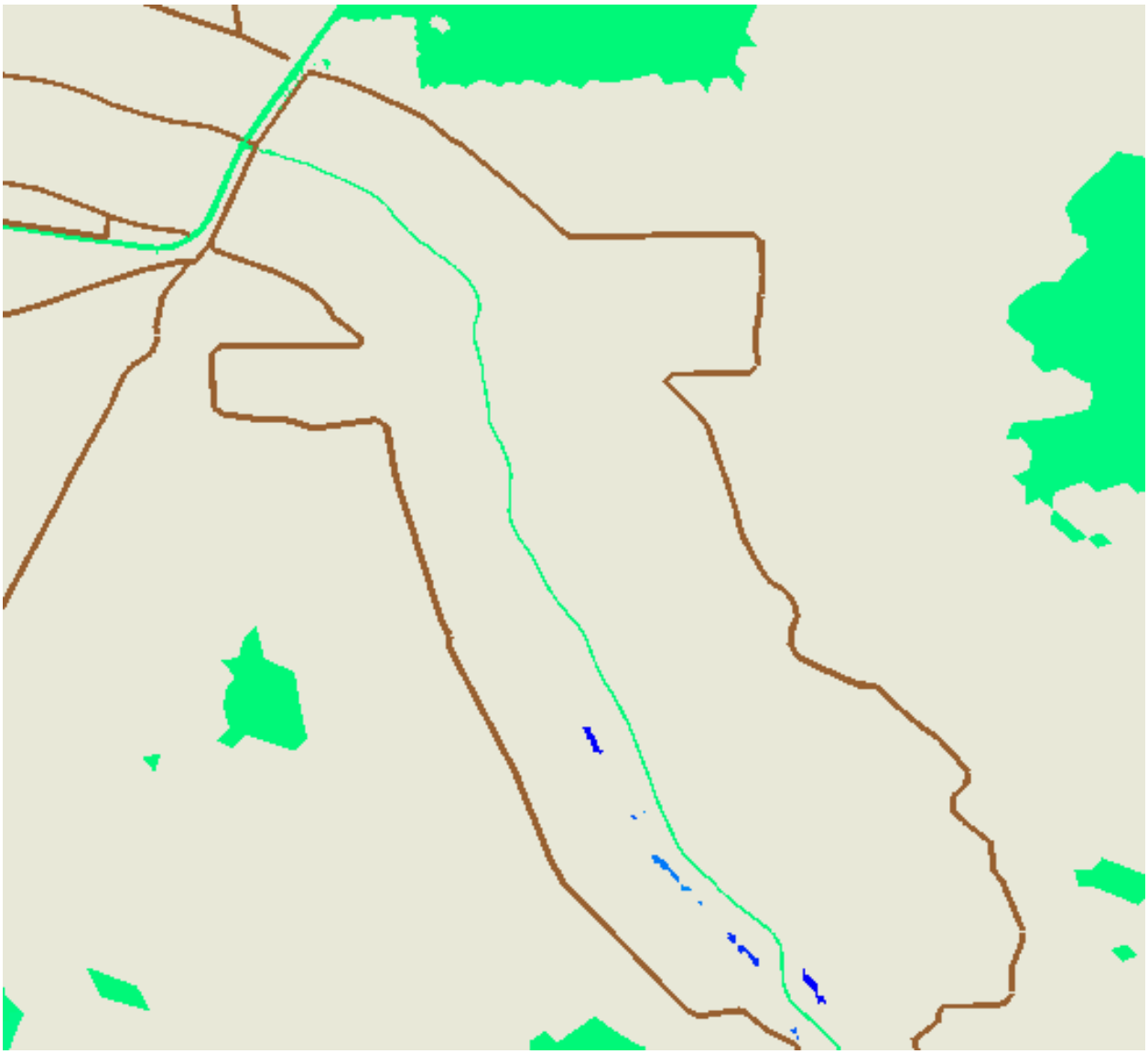

Figure 405: Zoom of the Golden Meadow region with the natural levees properly resolved, resulting in no artificial flooding.

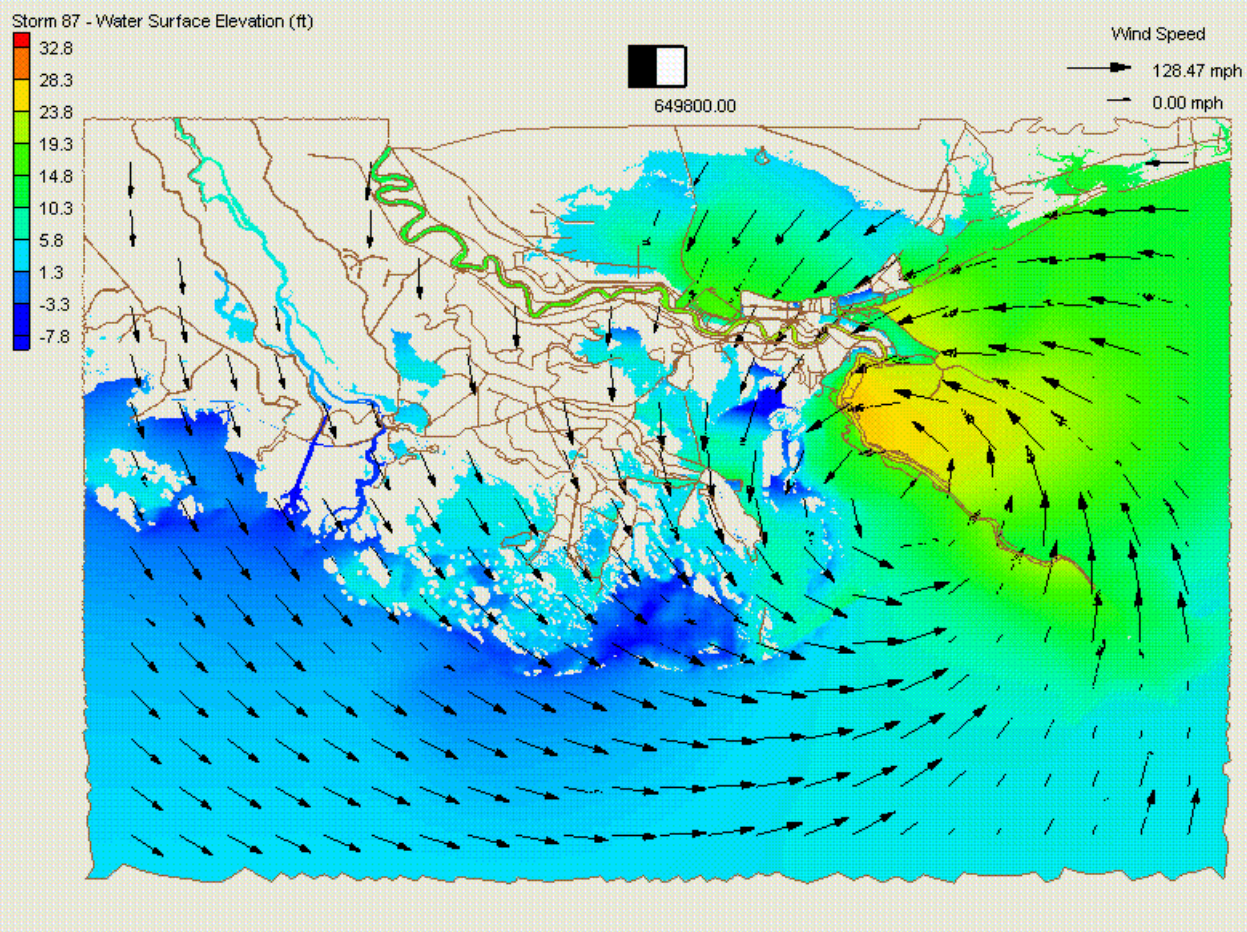

Figure 406: Snapshot from a quality assurance/quality control movie product that animates surface water elevation (color contours) and wind field (black vectors) for storm 087.

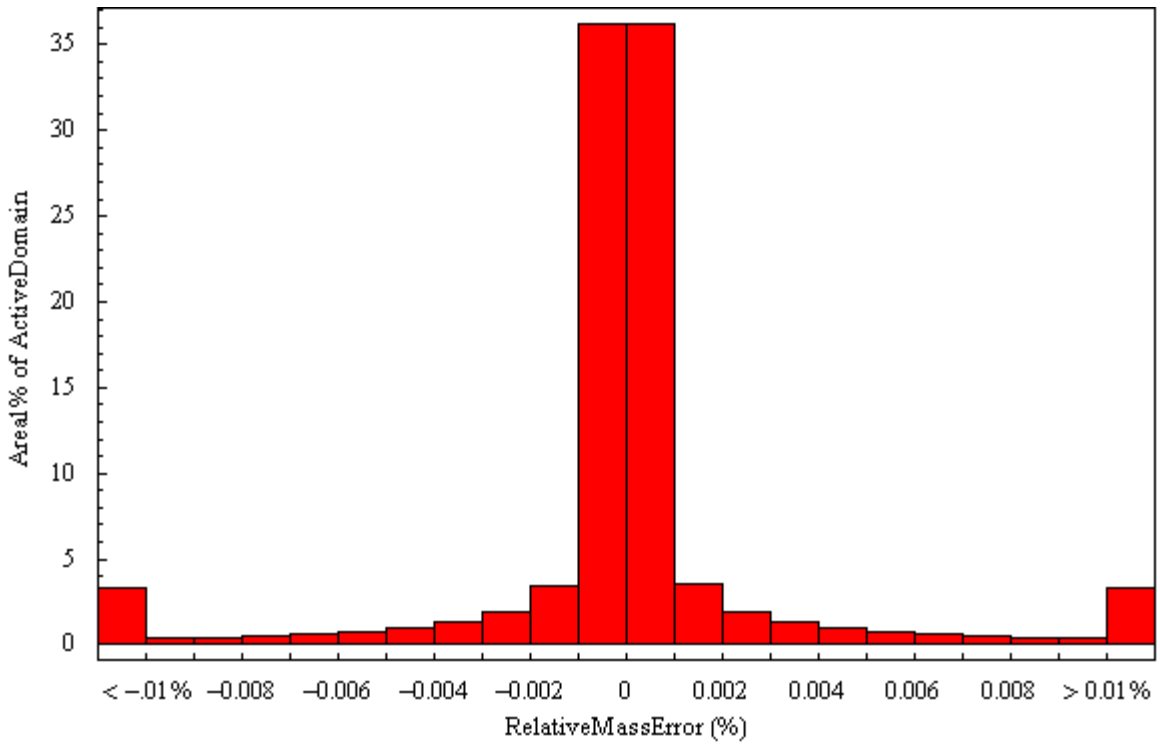

Figure 407: Histogram of relative mass balance error that is relative to still water volume, for storm 002; vertical axis is % of total domain area. Errors represent the average per time step error over the course of the simulation.

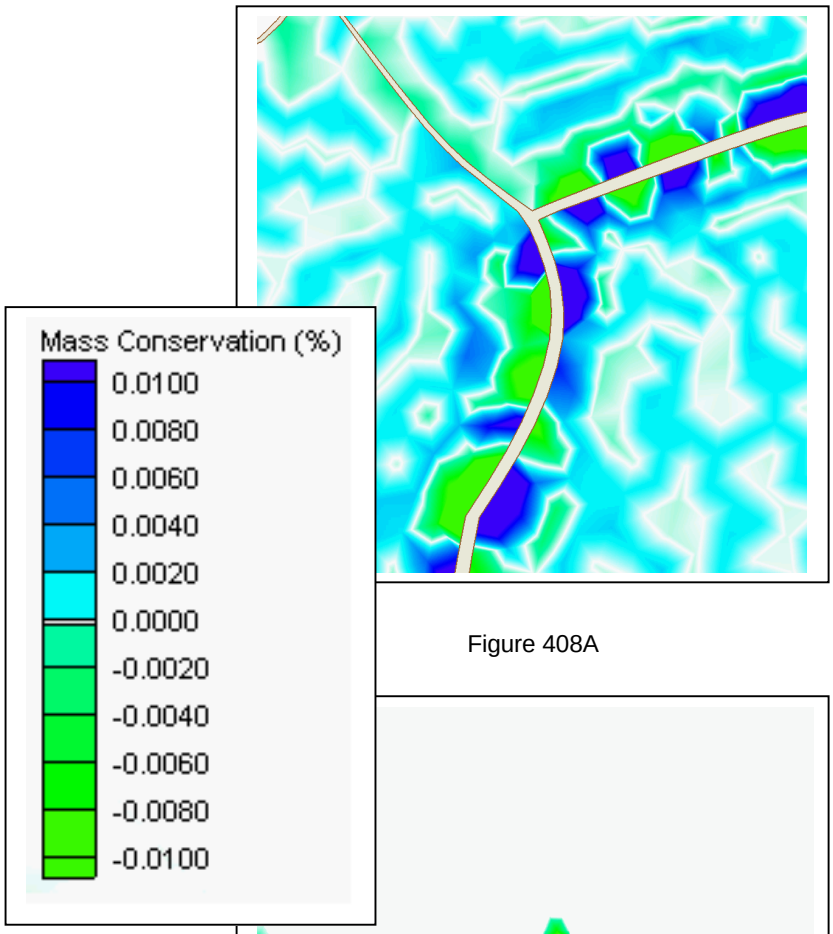

Figure 408A

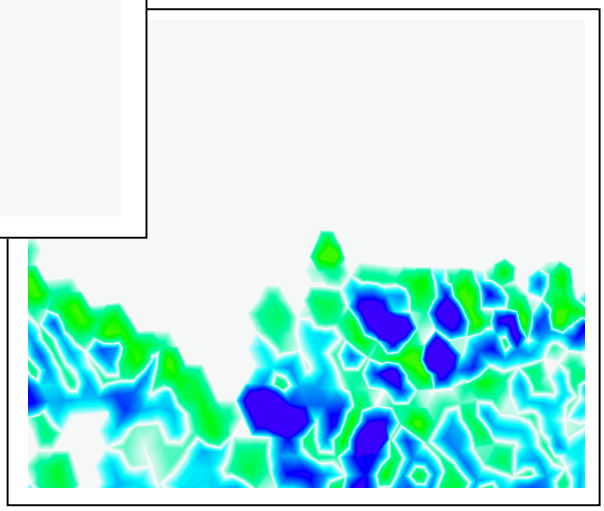

Figure 408B

Figure 408: Zoomed region near a levee (Figure 408A) and wetting front (Figure 408B) illustrating the spatial distribution of local mass balance error in these zones where the highest errors were clustered; note that the scale is stretched for illustrative purposes, and note that the wetting front errors tracked the propagation of the incoming surge. Scale is relative mass balance error per time step in percent of still water volume.

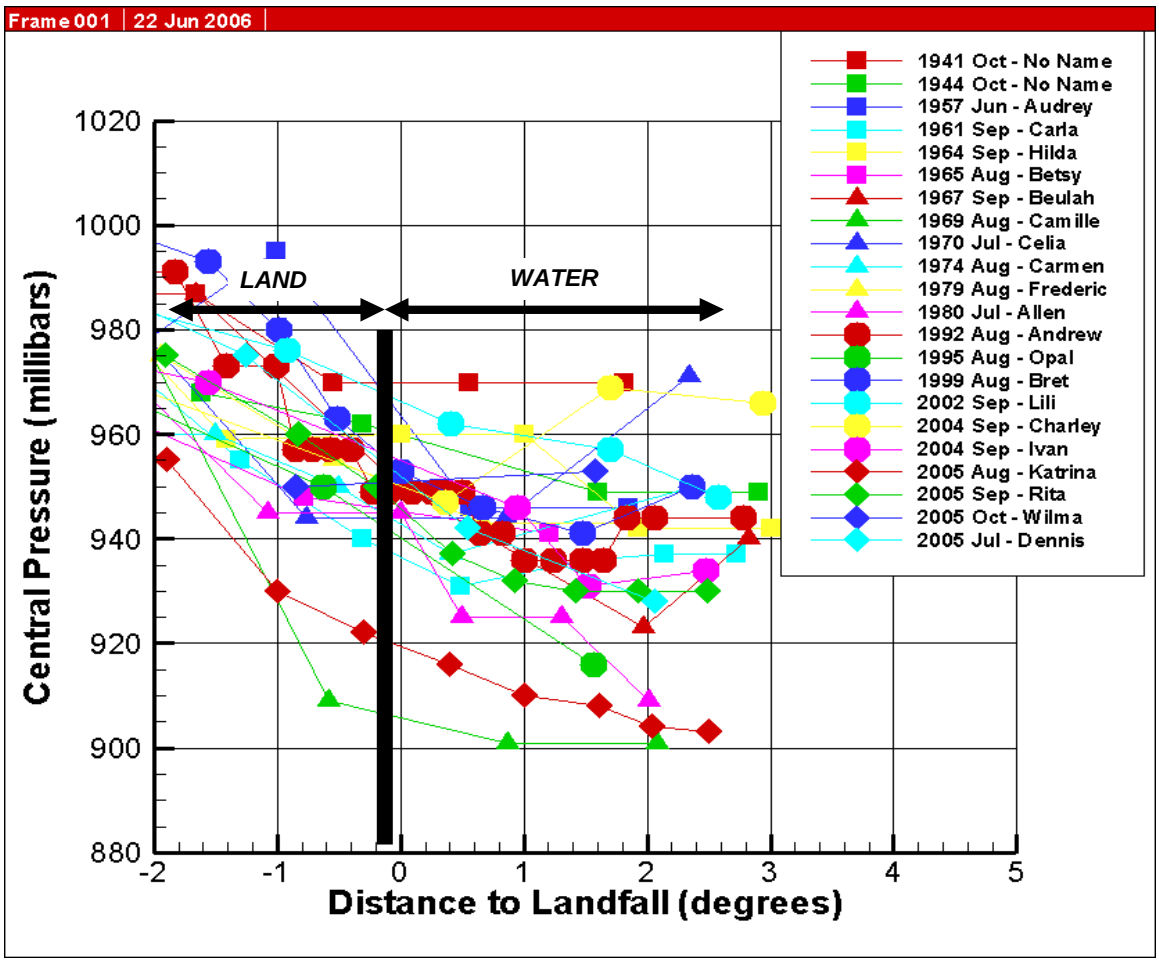

Figure 409: Central pressure in landfalling storms plotted against distance from the coast. Previously it was believed that storm decay began only after landfall. These data from Oceanweather, Inc., show clearly that decay begins offshore.

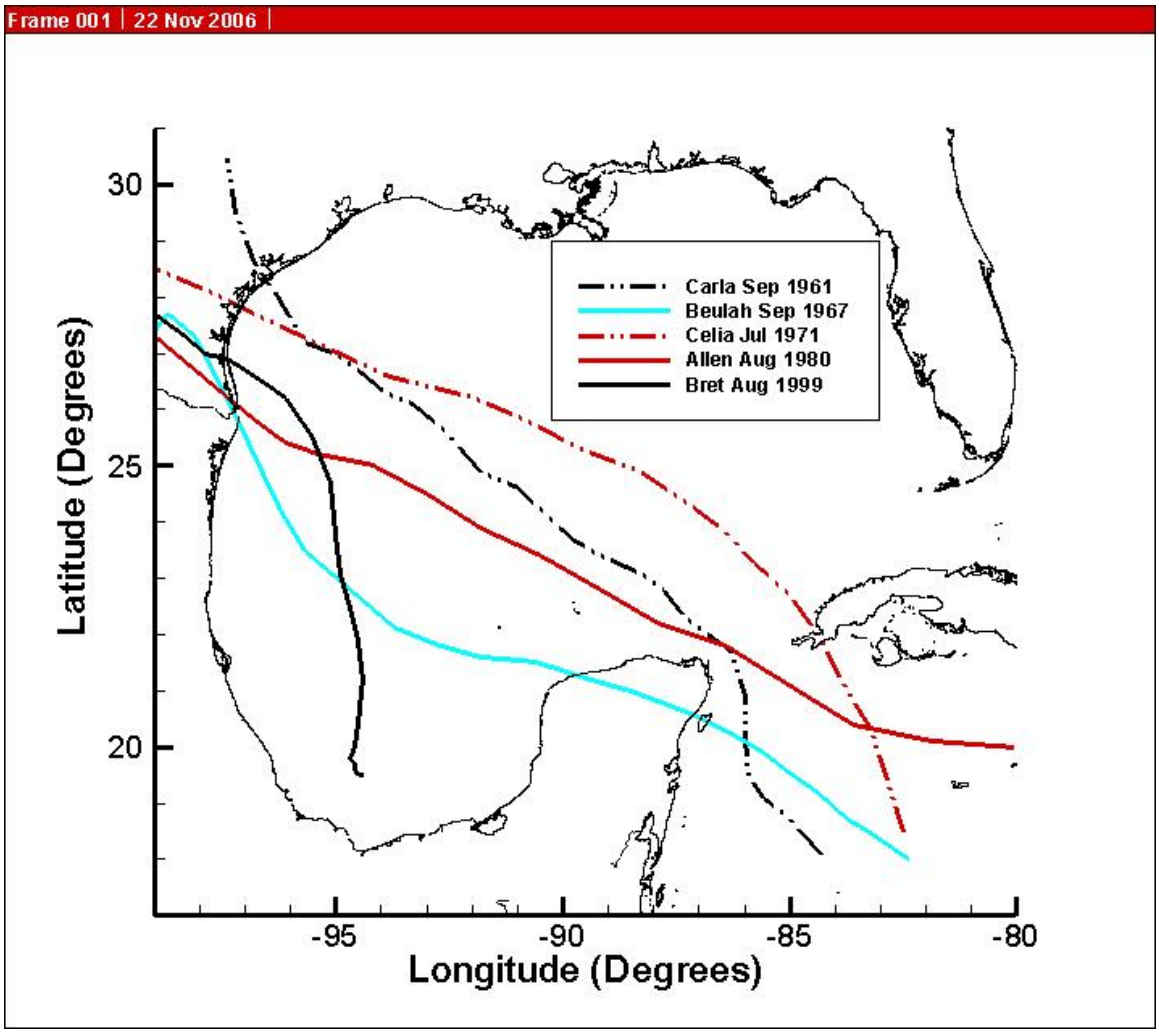

Figure 410: Tracks of all hurricanes (1941-2005) making landfall in the western Gulf of Mexico for storms that attained a central pressure of 955 millibars or lower during its transit through the Gulf of Mexico.

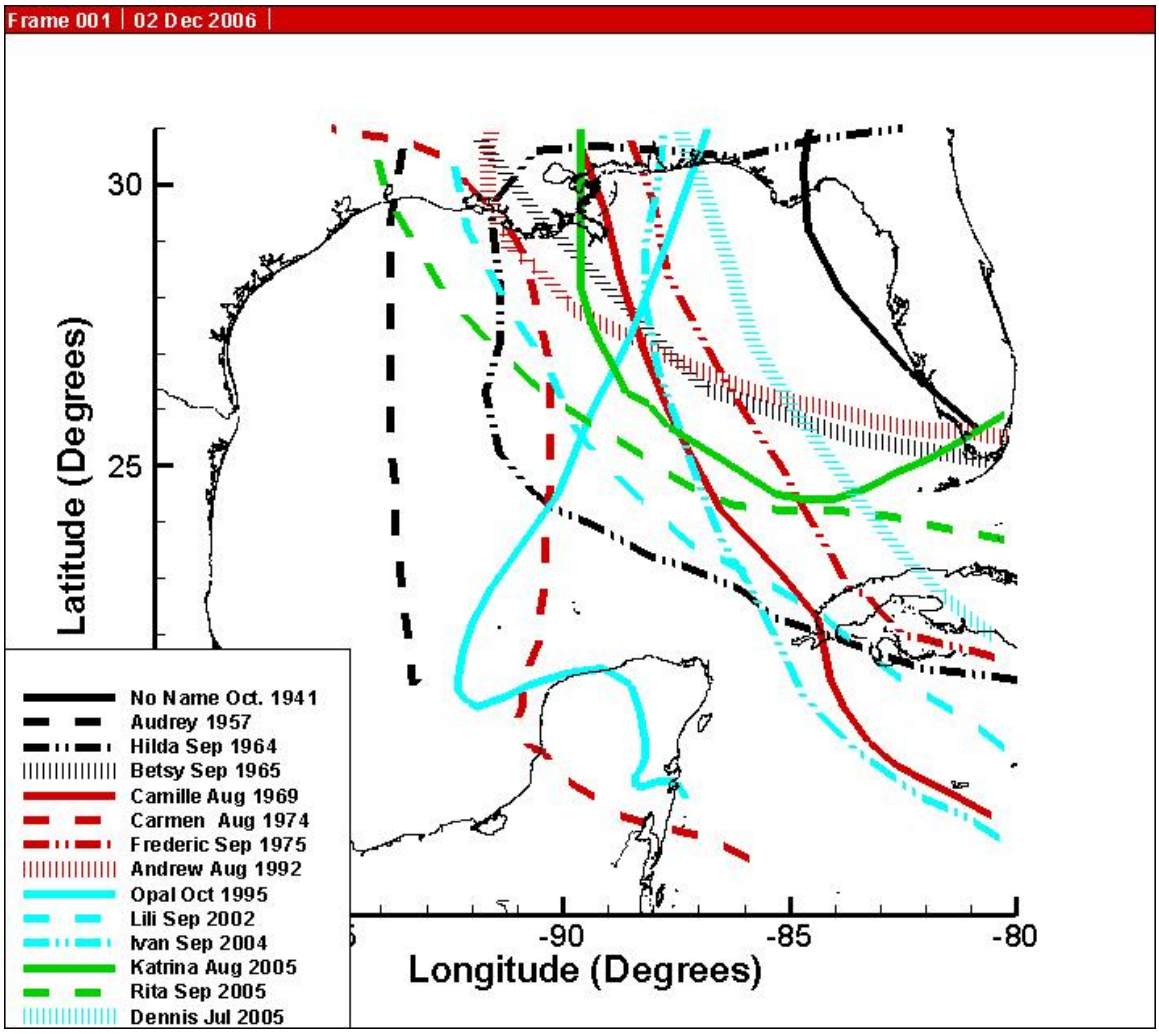

Figure 411: Tracks of all hurricanes (1941-2005) making landfall in the central Gulf of Mexico for storms that attained a central pressure of 955 millibars or lower during its transit through the Gulf of Mexico.

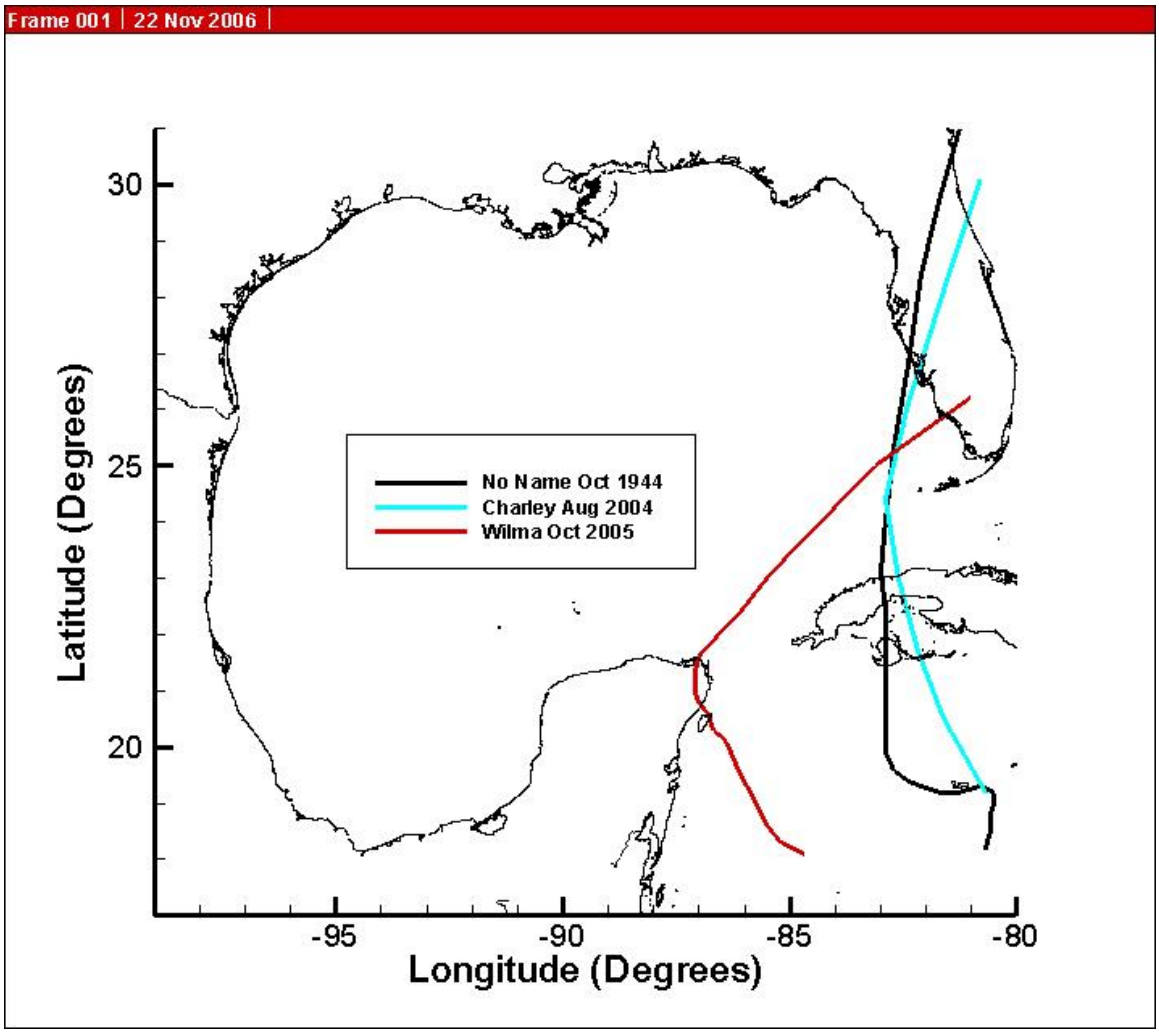

Figure 412: Tracks of all hurricanes (1941-2005) making landfall in the eastern Gulf of Mexico for storms that attained a central pressure of 955 millibars or lower during its transit through the Gulf of Mexico.

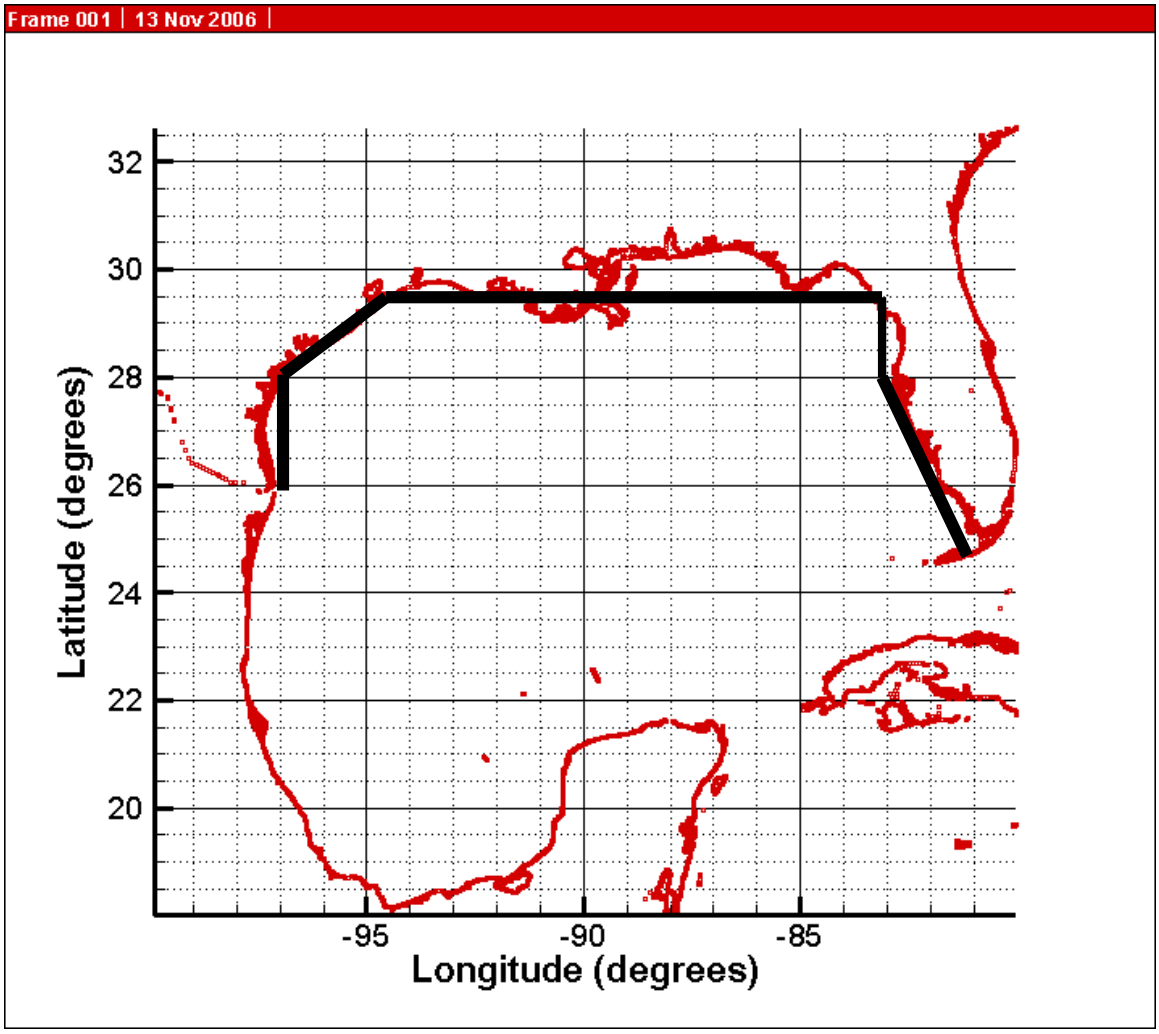

Figure 413: Location of line for analysis of hurricane landfalling characteristics. Throughout this white paper, one-degree increments of distance along this line from east to west, with the "zero-value" taken at -83 degrees longitude, will be used as a locator for discretized sections of coast. In this convention, the increment number for any section being analyzed is given by $N_{increment} = Integer(-83 - longitude)$. For example, any point with a longitude less or equal to -83 and greater than -84 would fall in increment 0, any point with a longitude less than or equal to -85 and greater than -85 would fall in increment 1, etc.

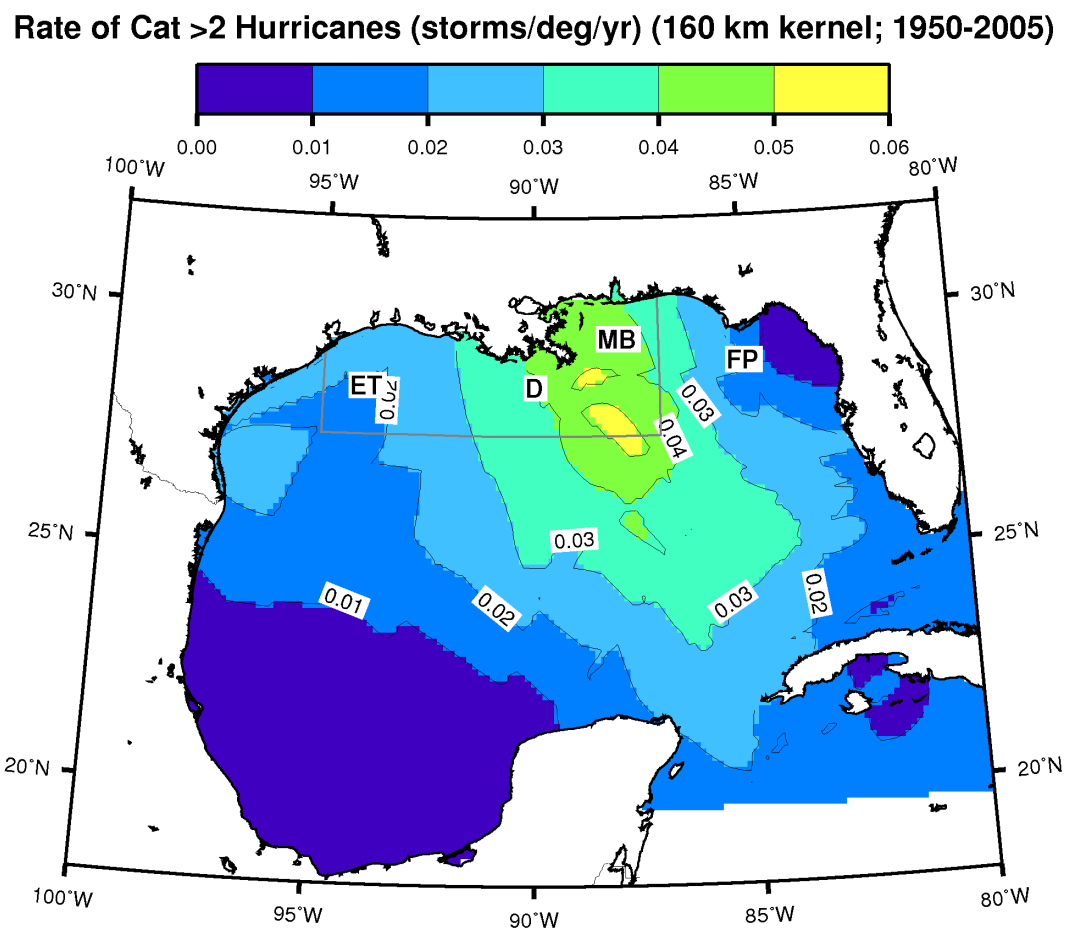

Figure 414: Analysis of hurricane frequency from Toro (Risk Engineering) from an analysis using an optimized spatial kernel.

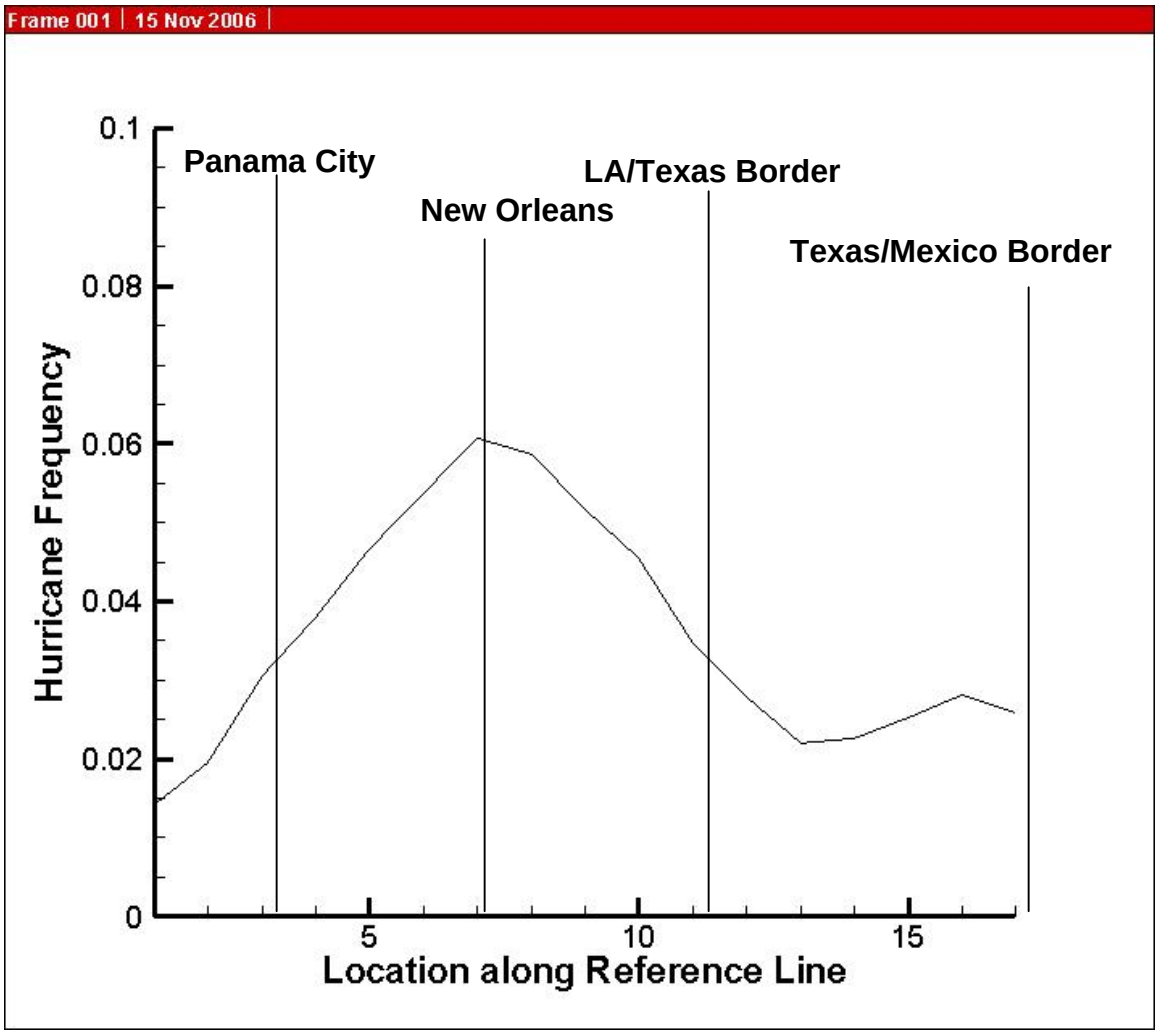

Figure 415: Frequency of hurricanes along reference line with annotated geographic locators, based on 22-storm sample. Location along this line can be taken as equivalent to 1-degree increments along the coast, with the New Orleans area falling within increment 7.

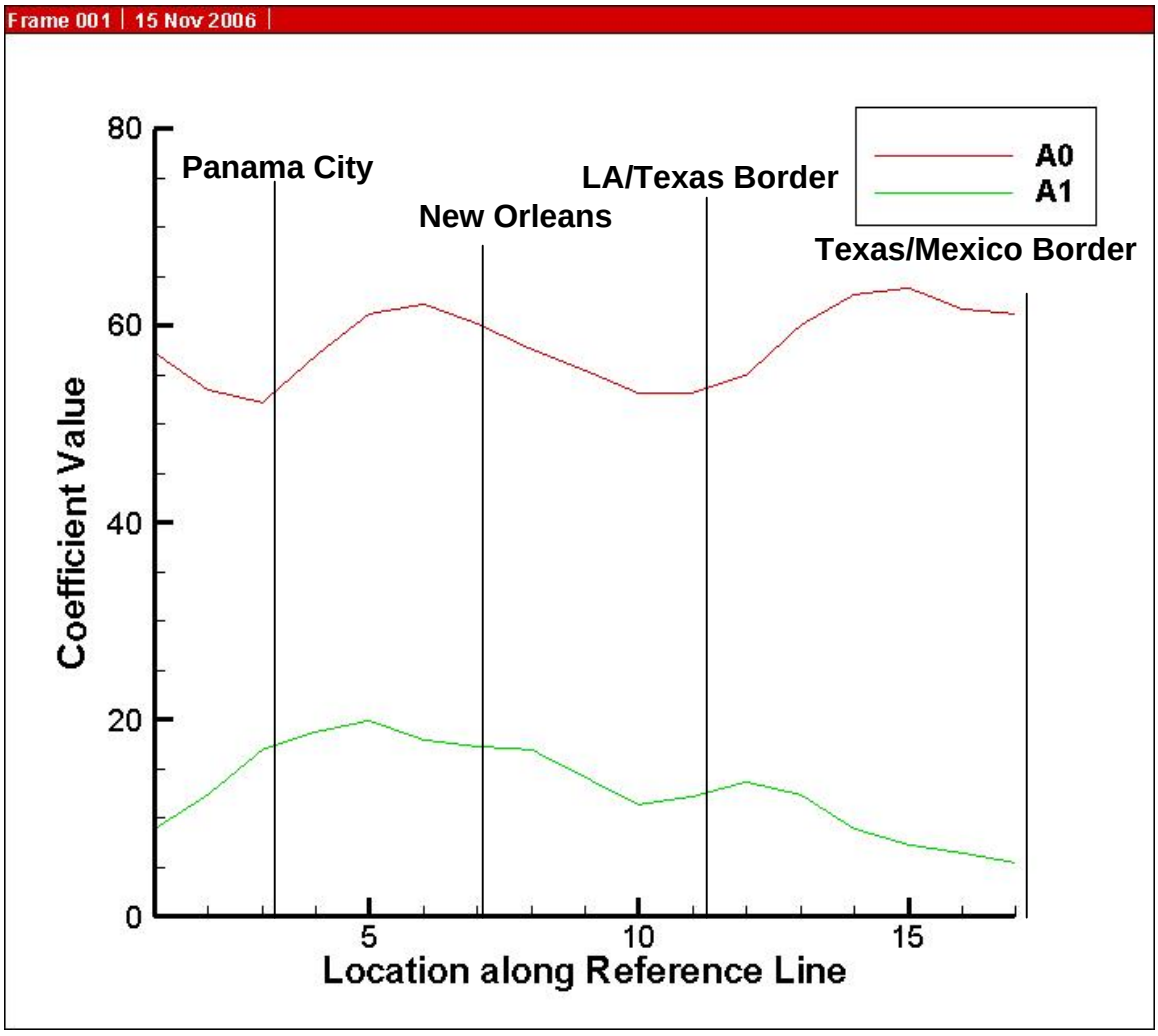

Figure 416: Gumbel coefficients for locations along reference line, based on 22-storm sample. For reference, the Gumbel equation is reproduced here in terms of its explicit dependence on x:

$$F(\Delta P \mid x) = \exp - \left\{ \exp - \left[\frac{\Delta P - a_0(x)}{a_1(x)} \right] \right\}$$

, where ΔP is the pressure differential (peripheral pressure minus central pressure). It should be recognized that the frequency is assumed to be equal to 1 in this equation. Location along this line can be taken as equivalent to 1-degree increments along the coast, with the New Orleans area falling within increment 7.

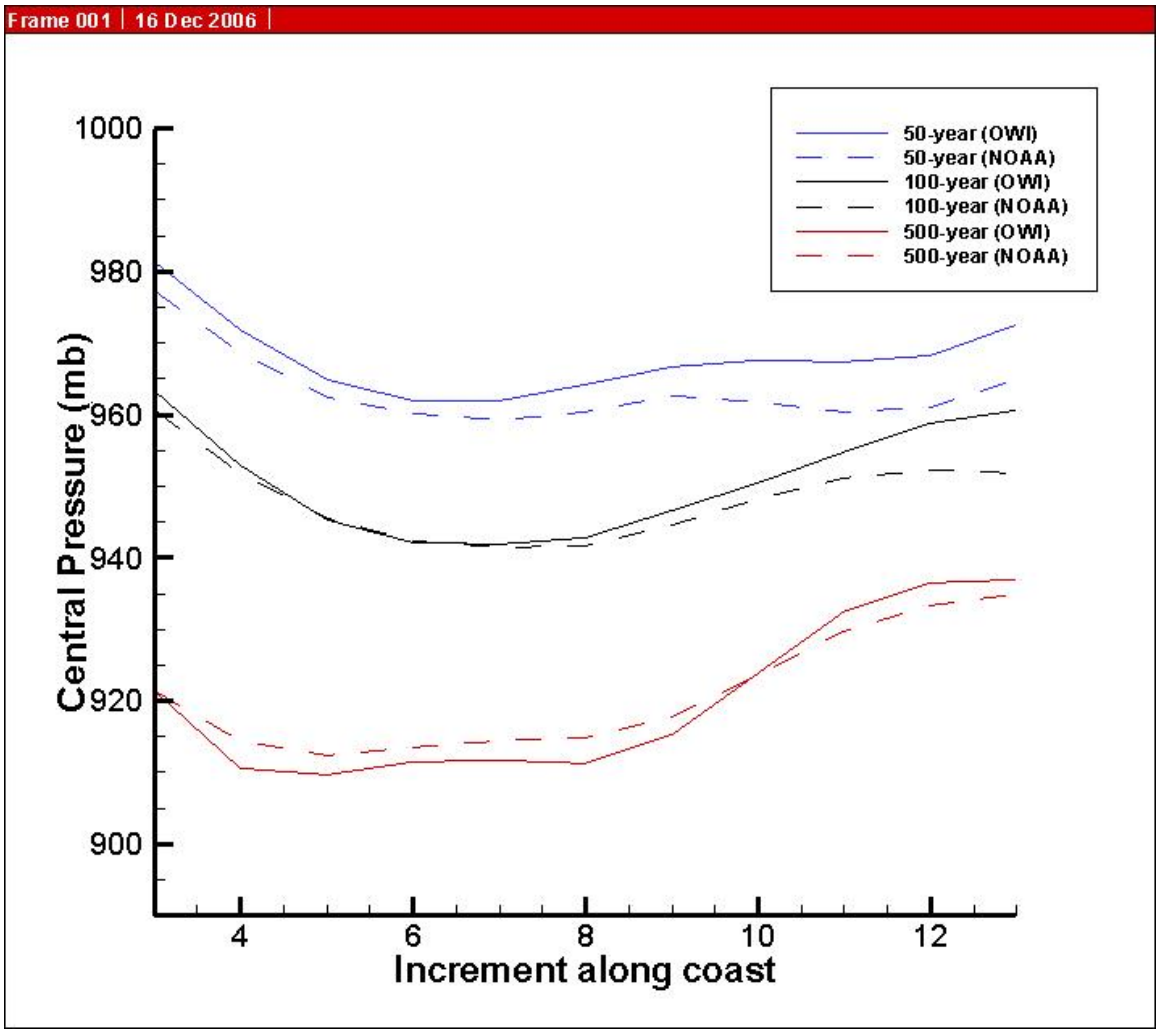

Figure 417: Distribution of 50-year, 100-year, and 500-year central pressures along the reference line shown on Figure 415, using both Oceanweather, Inc., data and official NOAA values. Location along this line can be taken as equivalent to 1-degree increments along the coast, with the New Orleans area falling within increment 7.

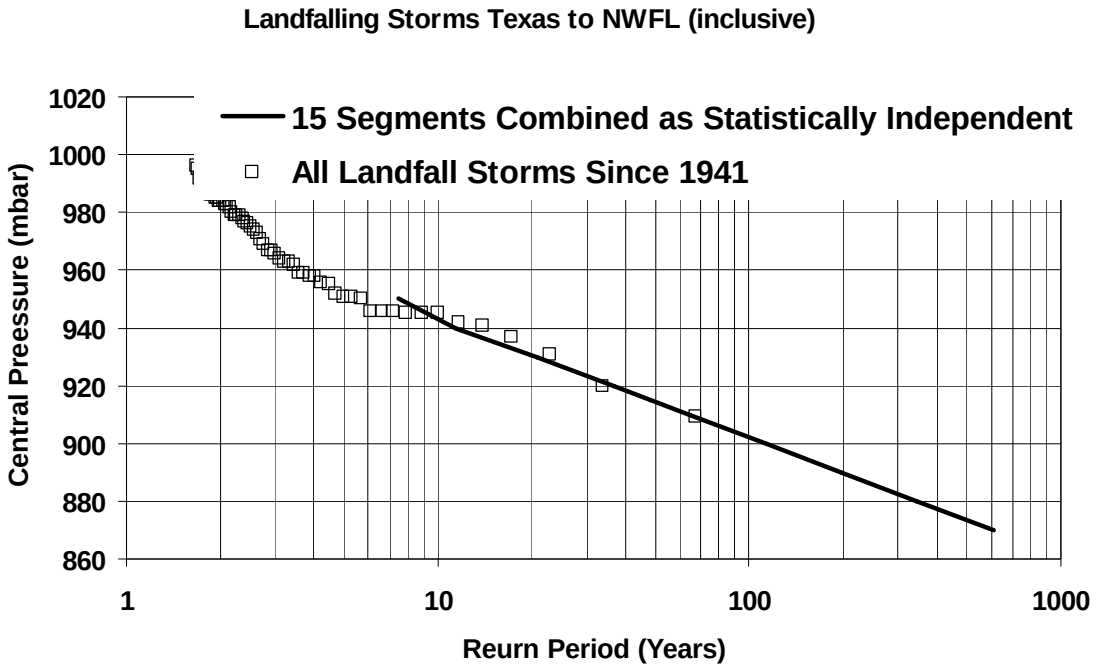

Figure 418: Comparison of Vickery's analysis of the combination of distributions for landfalling central pressures from all coastal segments (taken from the NOAA results shown on Figure 417) compared to the distribution of all (NOAA) landfalling central pressures within the Gulf of Mexico.

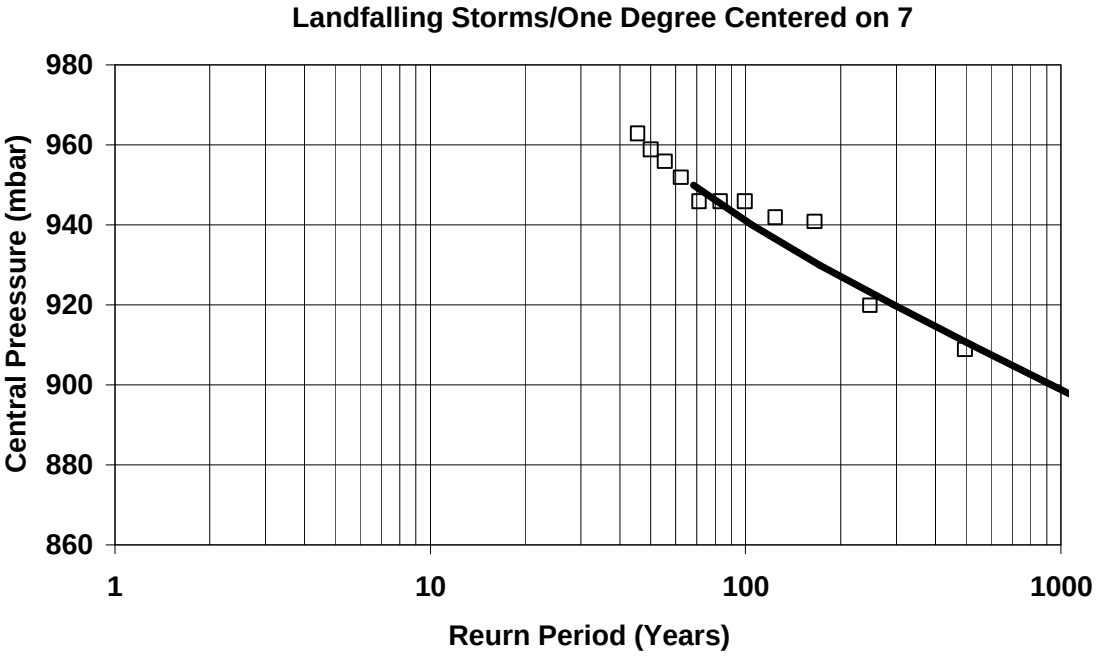

Figure 419: Same as Figure 418 except specific to the 1-degree increment centered on 7.

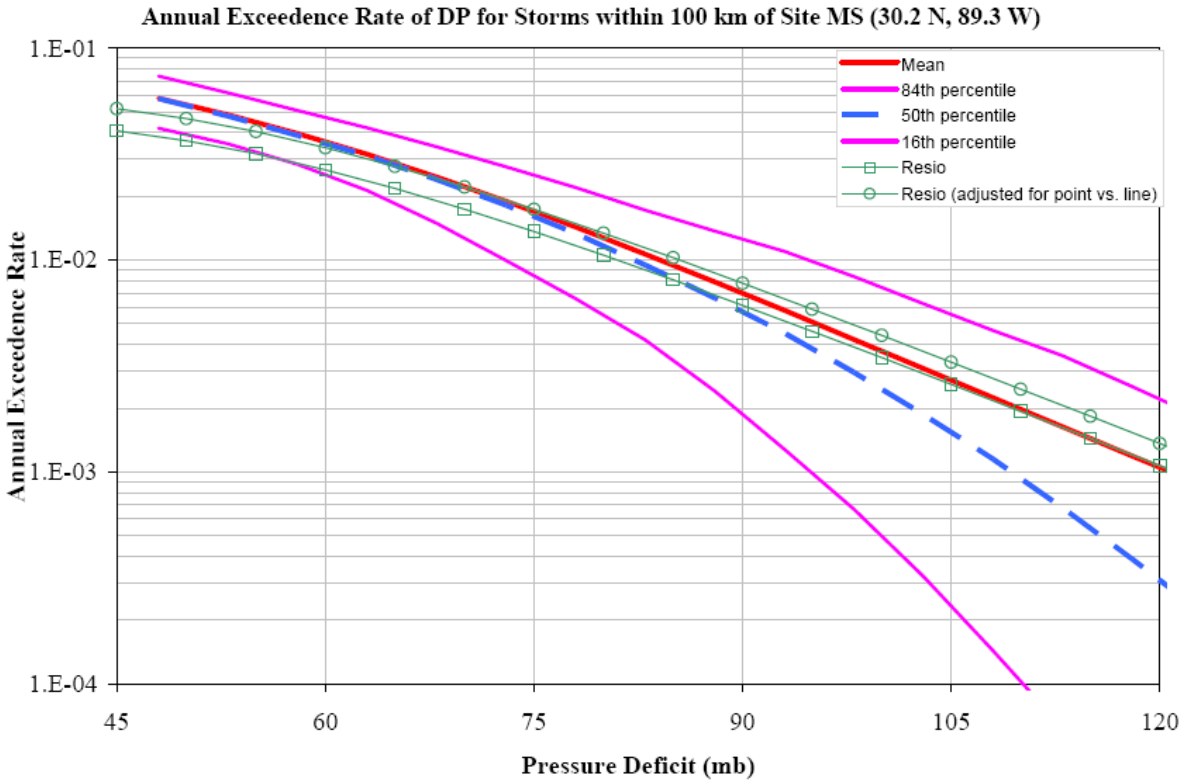

Figure 420: Independent estimate of storm probabilities in the Mississippi coastal area by Gabriel Toro (for FEMA Region 4) compared to estimate based on Gumbel segments developed in this white paper. As can be seen here the mean curve is in very good agreement with Toro's results.

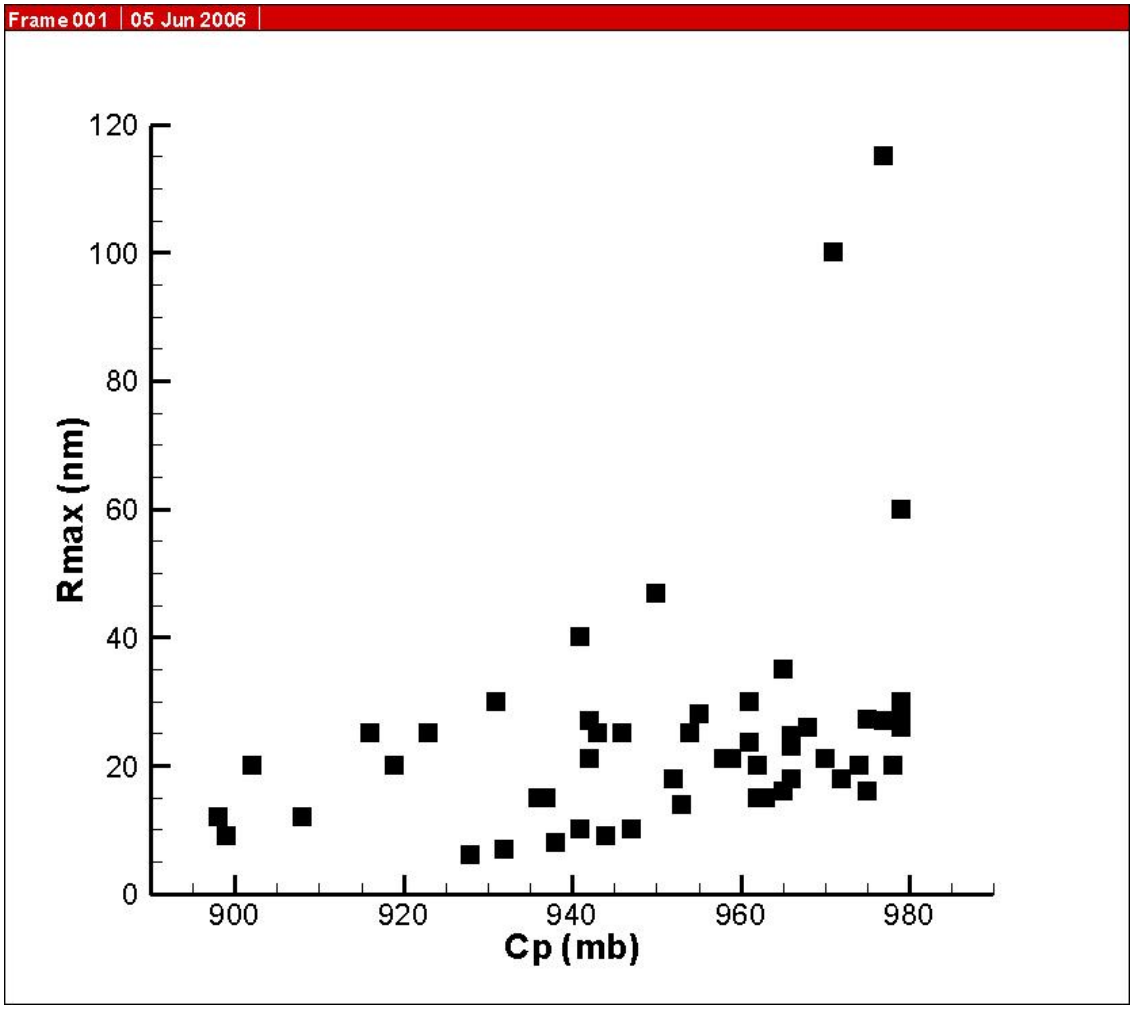

Figure 421: Relationship between size scaling parameter (Rp) versus Central Pressure for the 52-storm set in Gulf of Mexico (off coast; all storms > Cat 2).

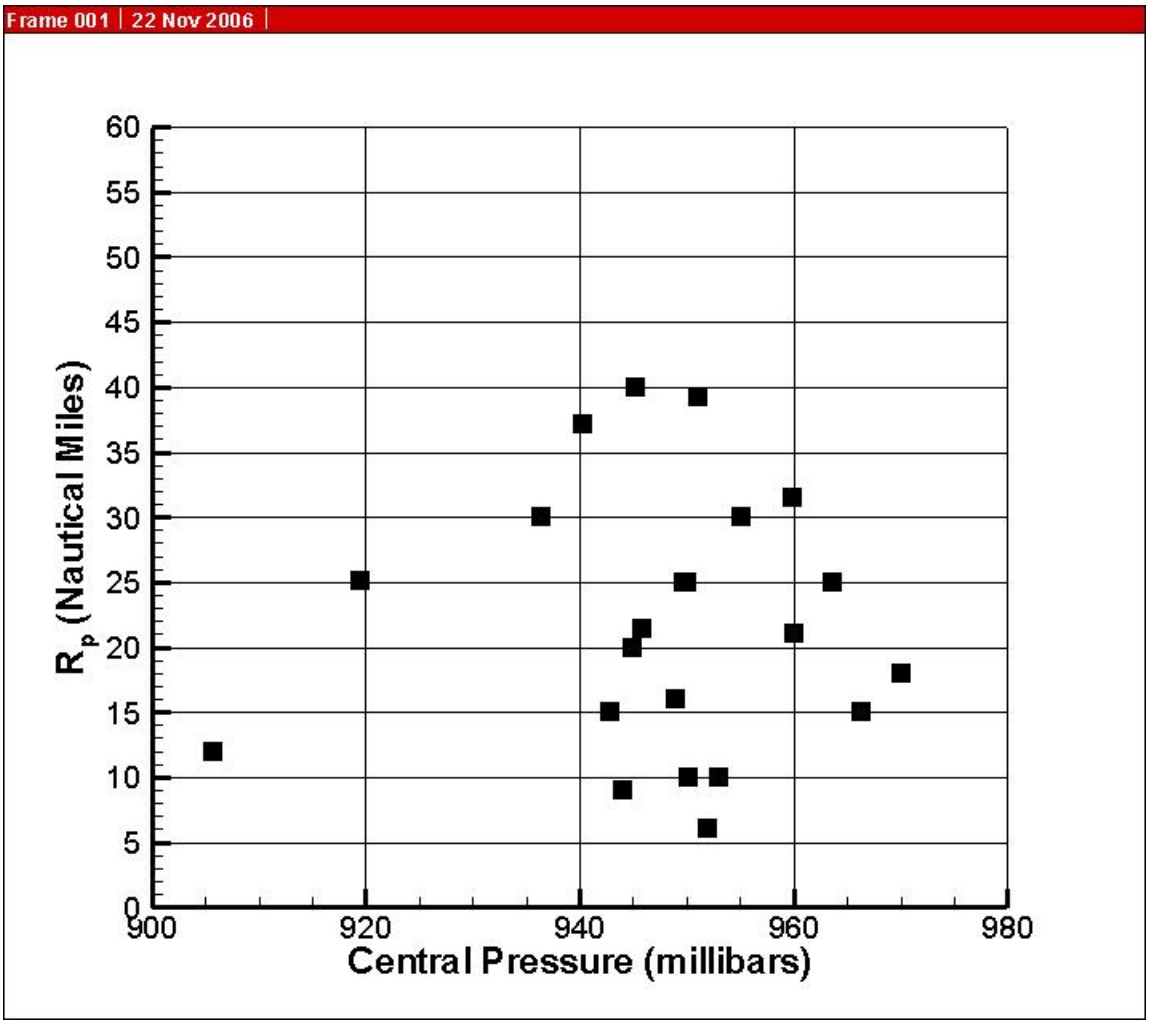

Figure 422: Relationship between size scaling parameter (Rp) at landfall versus Central Pressure for the 22-storm set in Gulf of Mexico (off coast; all storms with central pressure < 955 at time of minimum pressure in the Gulf of Mexico).

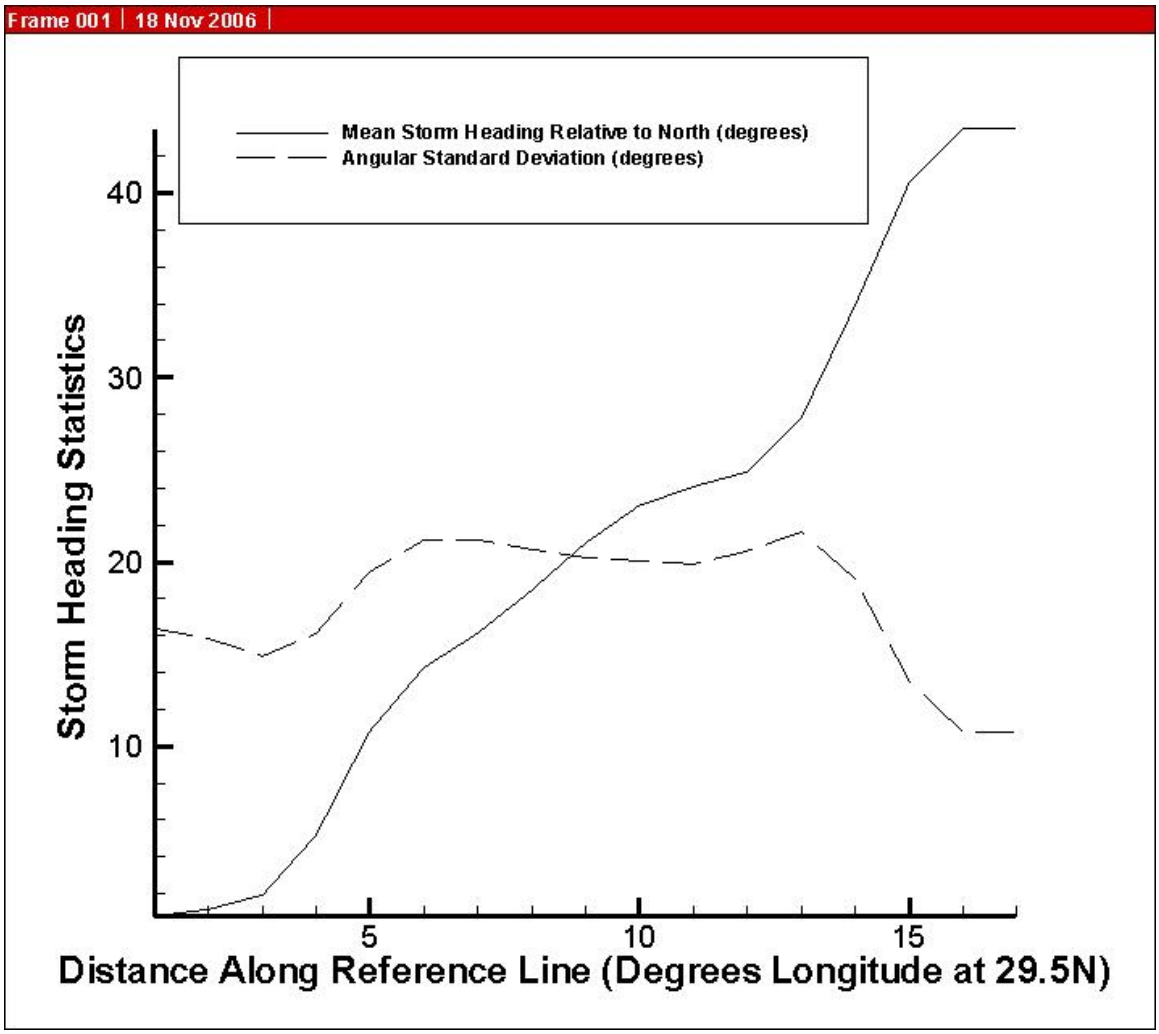

Figure 423: Plot of mean storm heading angle and standard deviation around this angle as a function of location along reference line. Distance along the x-axis can be taken as equivalent to 1-degree increments along the coast, with the New Orleans area falling within increment 7.

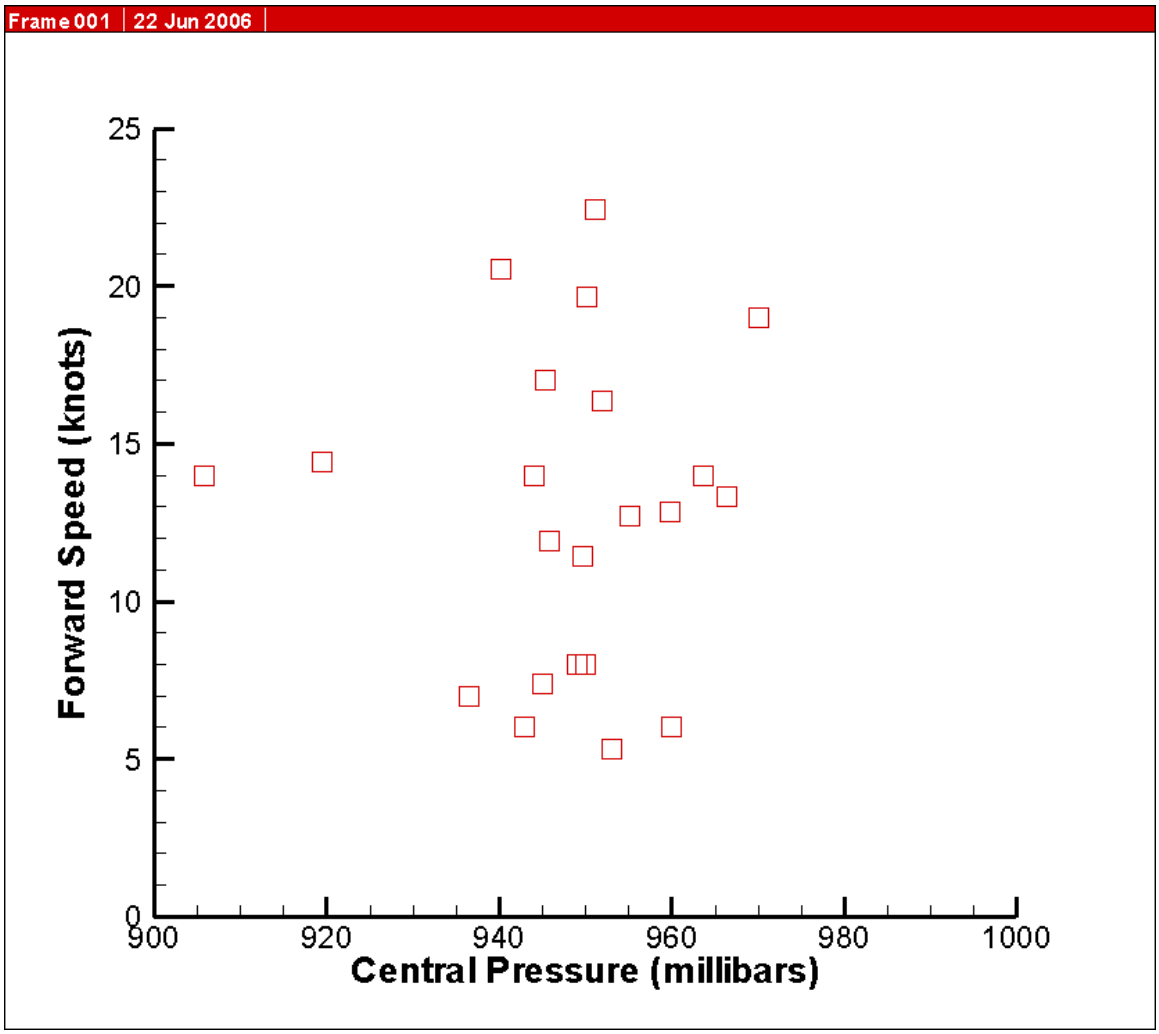

Figure 424: Plot of forward speed of storm at landfall versus central pressure at landfall.

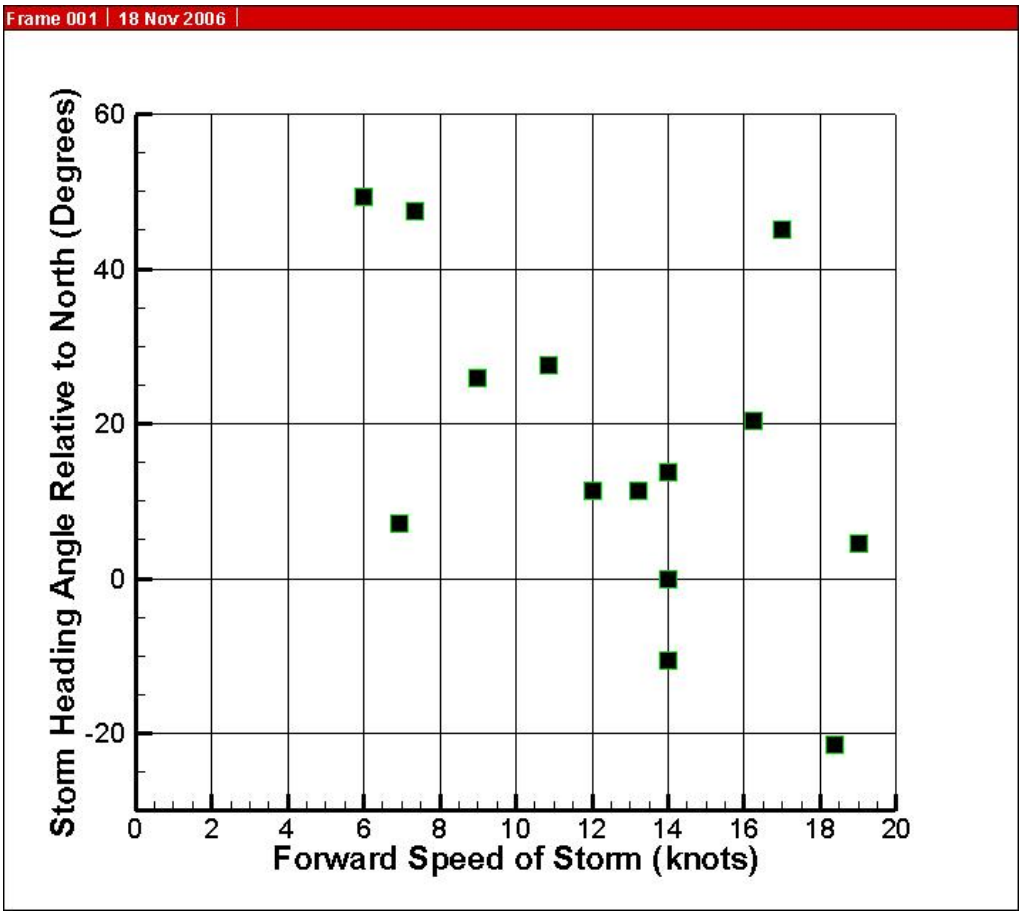

Figure 425: Plot of storm heading and forward speed at time of landfall for only central Gulf landfalling storms.

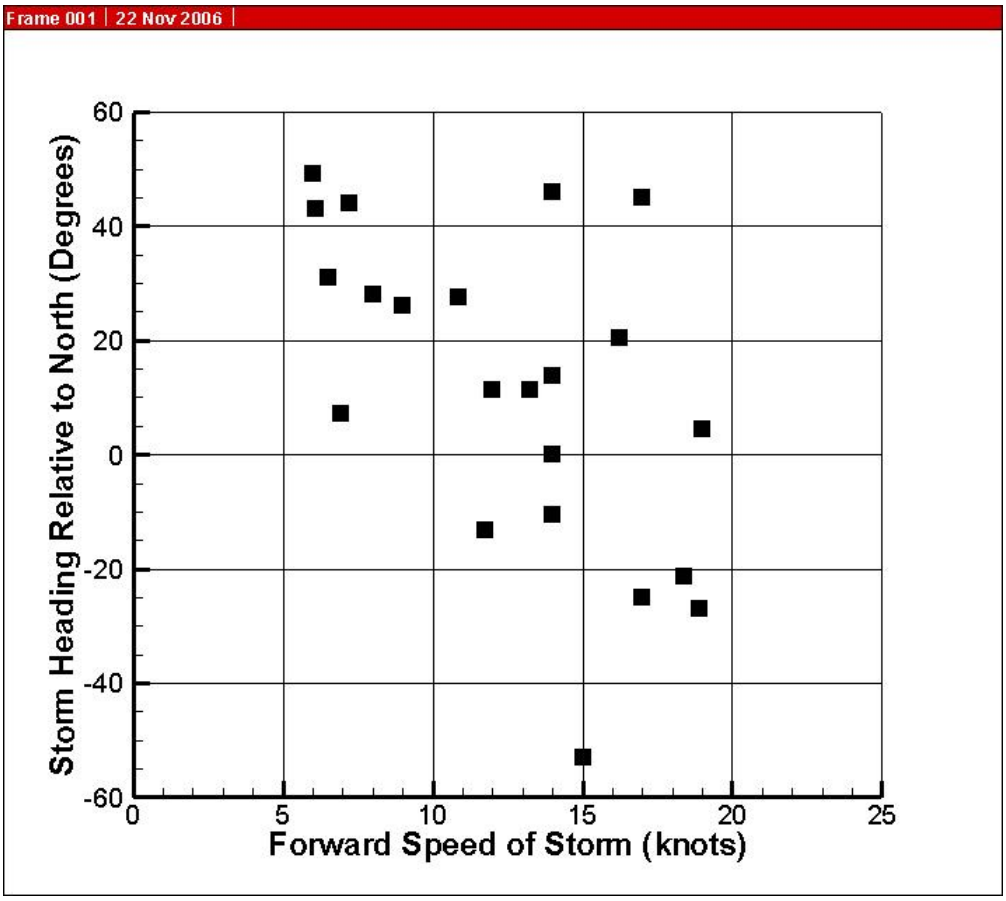

Figure 426: Plot of storm heading and forward speed at time of landfall for the entire 22-storm sample.

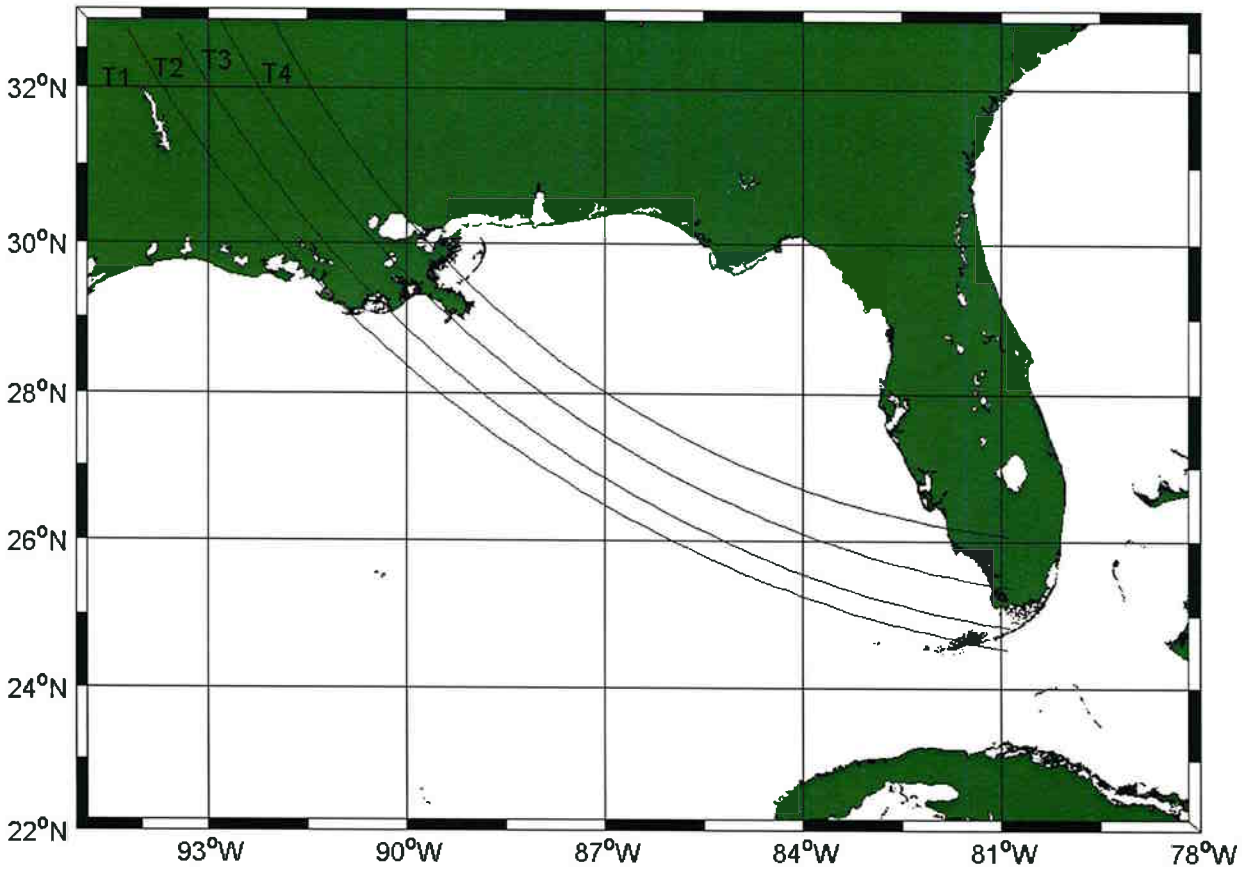

Figure 427: Tracks from southeast at 45-degree angle to RICK-fan set.

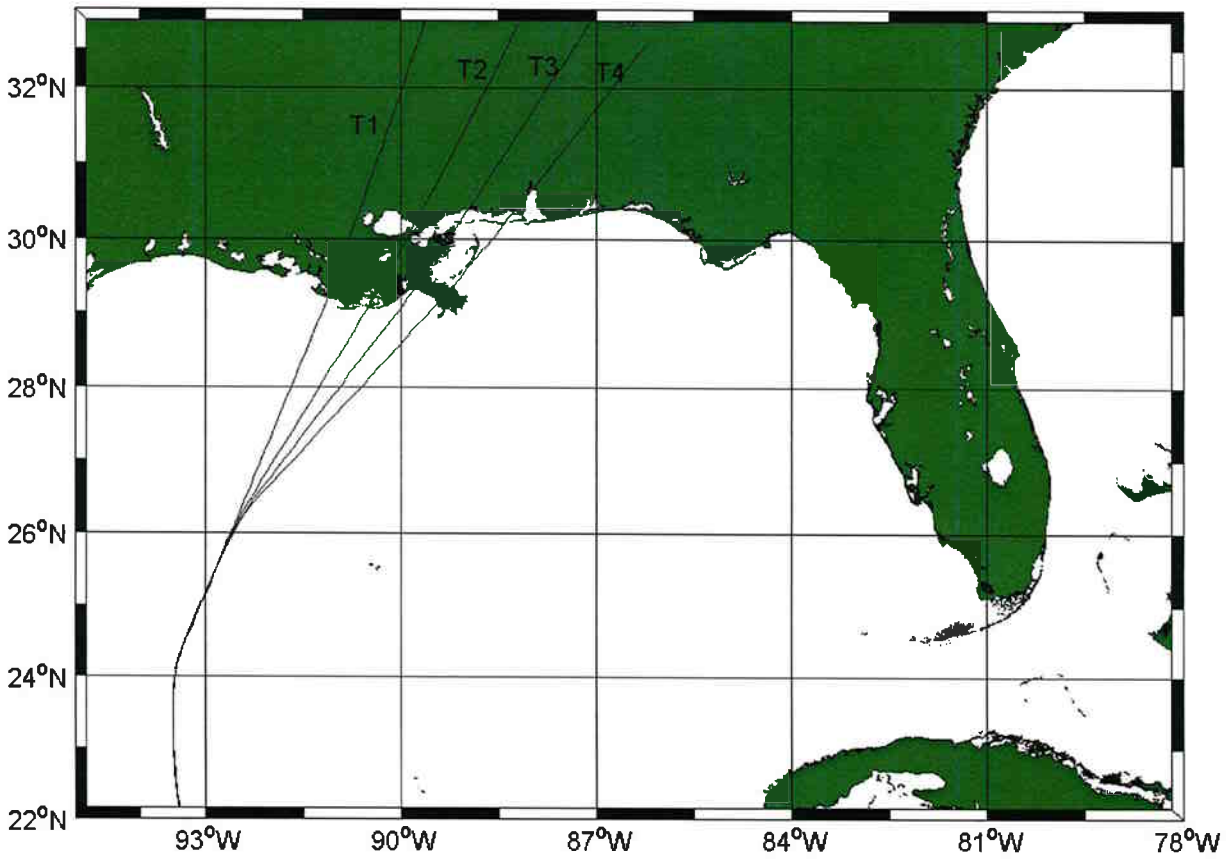

Figure 428: Tracks from southwest at 45-degree angle to RICK-fan set.

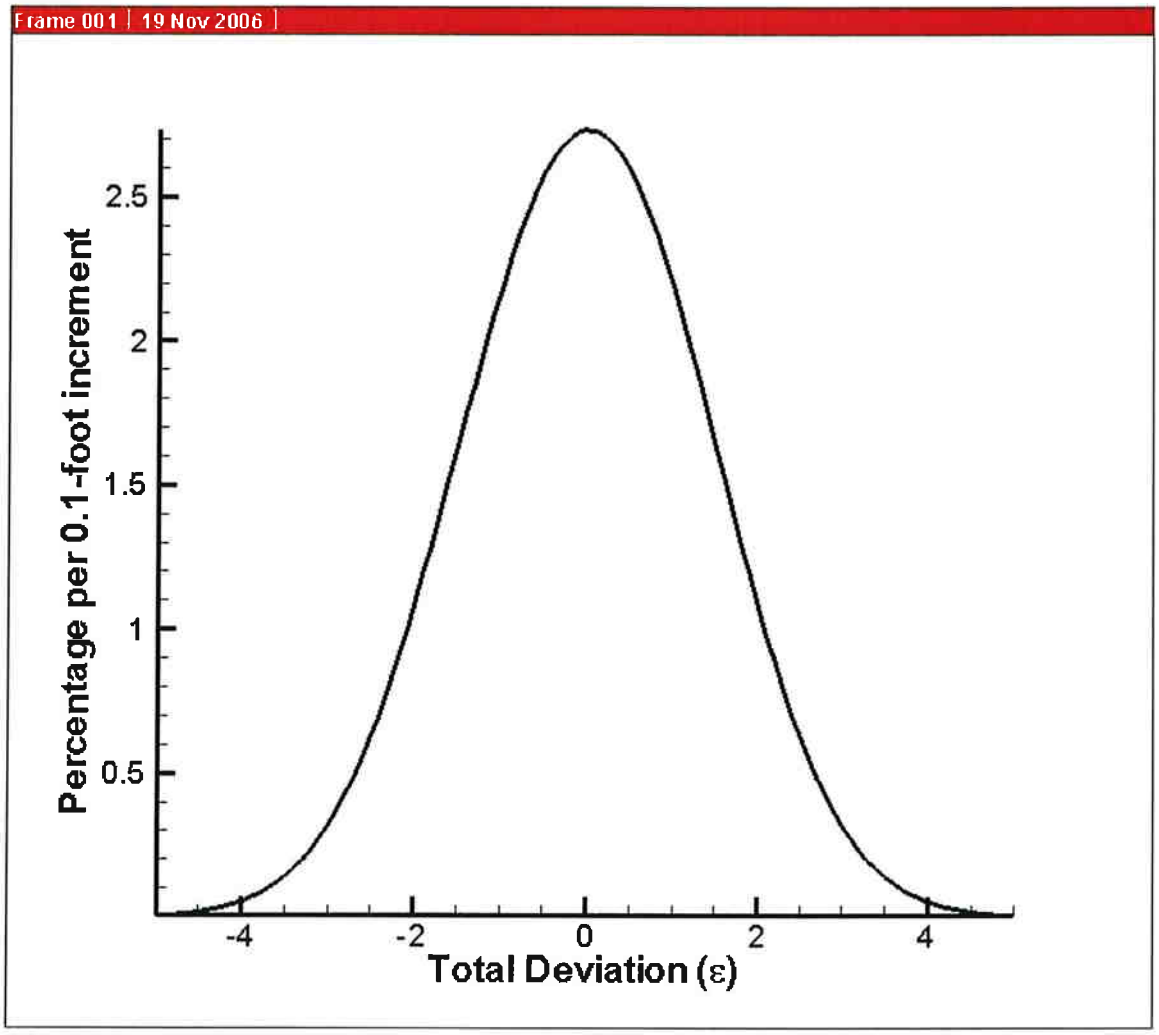

Figure 429: Percentage of deviations per 0.1-foot class as a function of deviation in feet.

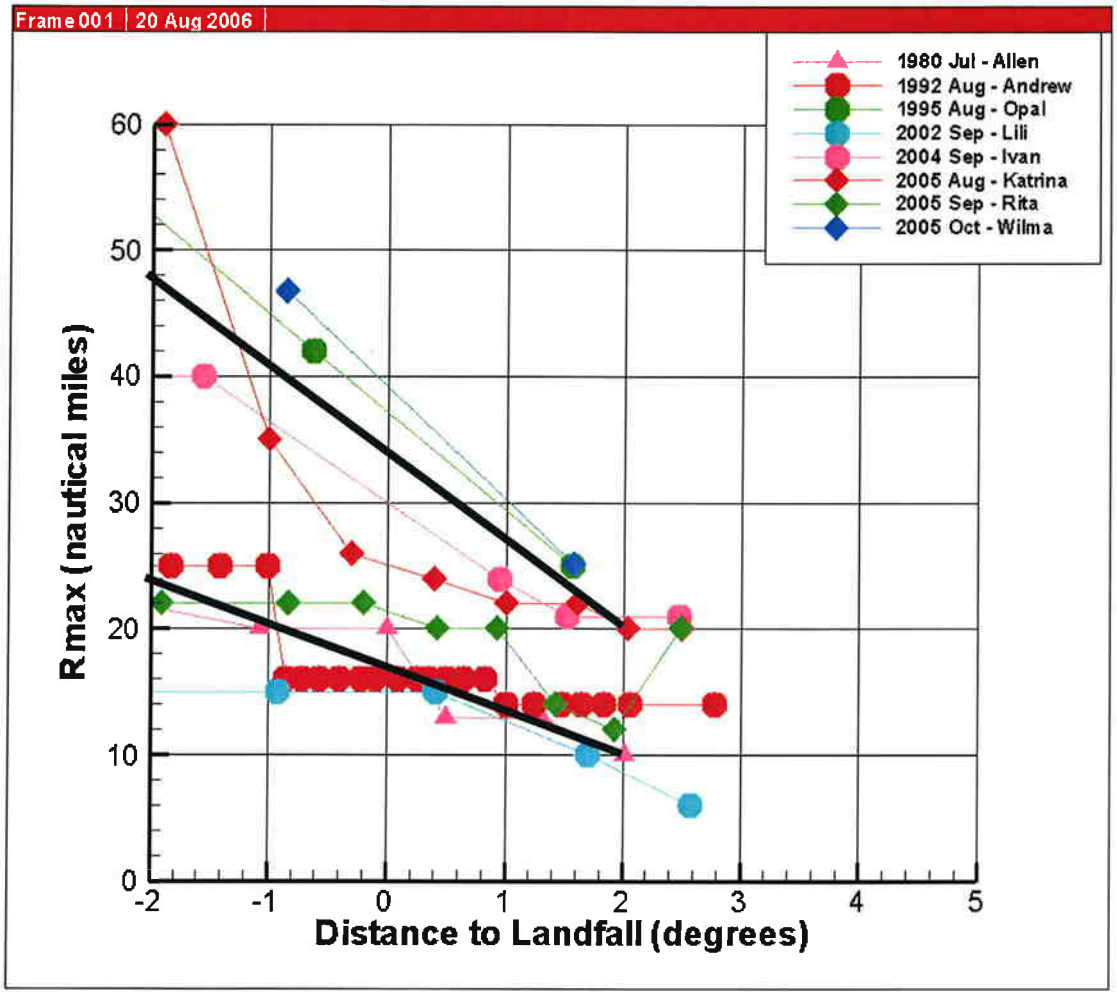

Figure 430: Increase in hurricane size during approach to coast, as seen in recent, well-documented storms.

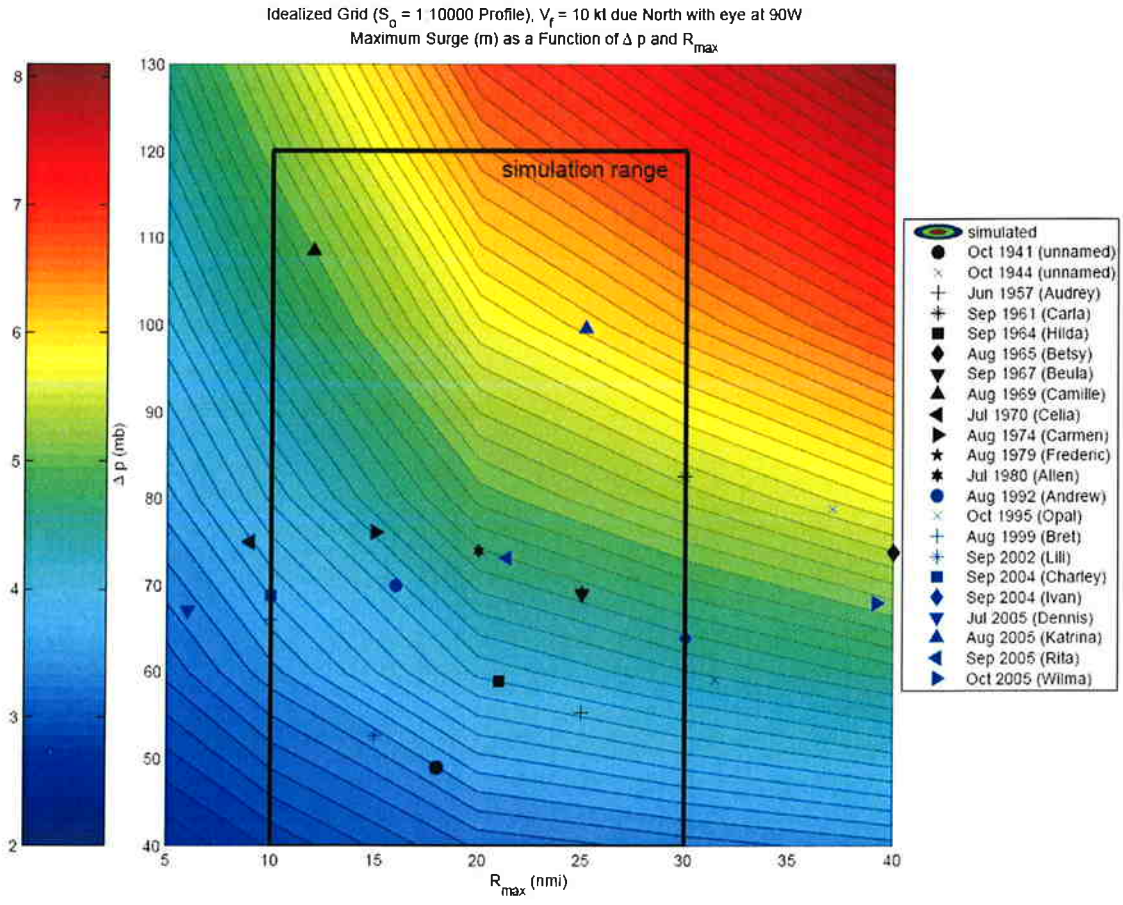

Figure 431: Contour plot of peak surge levels along a straight coast with a constant offshore slope as a function of storm size ($R_{\max} = R_p$ in our terminology) and storm intensity (peripheral pressure minus central pressure). The storm values used in this plot are the offshore conditions, rather than the conditions at the coast.

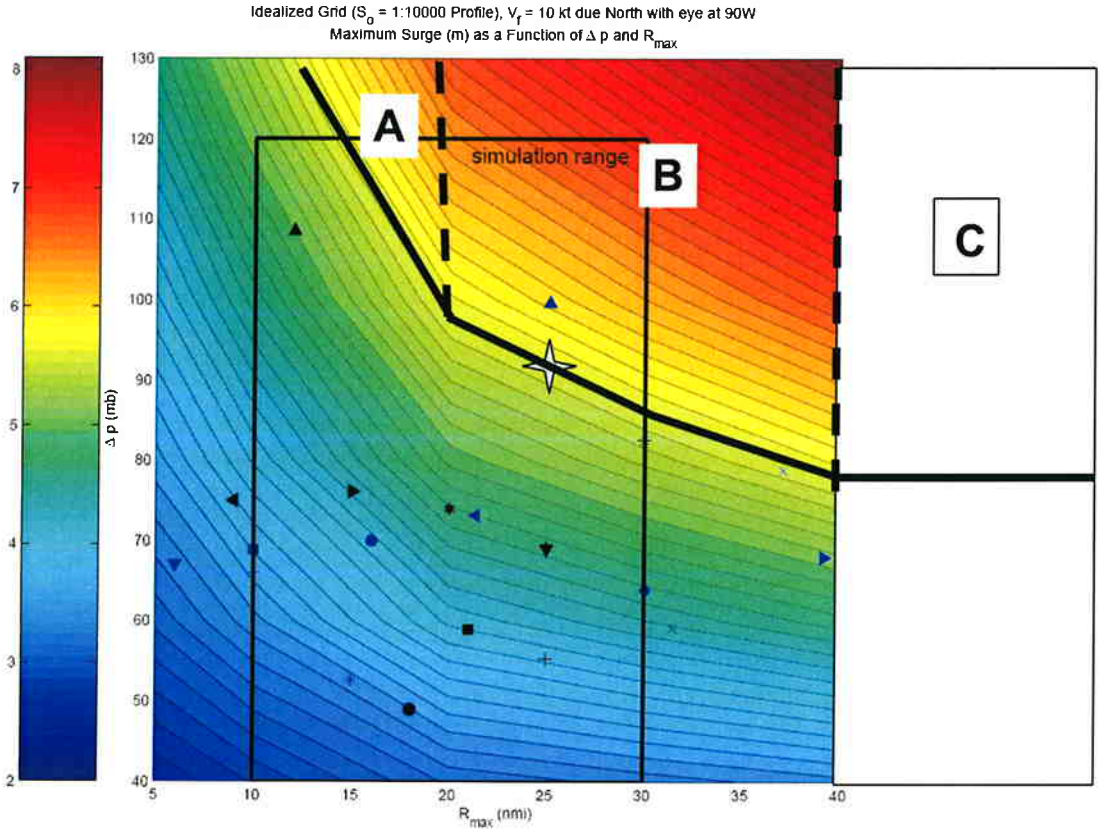

Figure 432: Regions of size-intensity domain expected to contribute to surges greater than or equal to that of Hurricane Katrina. The Blue "star" represents Katrina's characteristics at time of landfall, with a somewhat lower intensity than shown on Figure 431.

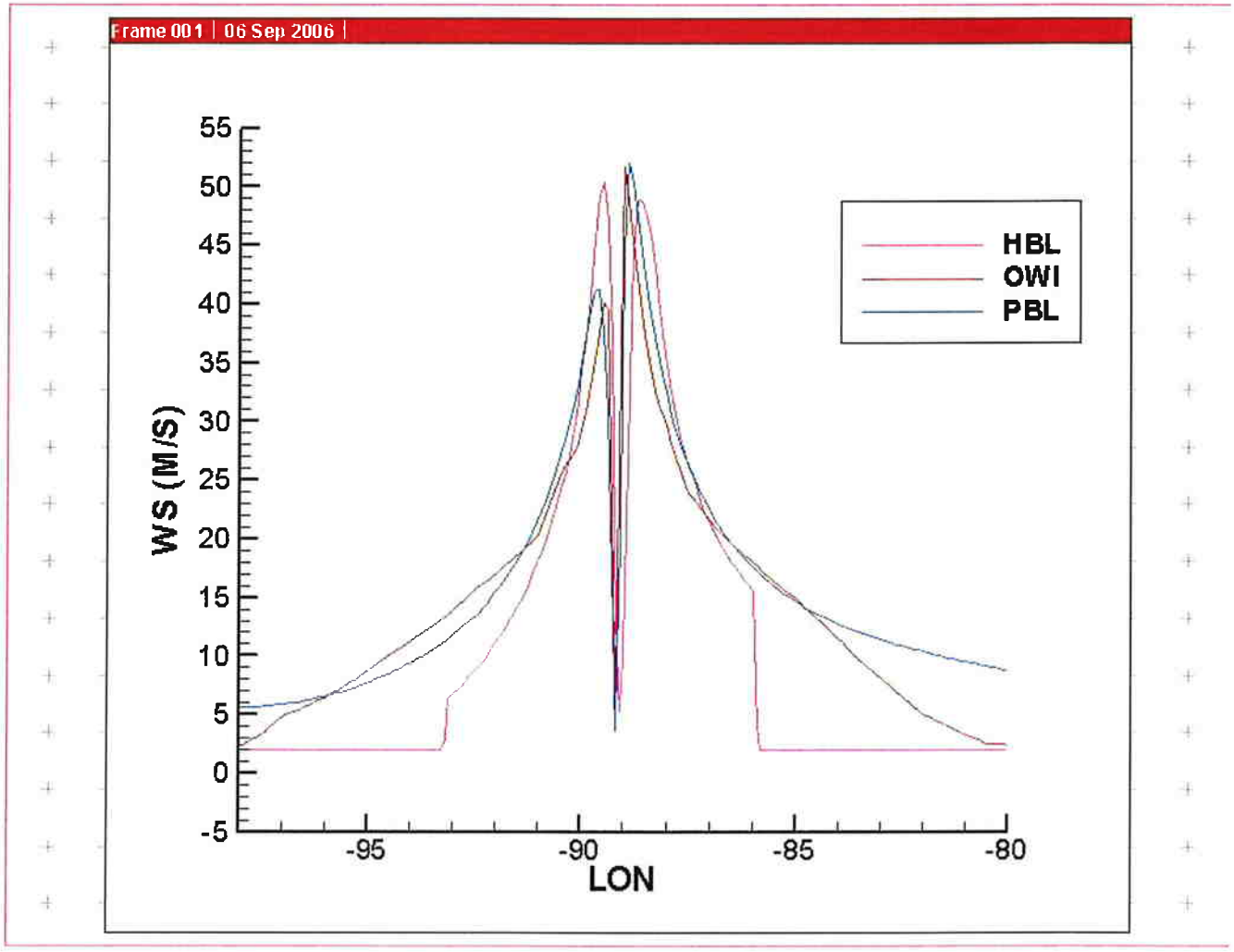

Figure 433: Plot of wind speeds (in meters per second) along east-west transects through Hurricane Katrina. HBL denotes wind speeds from the Vickery et al. (2000) hurricane boundary layer model. PBL denotes wind speeds from the Thompson and Cardone (1996) planetary boundary layer (PBL) model; and OWI denotes wind speeds from the "best-available" wind speeds from analysts at Oceanweather, Inc., which include the HWIND inputs from Mark Powell in NOAA's Hurricane Research Division.

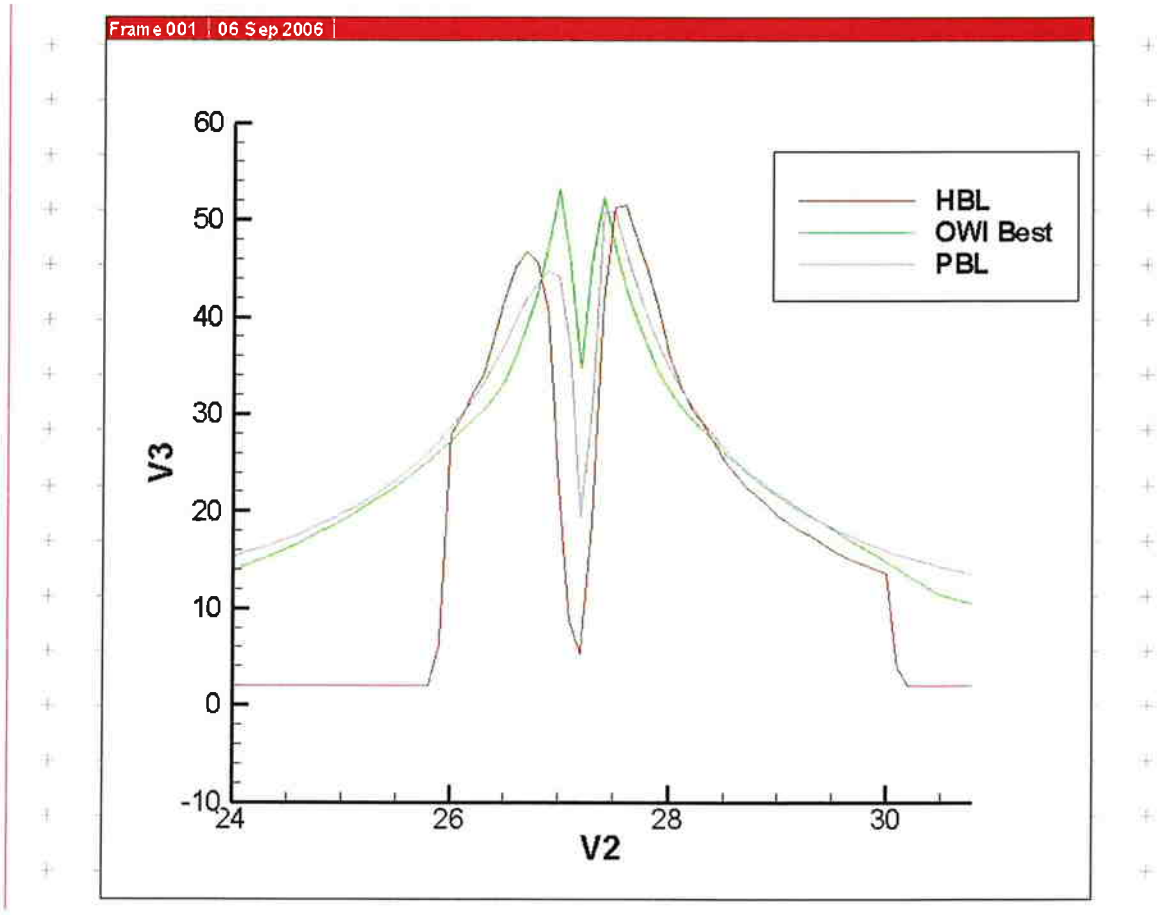

Figure 434: Plot of wind speeds (in meters per second) along north-south transects through Hurricane Katrina. HBL denotes wind speeds from the Vickery et al. (2000) hurricane boundary layer model. PBL denotes wind speeds from the Thompson and Cardone (1996) planetary boundary layer (PBL) model; and OWI denotes wind speeds from the "best-available" wind speeds from analysts at Oceanweather, Inc., which include the HWIND inputs from Mark Powell in NOAA's Hurricane Research Division.

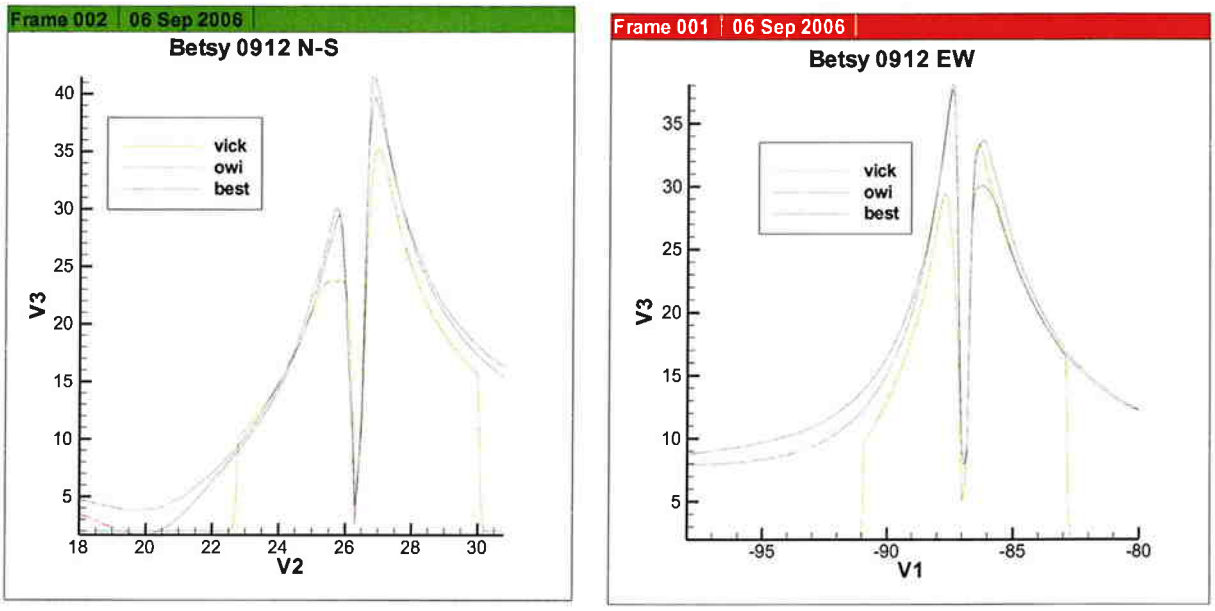

Figure 435: Plot of wind speeds (in meters per second) along north-south (N-S) and east-west (E-W) transects through Hurricane Betsy. Vick denotes wind speeds from the Vickery et al. (2000) hurricane boundary layer model. OWI denotes wind speeds from the Thompson and Cardone (1996) planetary boundary layer (PBL) model; and "best-available" denotes wind speeds from the "best-available" wind speeds from analysts at Oceanweather, Inc.

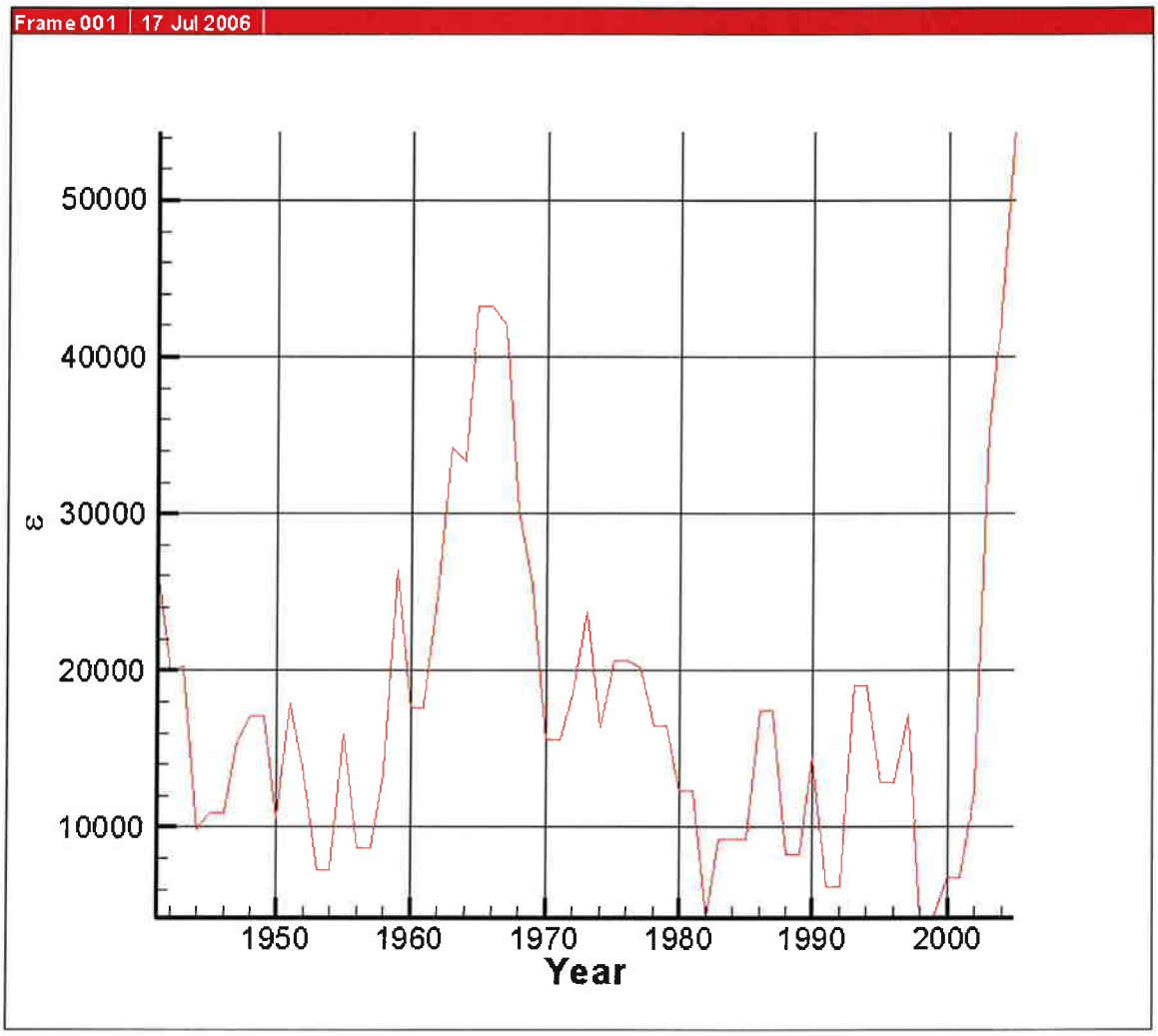

Figure 436: Plot of estimated cumulative kinetic energy for all storms at time of maximum surface winds within each year: 1941-2005. The units of ε are l^4/t^2 because we have factored out the mass term (consistent with equation C1). Note: ε is termed E_k in Section 4.4.

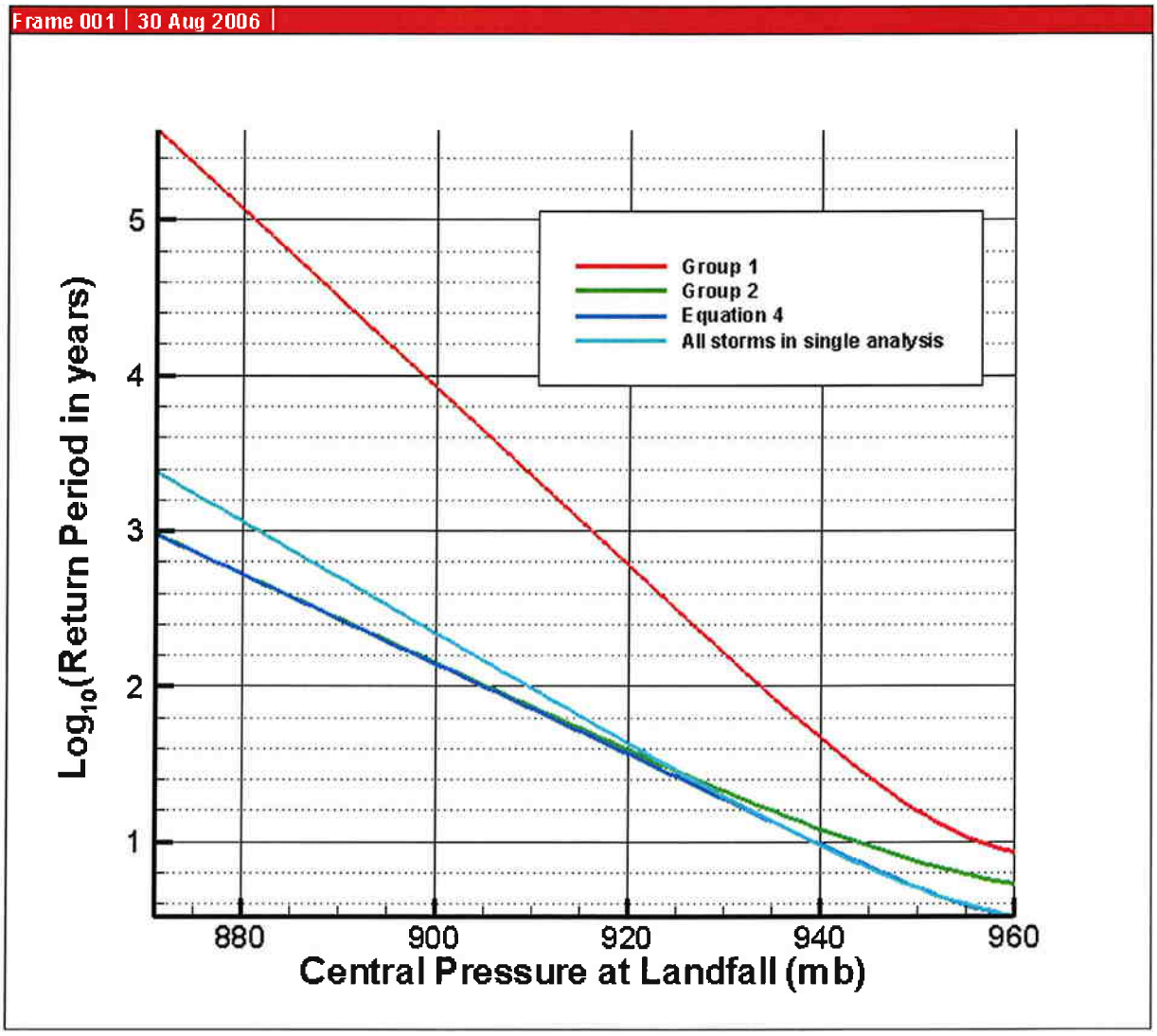

Figure 437: Estimated return periods for 4 separate analyses: Low-Activity years only (Group 1 – red line); High-Activity Years only (Group 2 – green line); All years into a single analysis (light blue line); and estimate based on combined analysis of two populations (Equation 4 from Resio and Orelup - dark blue line).

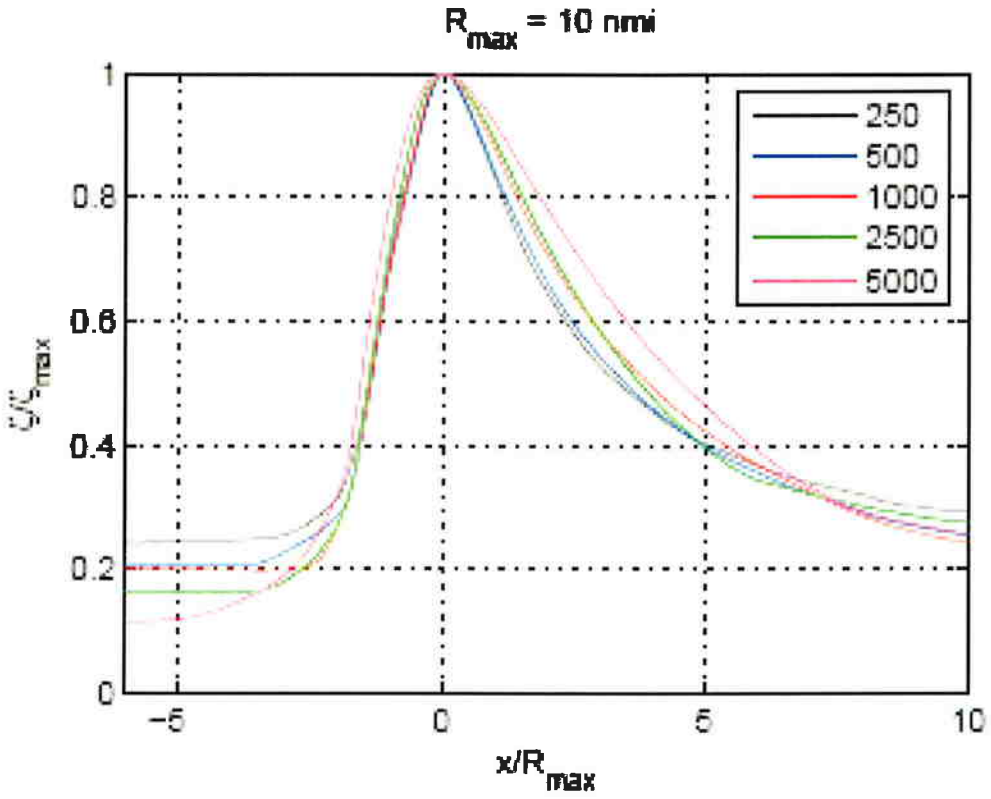

Figure 438: Distribution of normalized maximum surges along the coast (local surge maximum (ζ) divided by the maximum surge within the entire storm (ζ_{max}) versus normalized distance along the coast (distance from storm peak divided by radius scaling parameter, R_{max} ,for offshore slopes in the range of 1:250 to 1:5000. Results are from numerical simulations on an idealized, straight coast for hurricanes for relatively small storm:

R_{max}(= R_p scaling radius in Cardone PBL model)=10nm

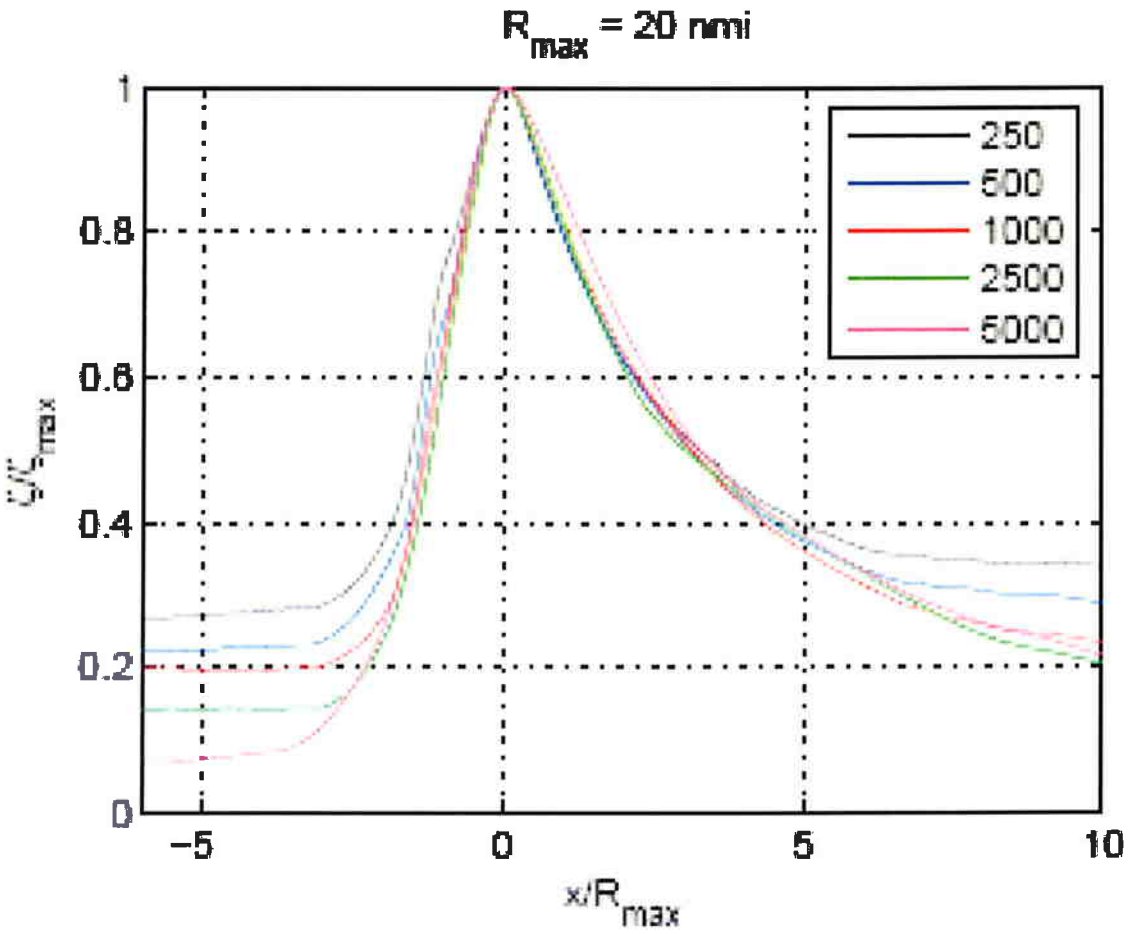

Figure 439: Distribution of normalized maximum surges along the coast (local surge maximum (ζ) divided by the maximum surge within the entire storm (ζ_{max}) versus normalized distance along the coast (distance from storm peak divided by radius scaling parameter, R_{max} ,for offshore slopes in the range of 1:250 to 1:5000. Results are from numerical simulations on an idealized, straight coast for hurricanes for relatively small storm:

$R_{max}(= R_p$ scaling radius in Cardone PBL model)=20nm

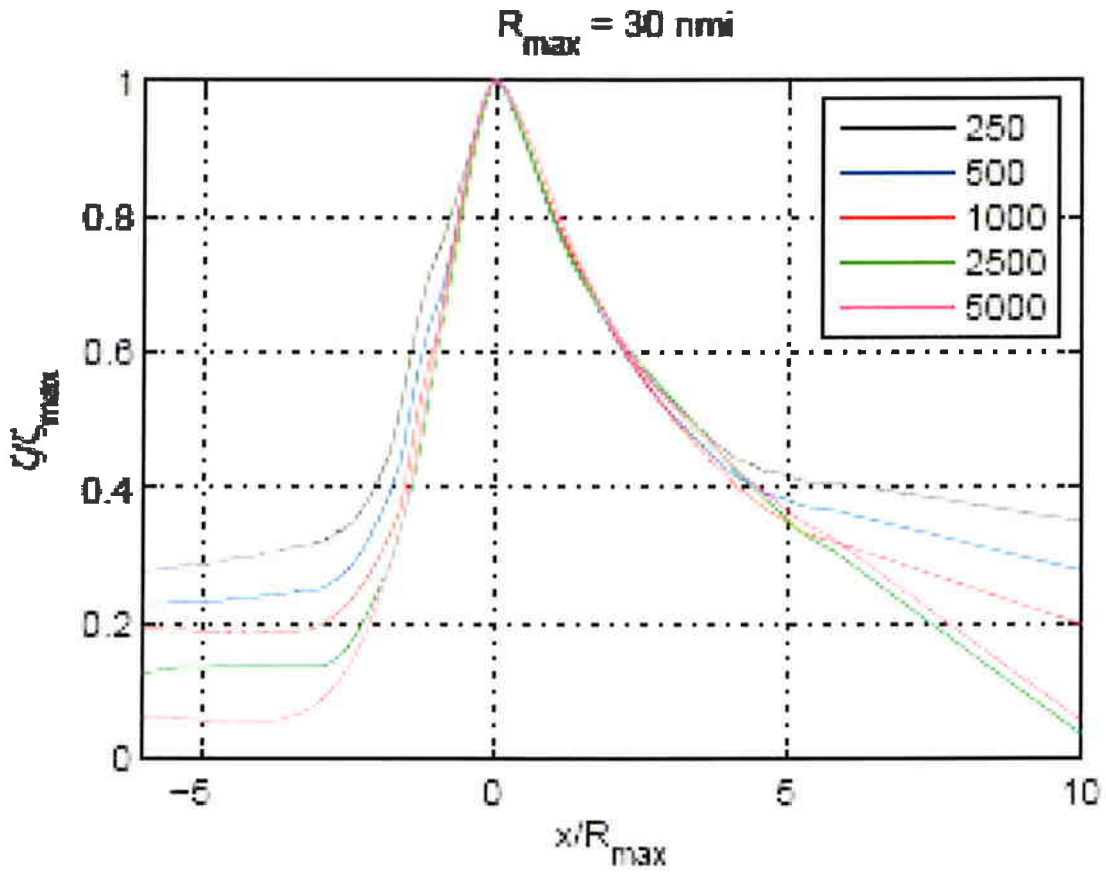

Figure 440: Distribution of normalized maximum surges along the coast (local surge maximum (ζ) divided by the maximum surge within the entire storm $(\zeta_{\max})$ versus normalized distance along the coast (distance from storm peak divided by radius scaling parameter, $R_{\max}$,for offshore slopes in the range of 1:250 to 1:5000. Results are from numerical simulations on an idealized, straight coast for hurricanes for relatively small storm:

R_{max}(= R_p scaling radius in Cardone PBL model)=30nm

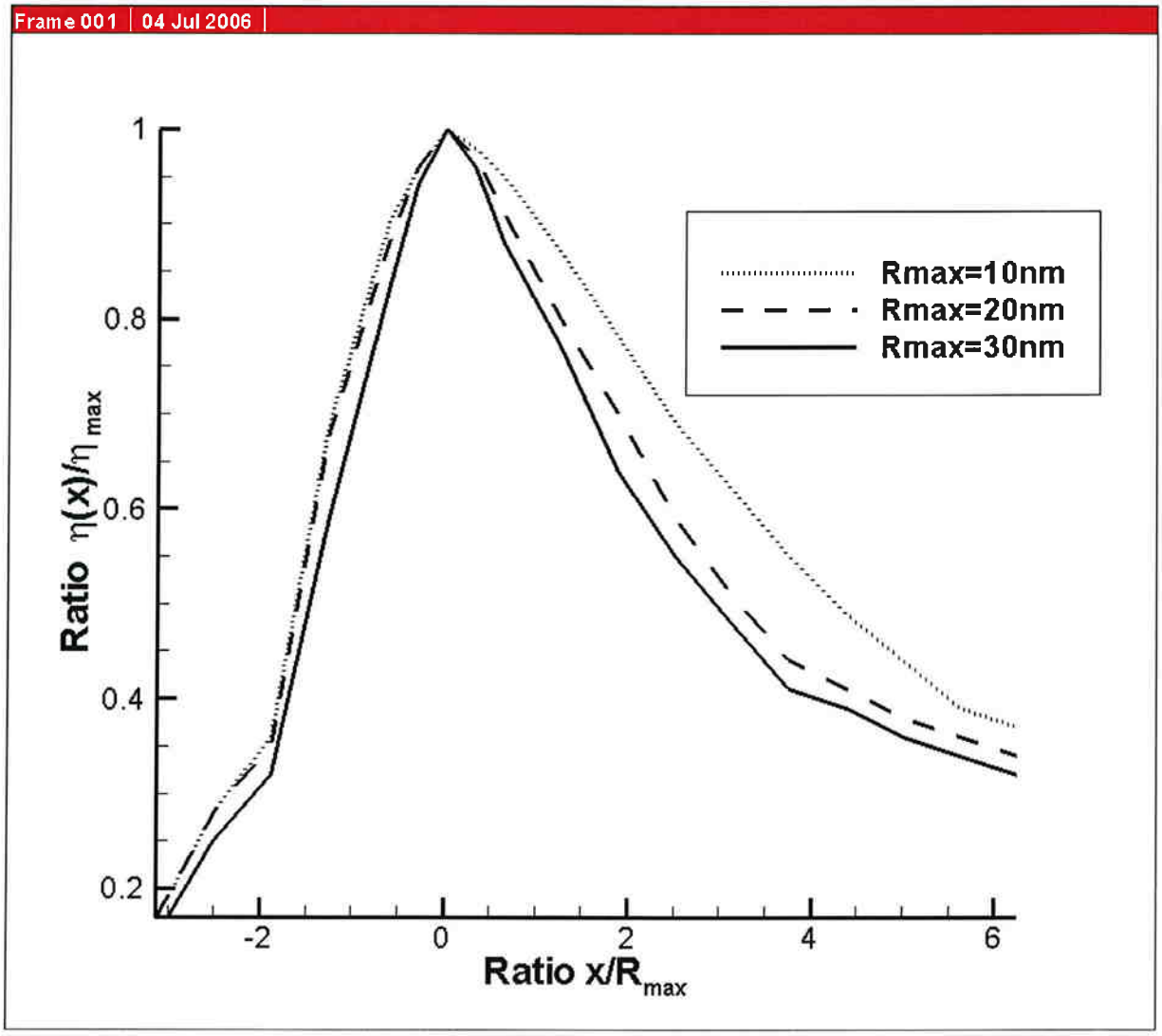

Figure 441: Distribution of normalized storm surge (local maximum ($[\eta(x)]$ divided by maximum over entire storm (η_{max})) as a function of normalized distance along the coast.

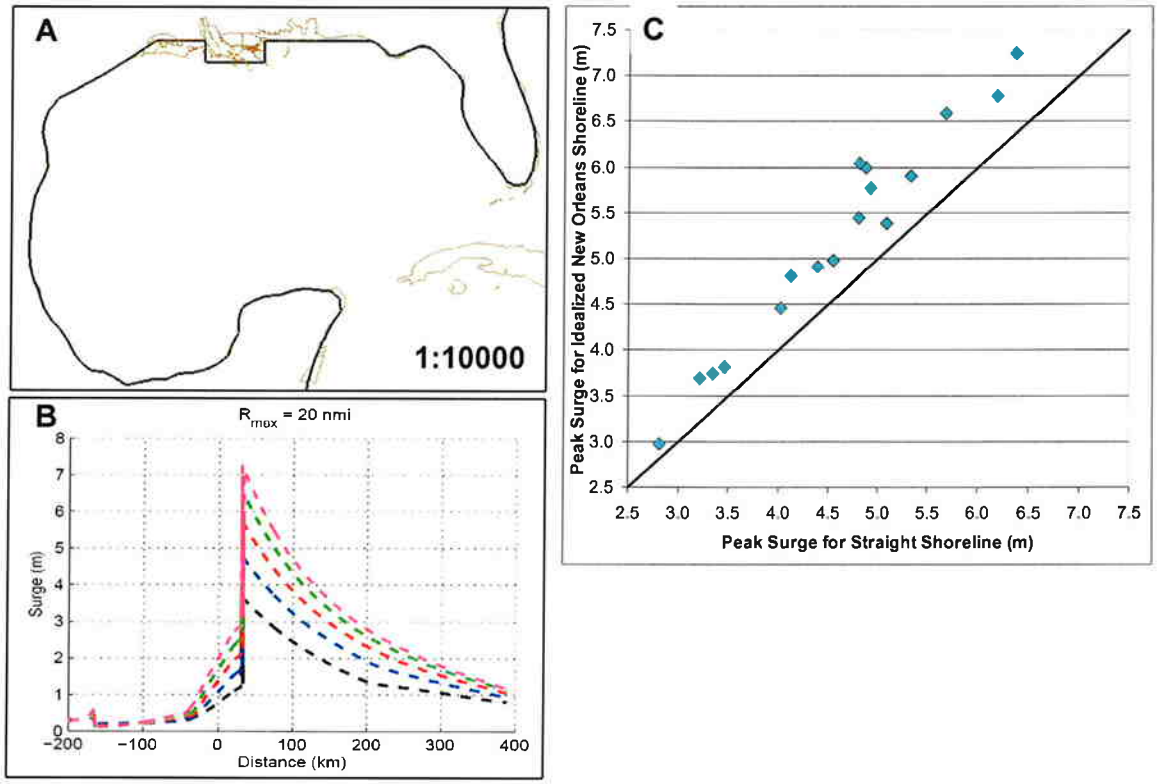

Figure 442 (A-C): Figure 442-A shows an idealized representation of the New Orleans coastal area, with a section of land protruding from a generalized straight-line coast. Figure 442-B shows that the resulting surge distributions along the coast. Figure 442-C shows that surge values for this coastal configuration tend to be about 10 to 20 percent higher than the corresponding surges on a straight-line coast.

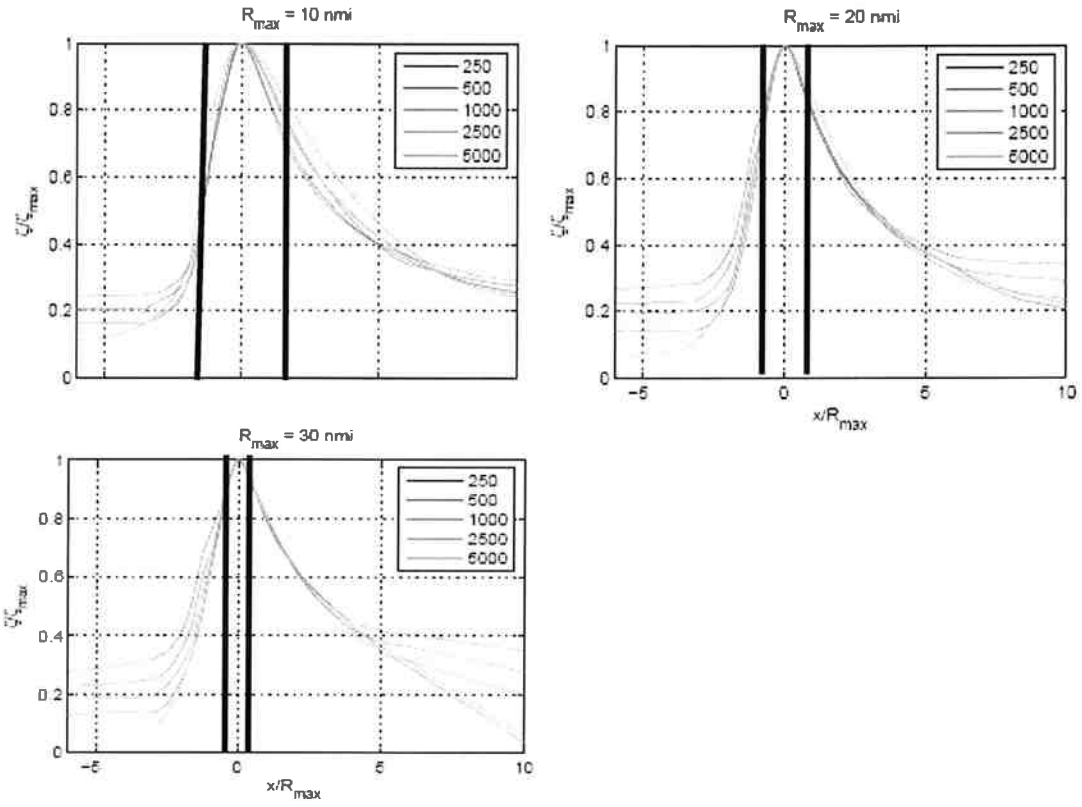

Figure 443: Figures 443-A through 443-C re-plotted with lines approximately 31 nautical miles drawn for the case in which the peak falls midway between the two tracks.

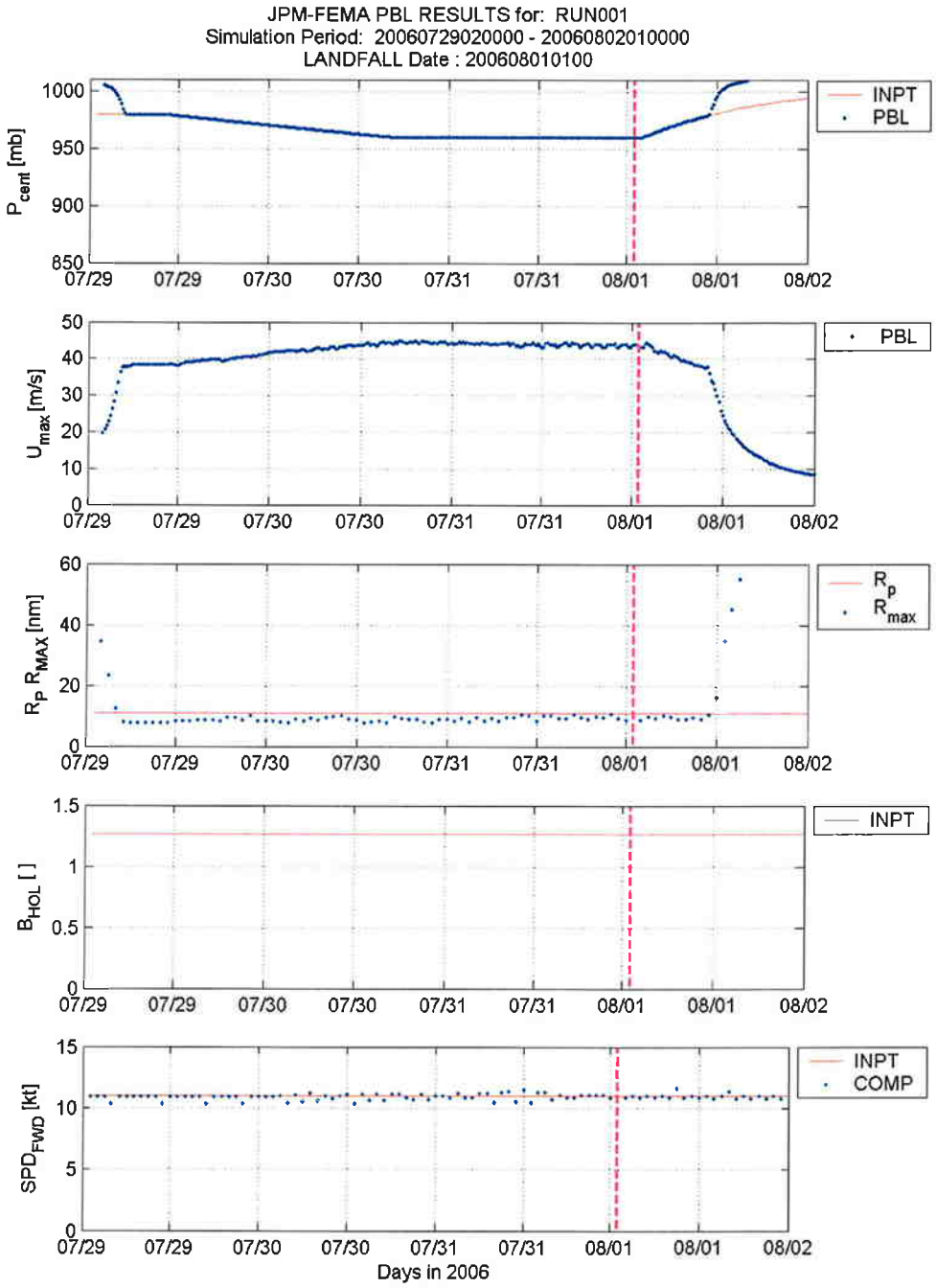

Figure 444: Sample time plot of the variation in central pressure, maximum wind speed, R_p, and forward storm speed used in quality control check of storm parameter behavior for first storm in JPM sequence.

Variation of surges related to angle of incidence of storm at the coast.

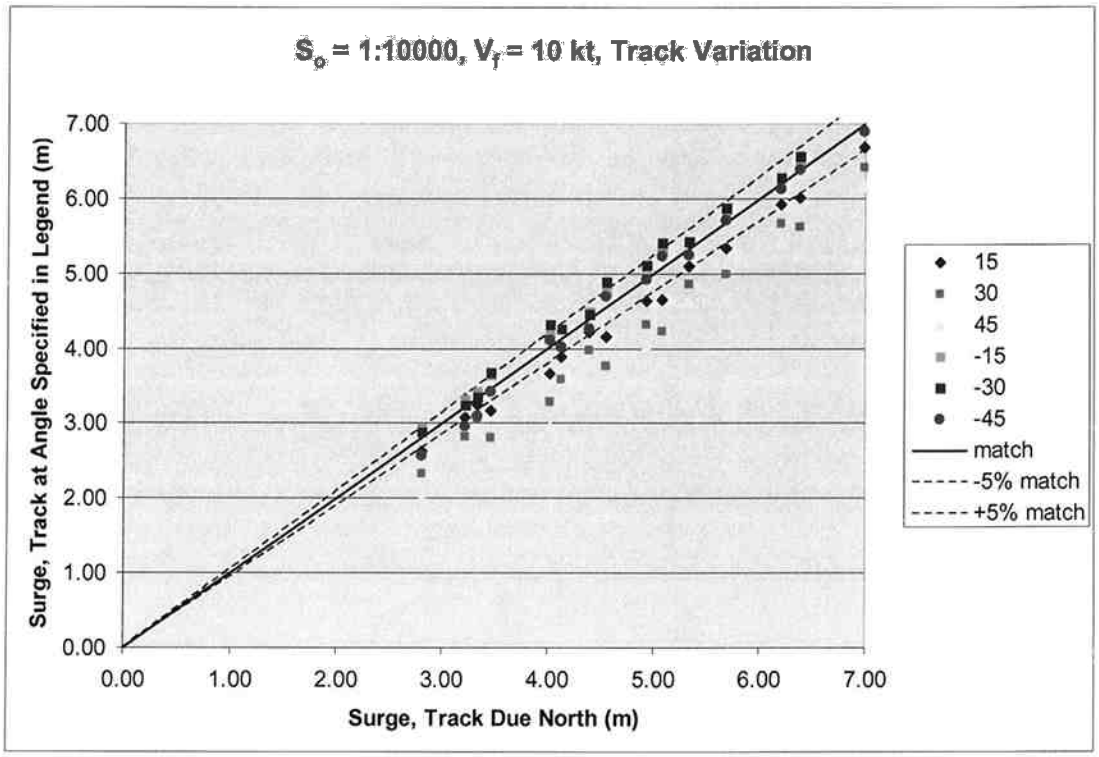

Figure 445: Variation in maximum storm surge produced by hurricanes approaching a straight, shallow-sloping (1:10,000) coast relative to the maximum surge produced by a storm moving perpendicularly to the coast.

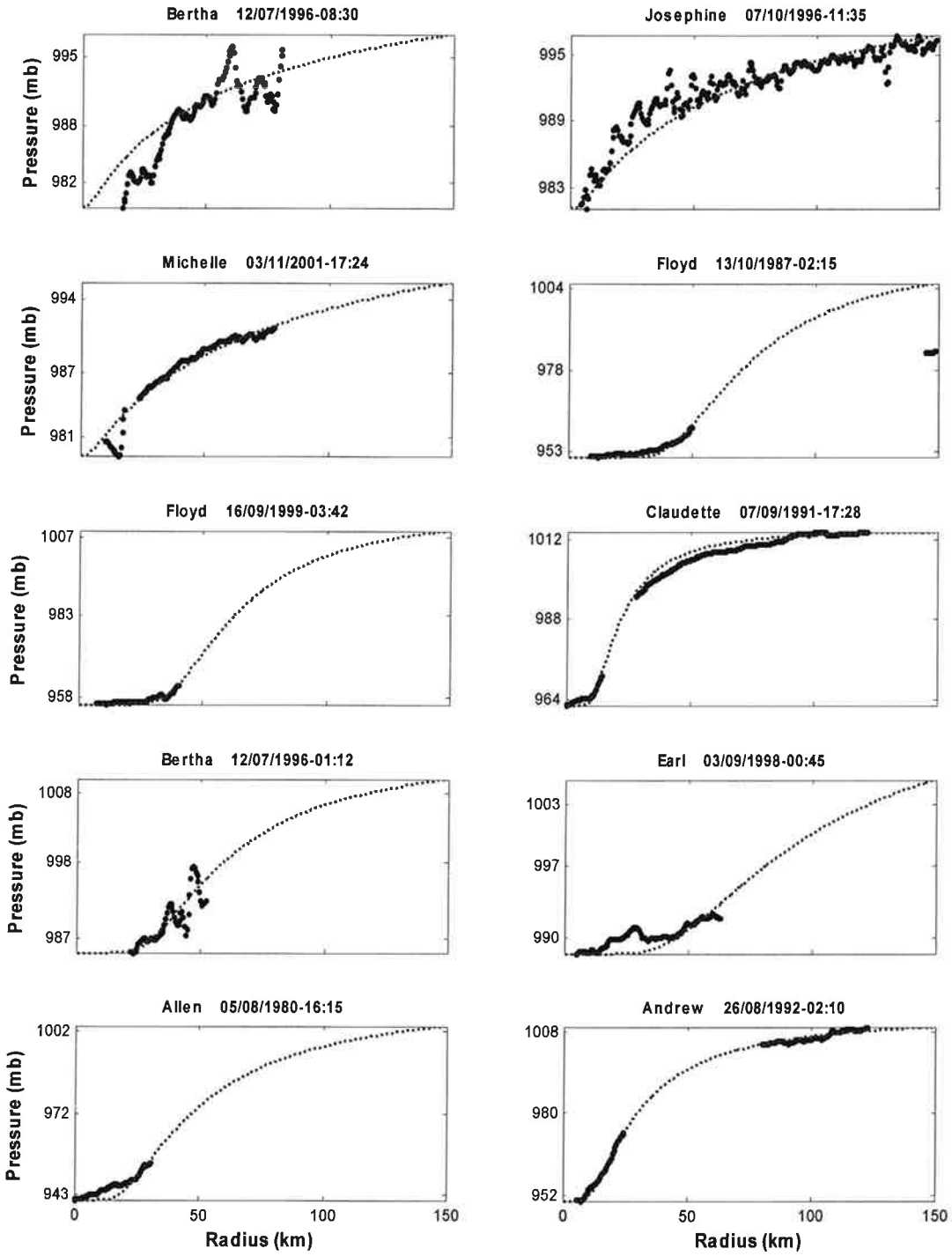

Figure 446: Examples of the eliminated profiles.

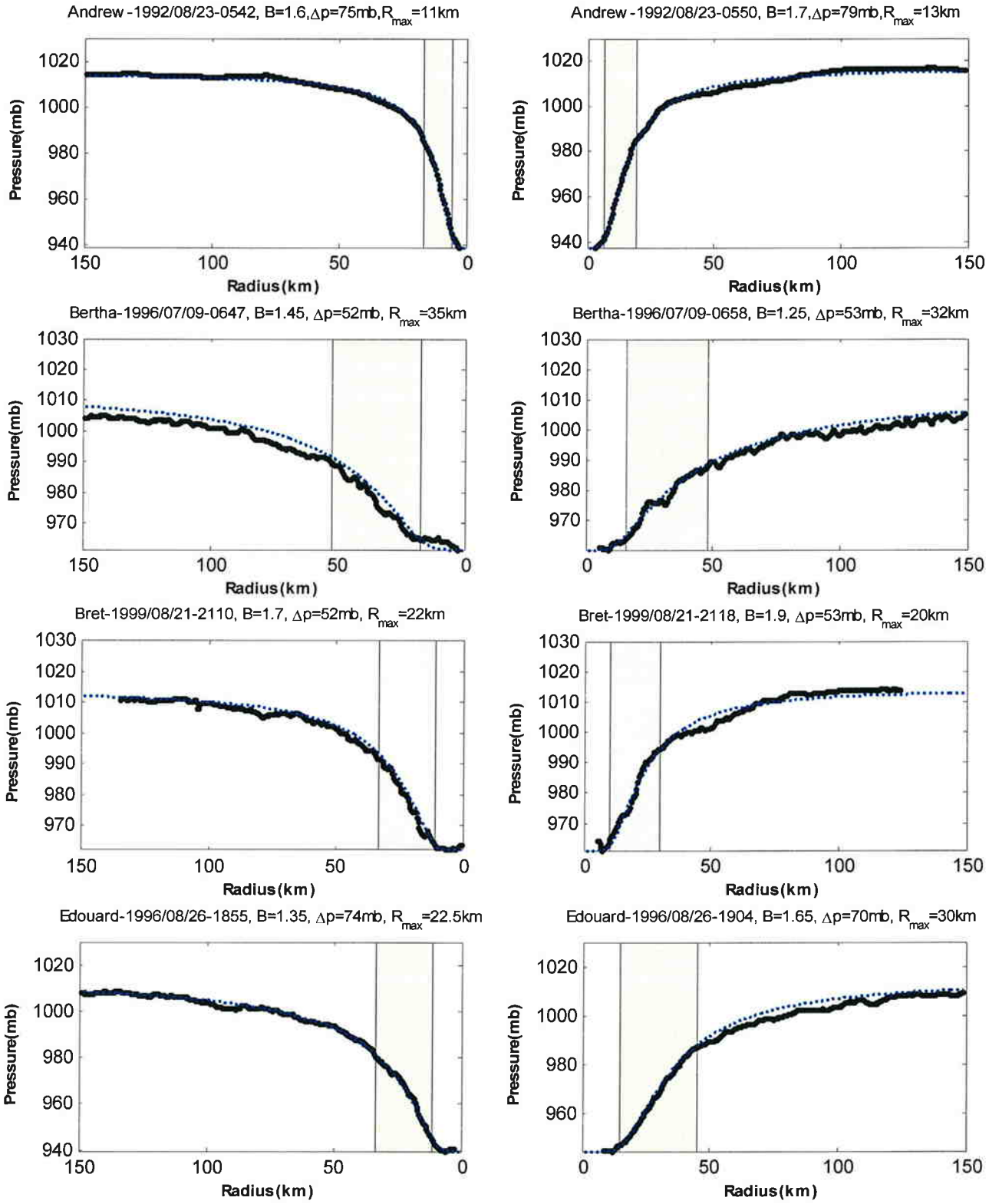

Figure 447: Examples of surface pressure profiles for a traverse across a given hurricane.

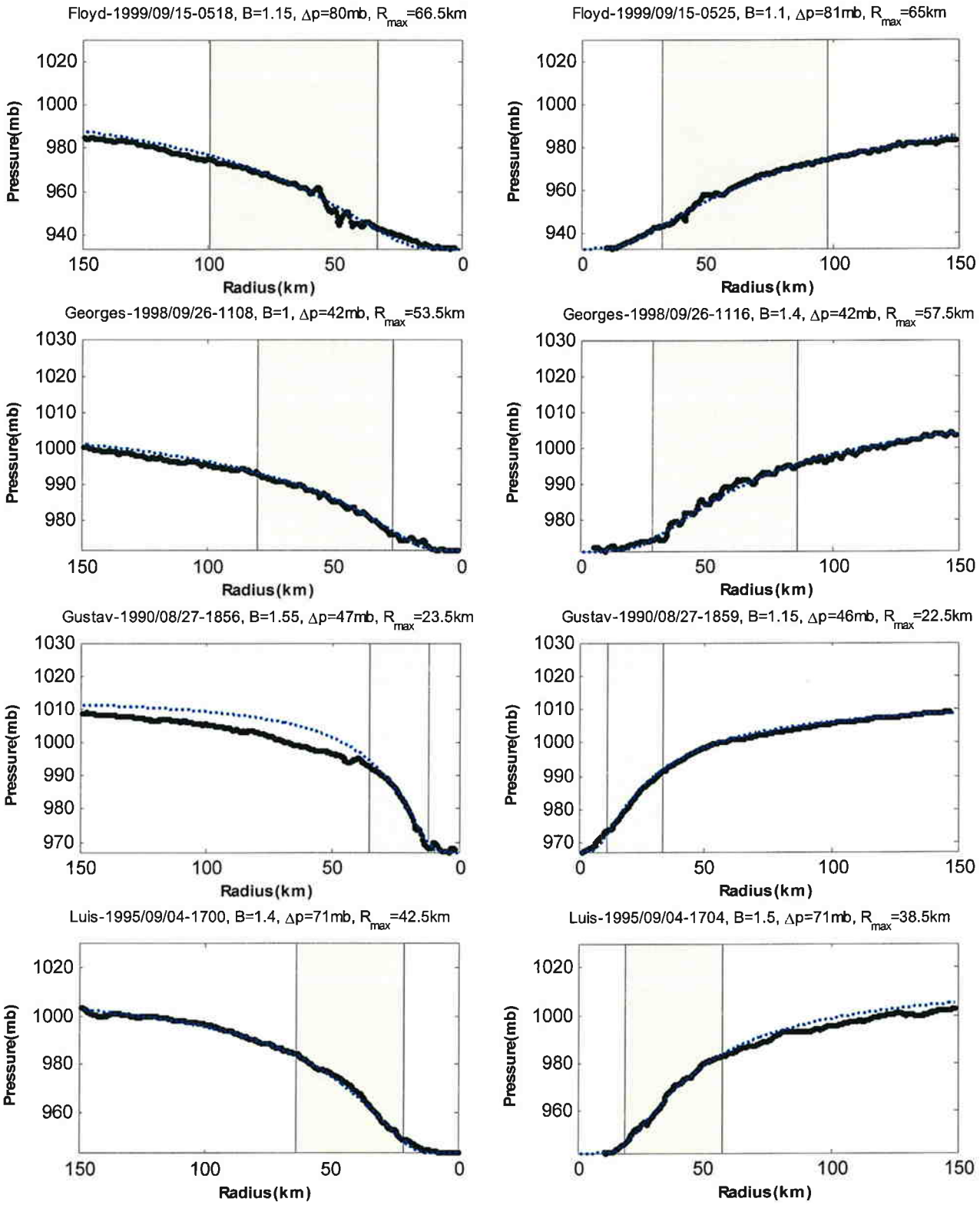

Figure 448: (continued) Examples of surface pressure profiles for a traverse across a given hurricane.

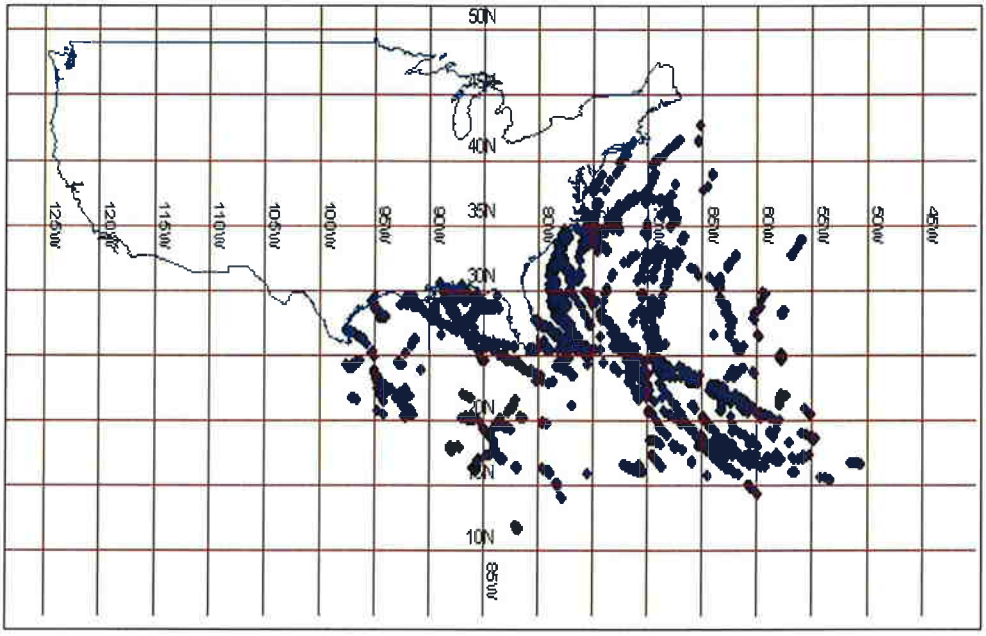

Figure 449: Geographical distribution of all the filtered profiles.

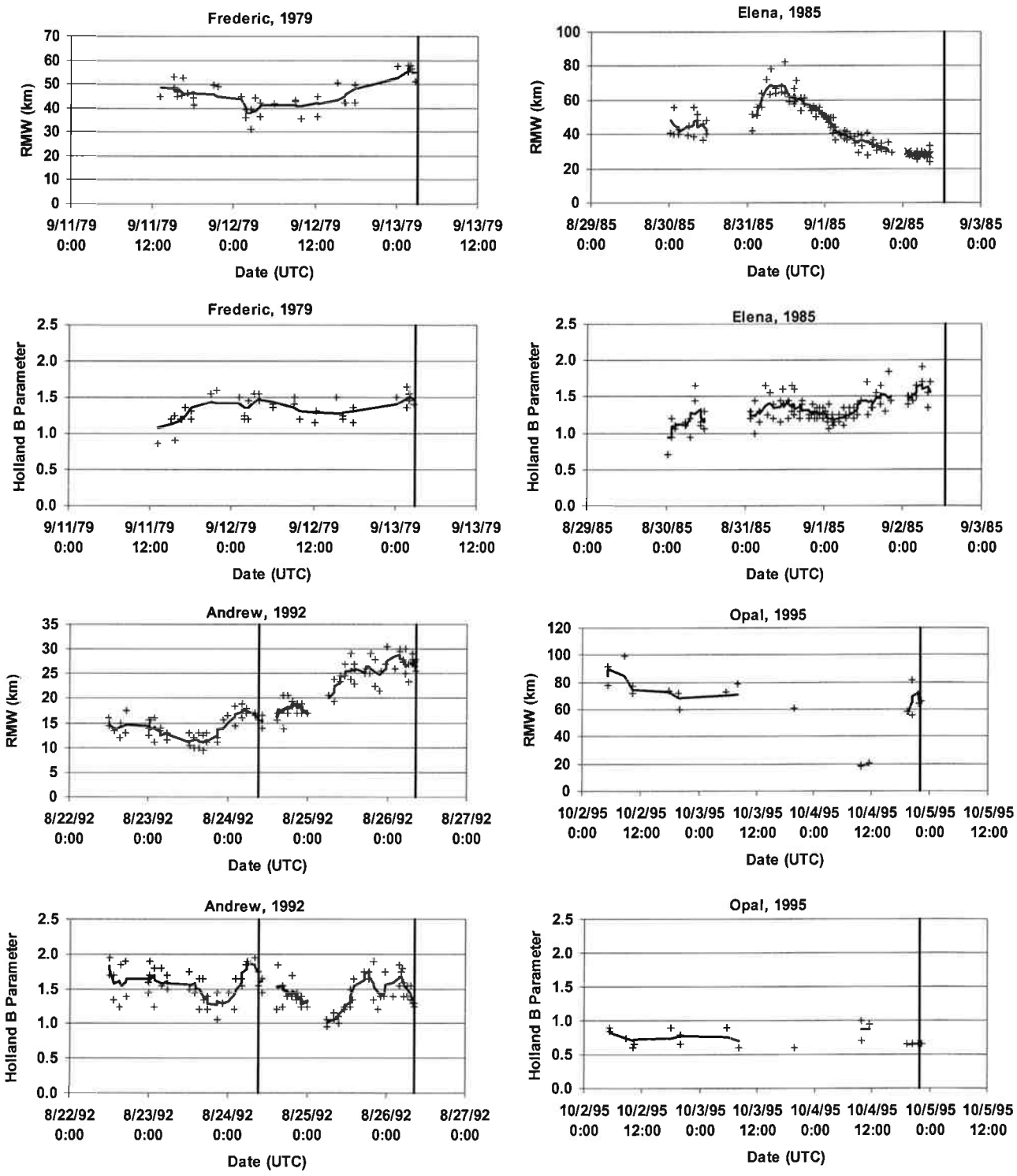

Figure 450: Examples of Smoothed (line) and Point Estimates (symbols) of RMW and B derived from 700-millibar level pressure data. Vertical line(s) represent time of landfall.

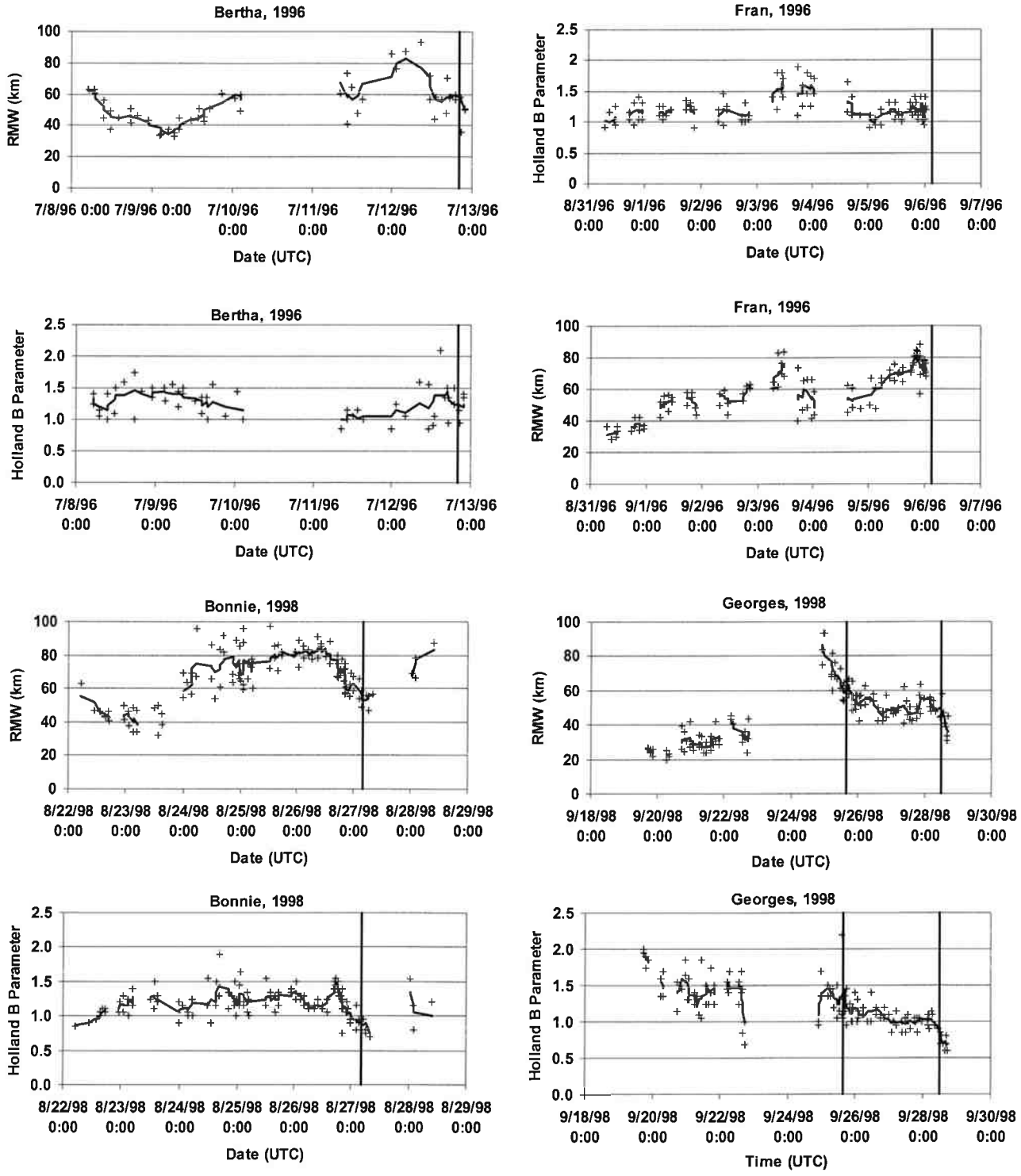

Figure 451: (continued) Examples of Smoothed (line) and Point Estimates (symbols) of RMW and B derived from 700-millibar level pressure data. Vertical line(s) represent time of landfall.

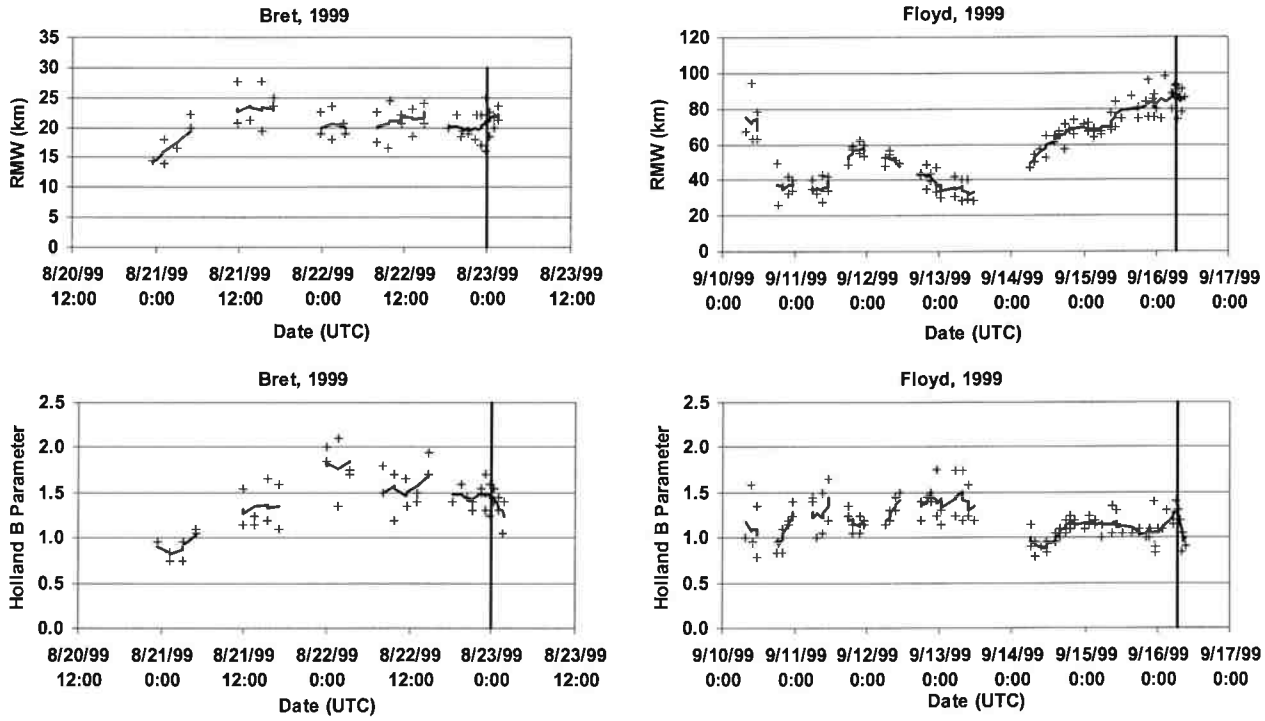

Figure 452: (concluded) Examples of Smoothed (line) and Point Estimates (symbols) of RMW and B derived from 700-millibar level pressure data. Vertical line(s) represent time of landfall.

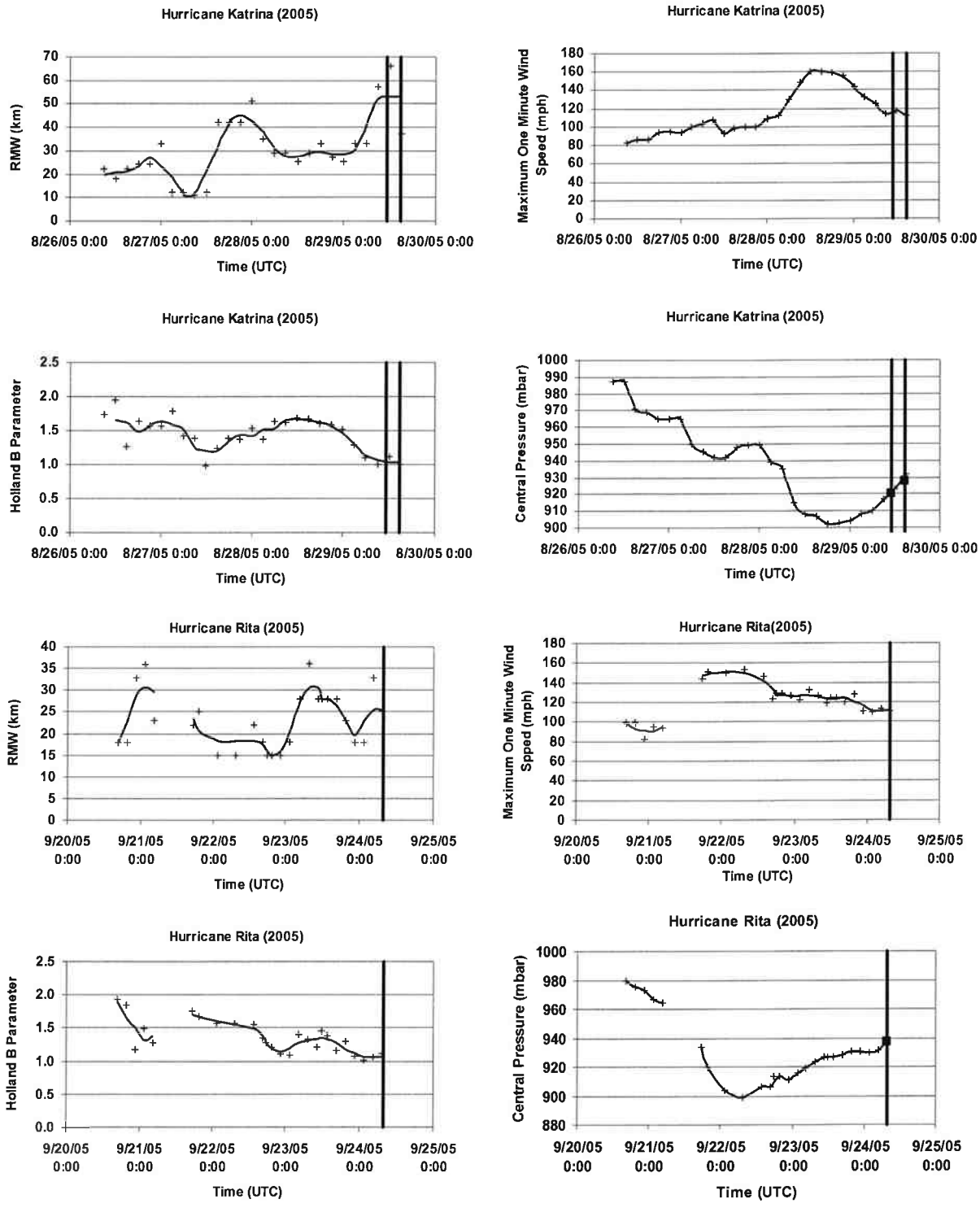

Figure 453: Smoothed (line) and Point Estimates (symbols) of RMW and B derived from H*Wind data. Vertical line(s) represent time of landfall. Solid square point at time of landfall represents NHC landfall pressure value.

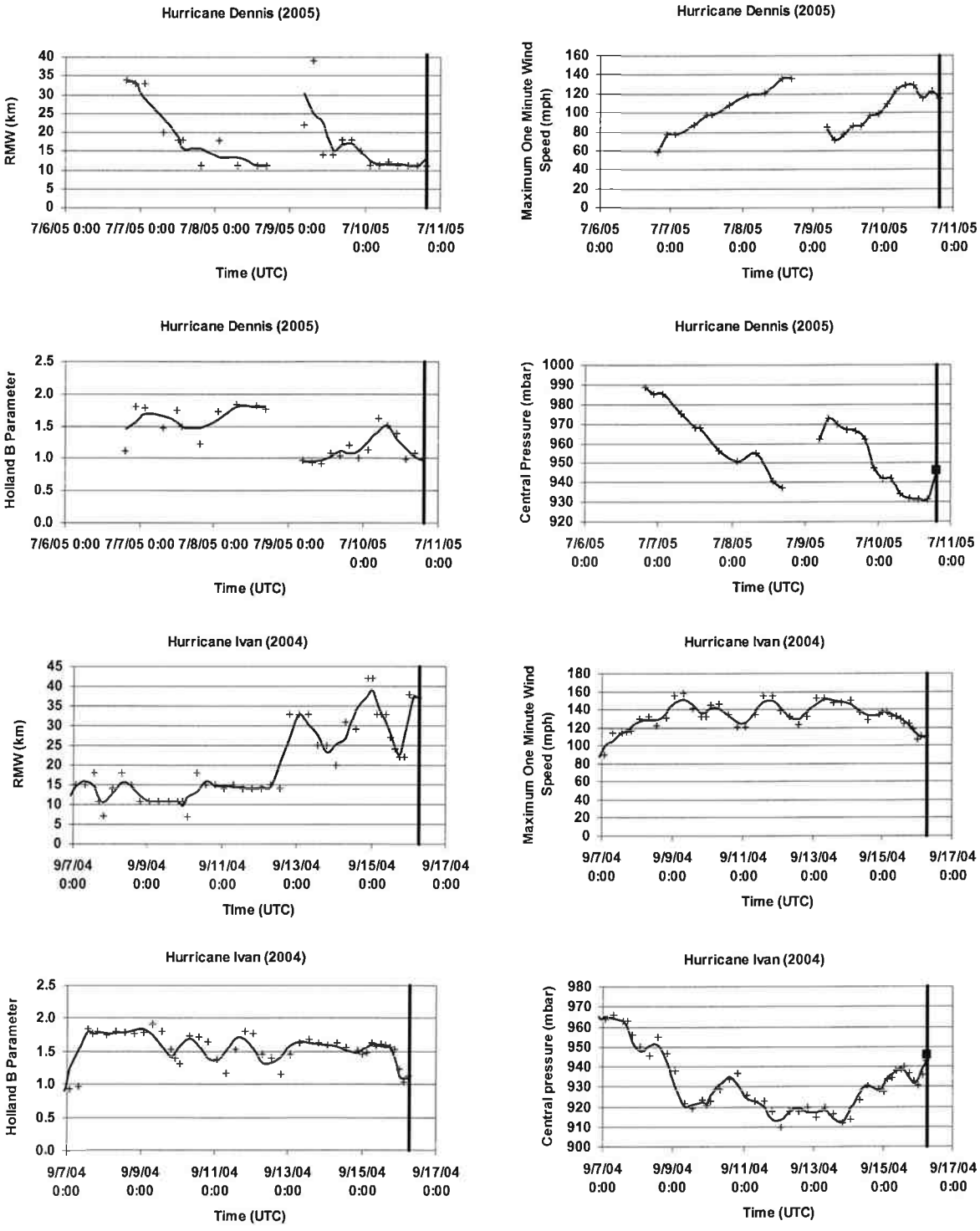

Figure 454: (continued) Smoothed (line) and Point Estimates (symbols) of RMW and B derived from H*Wind data. Vertical line(s) represent time of landfall. Solid square point at time of landfall represents NHC landfall pressure value.

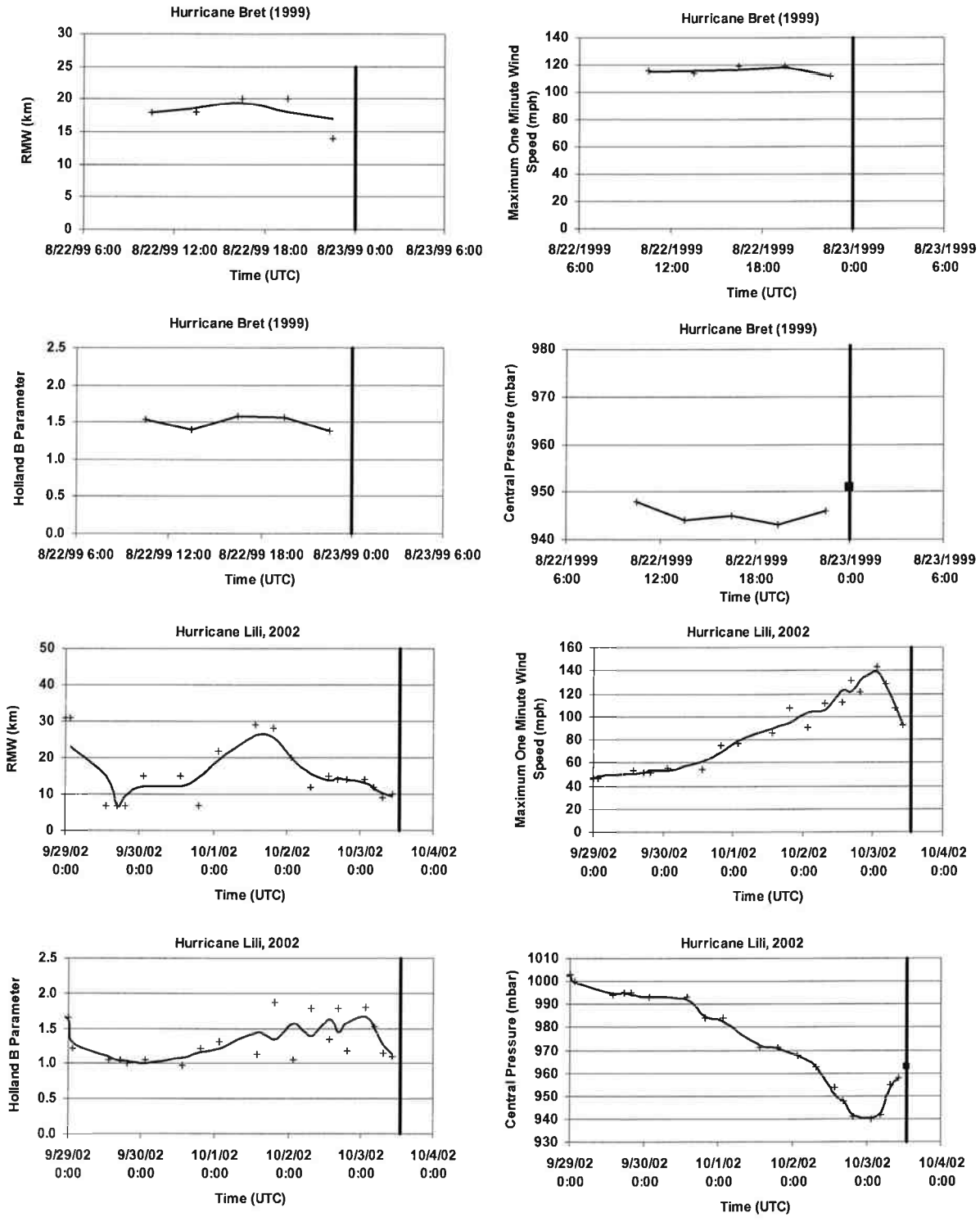

Figure 455: (concluded) Smoothed (line) and Point Estimates (symbols) of RMW and B derived from H*Wind data. Vertical line(s) represent time of landfall. Solid square point at time of landfall represents NHC landfall pressure value.

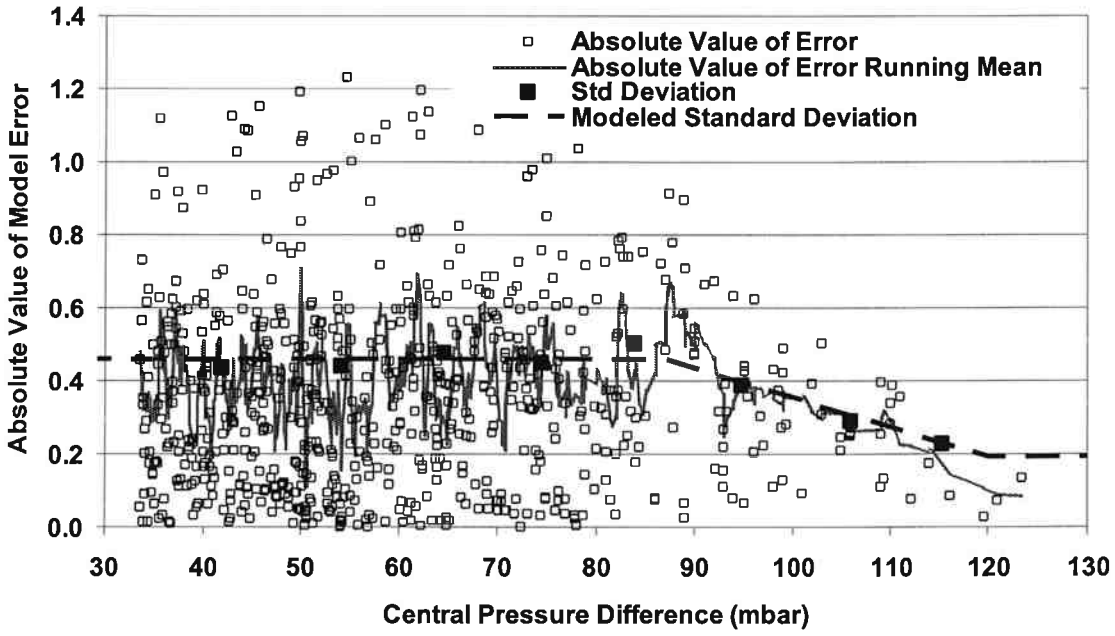

Figure 456: Absolute value of RMW model error vs. Δp

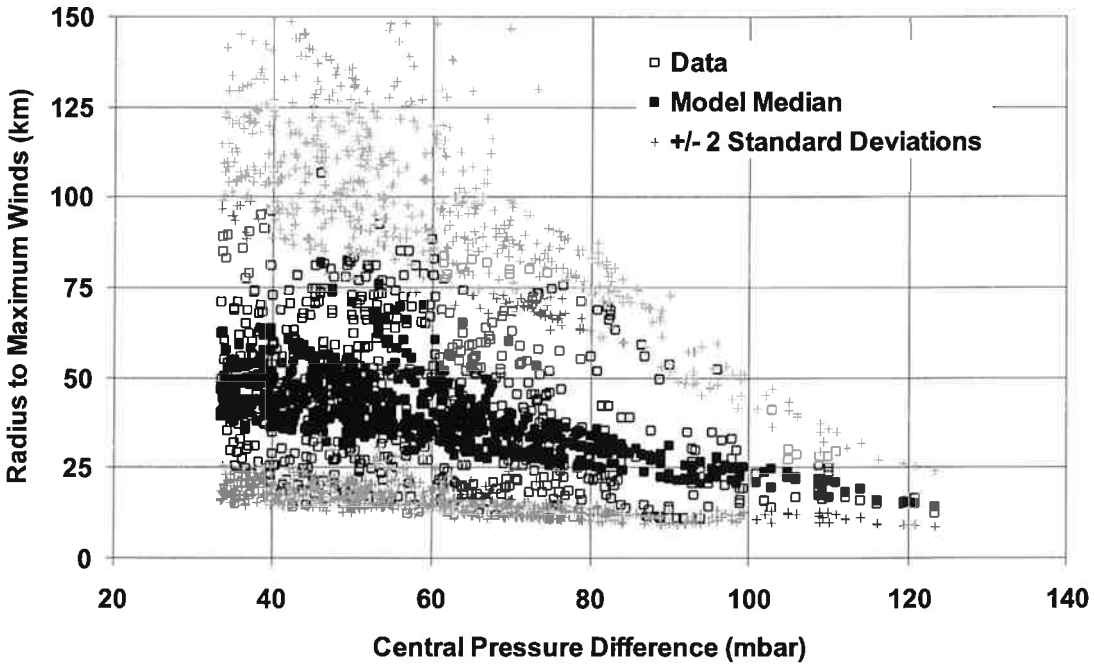

Figure 457: Modeled and observed RMW vs. Δp for all hurricanes

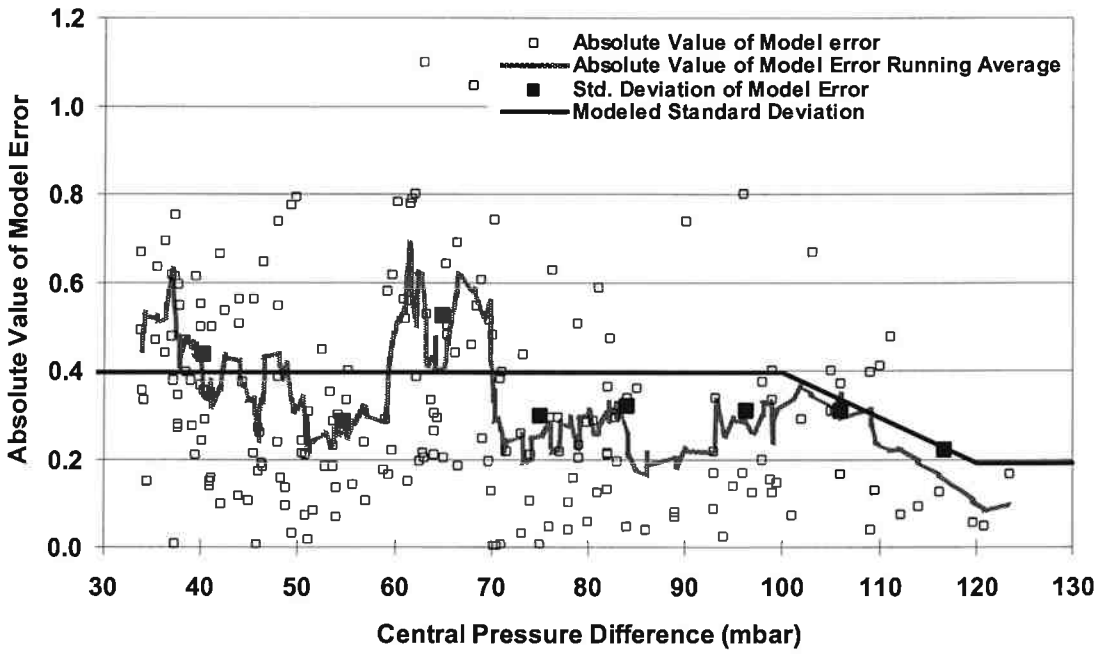

Figure 458: Absolute value of RMW model error vs. Δp for Gulf of Mexico hurricanes

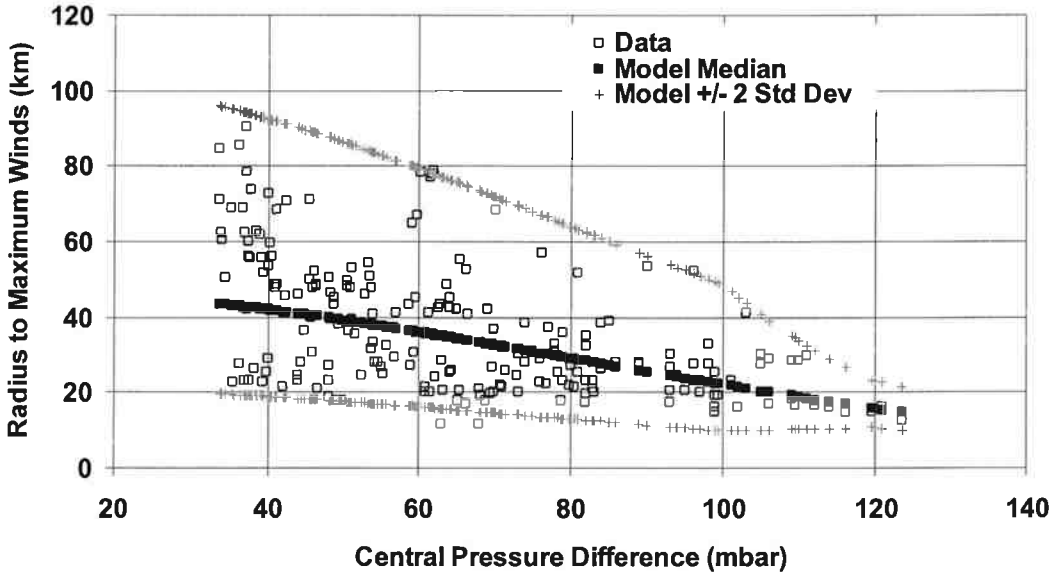

Figure 459: Modeled and observed RMW vs. Δp for Gulf of Mexico hurricanes.

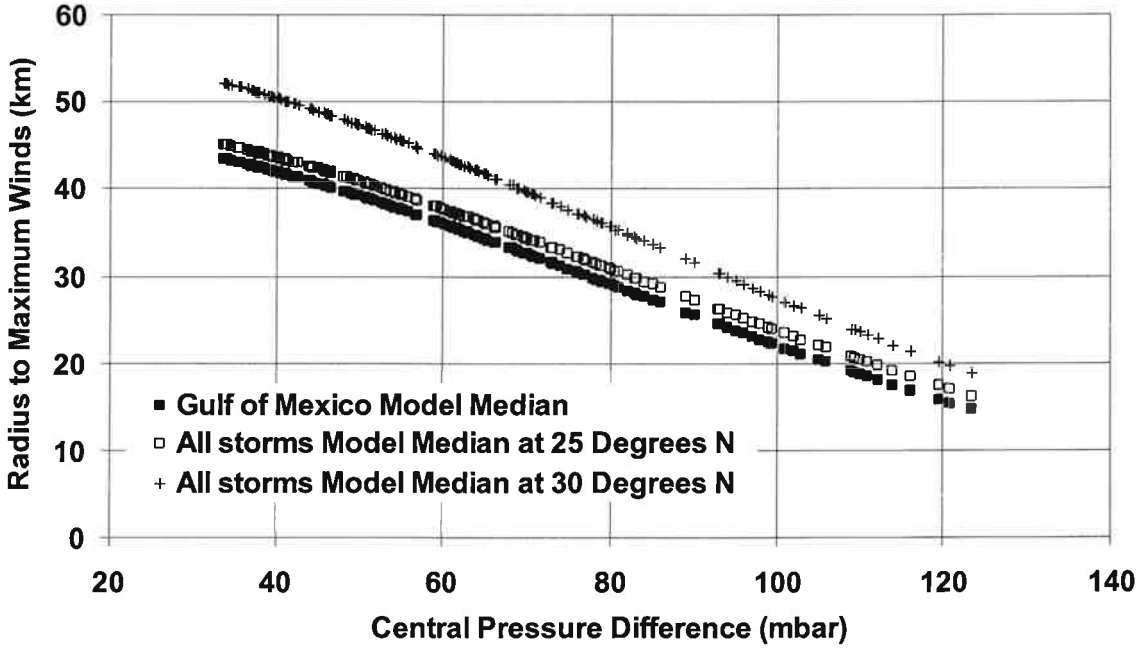

Figure 460: Comparison of all hurricanes model predicted median RMW to Gulf of Mexico model median RMW.

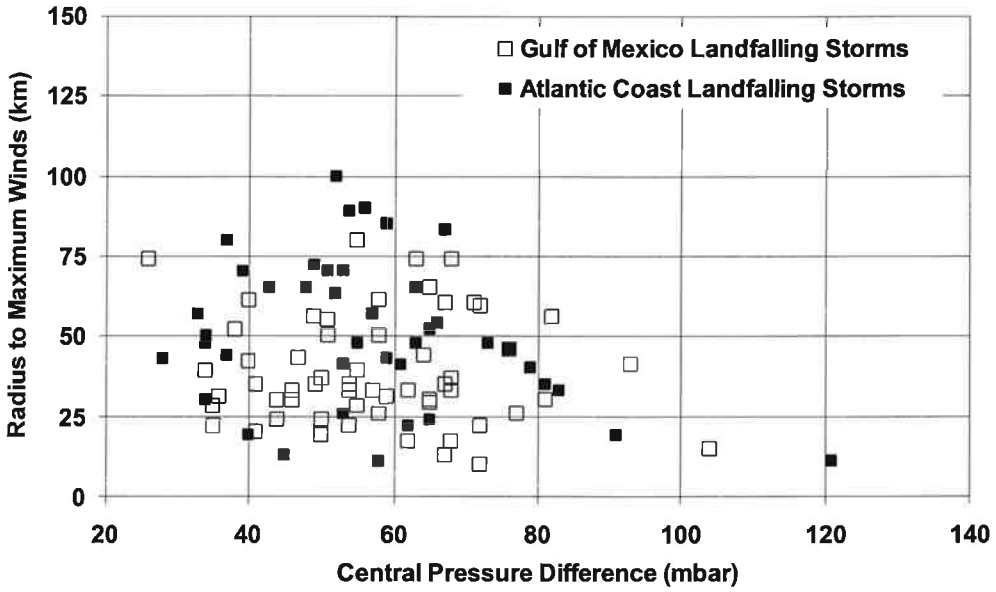

Figure 461: RMW for landfalling storms along the Gulf and Atlantic Coasts of the U.S.

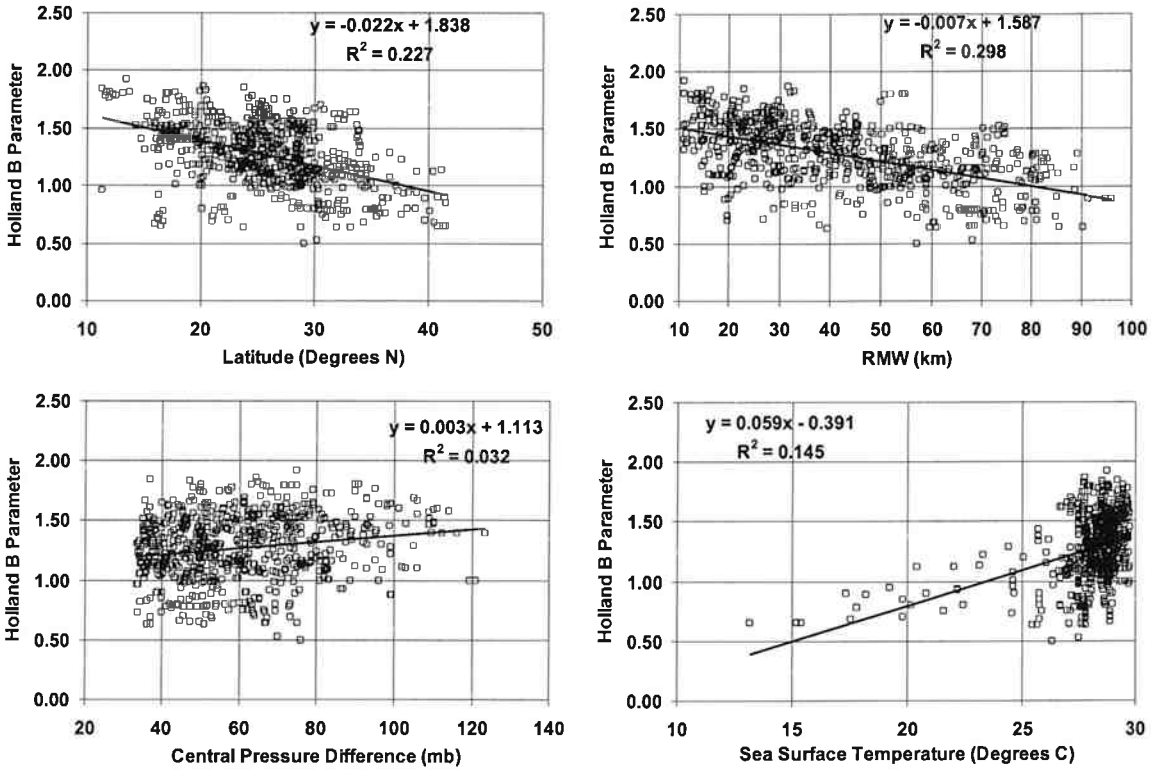

Figure 462: Relationships between the Holland B parameter, latitude, RMW, Δp, and Ts.

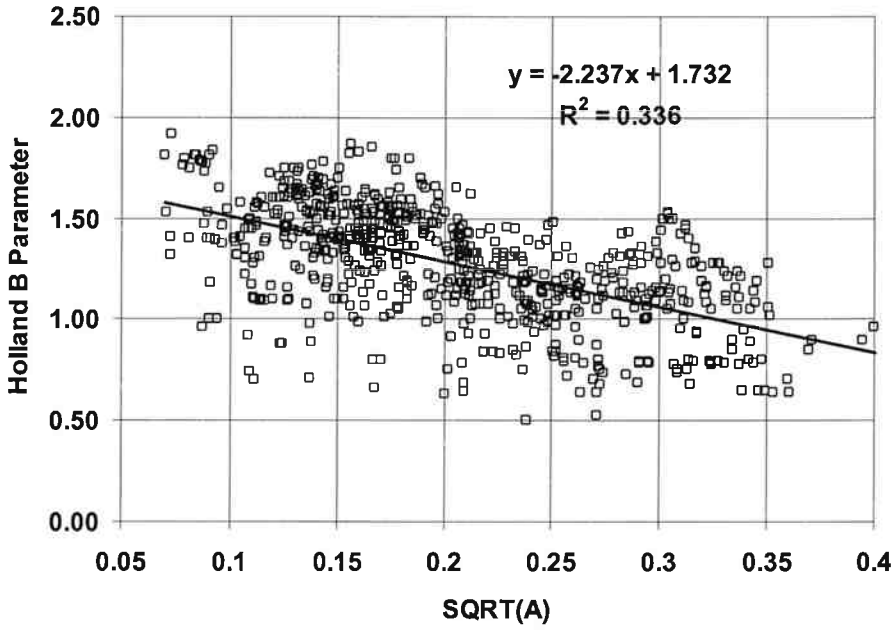

Figure 463: Relationship between the Holland B parameter dimensionless parameter, A.

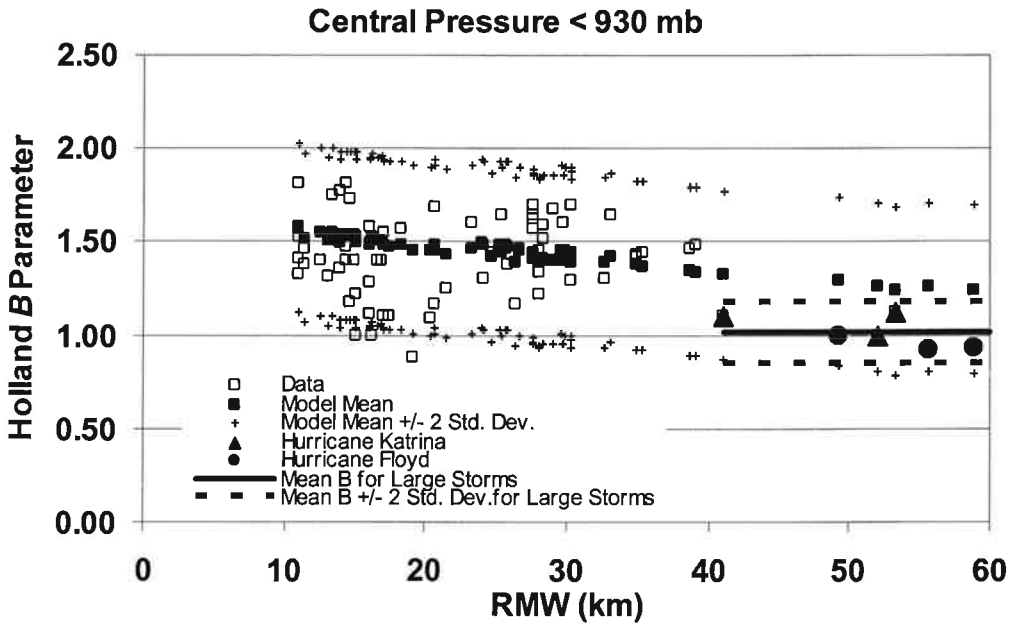

Figure 464: Holland B parameter vs. RMW for storms with central pressure < 930 millibars.

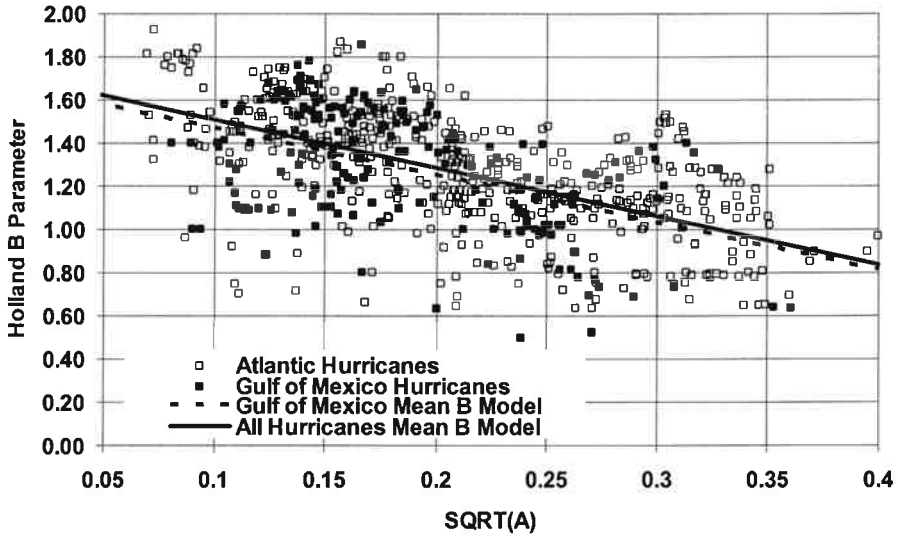

Figure 465: Relationship between the Holland B parameter and the dimensionless parameter, A, comparing all hurricane data with the Gulf of Mexico hurricane data.

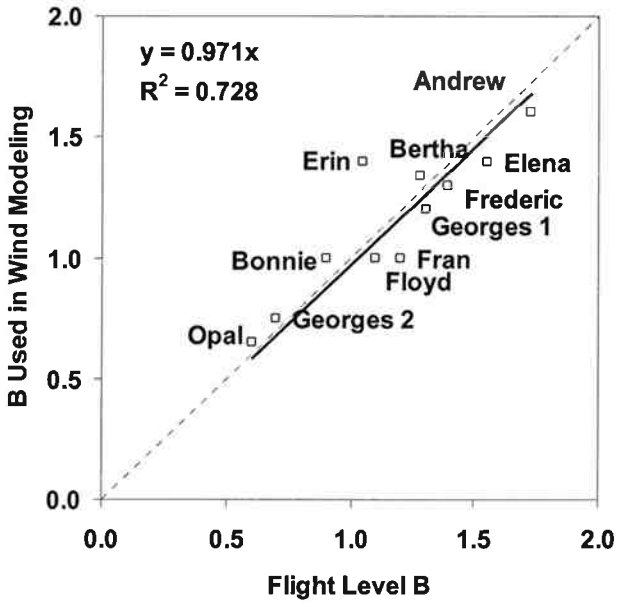

Figure 466: Comparison of Holland B parameters derived from flight level data to those derived using a post landfall windfield analysis.

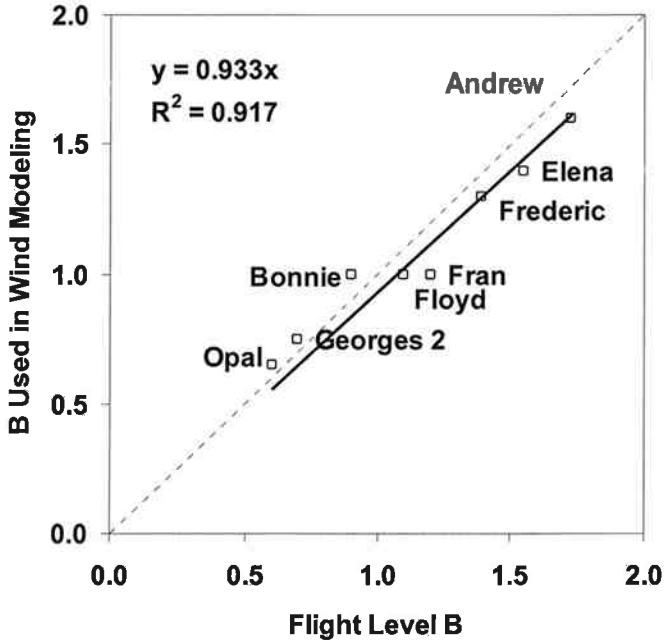

Figure 467: Comparison of Holland B parameters derived from flight level data to those derived using a post landfall windfield analysis for hurricanes with central pressures <= 964 millibars.

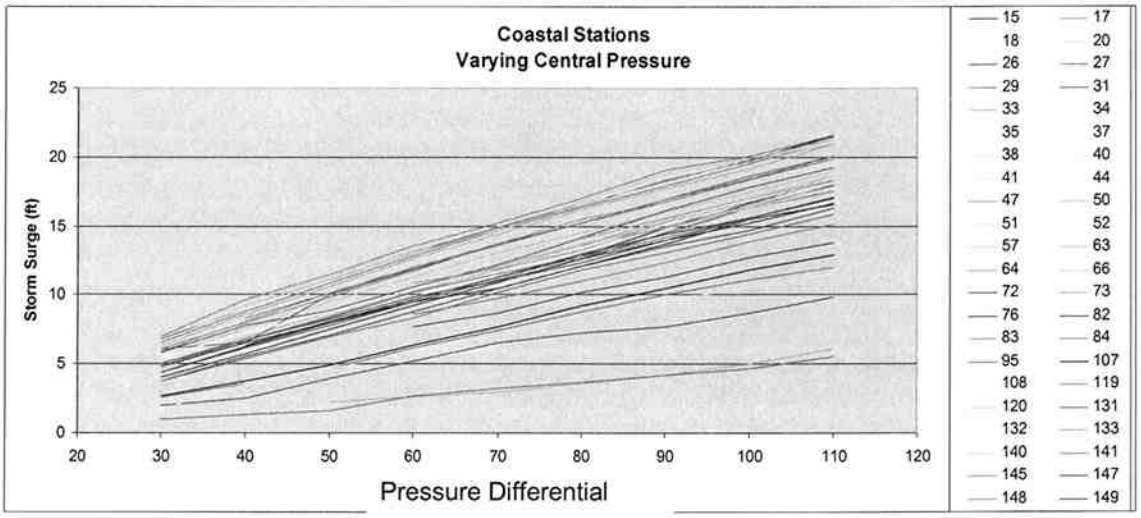

Figure 468: Surge levels (feet) at coastal stations (Station Numbers denoted on right hand side of chart) along Mississippi coast as a function of pressure differential (millibars).

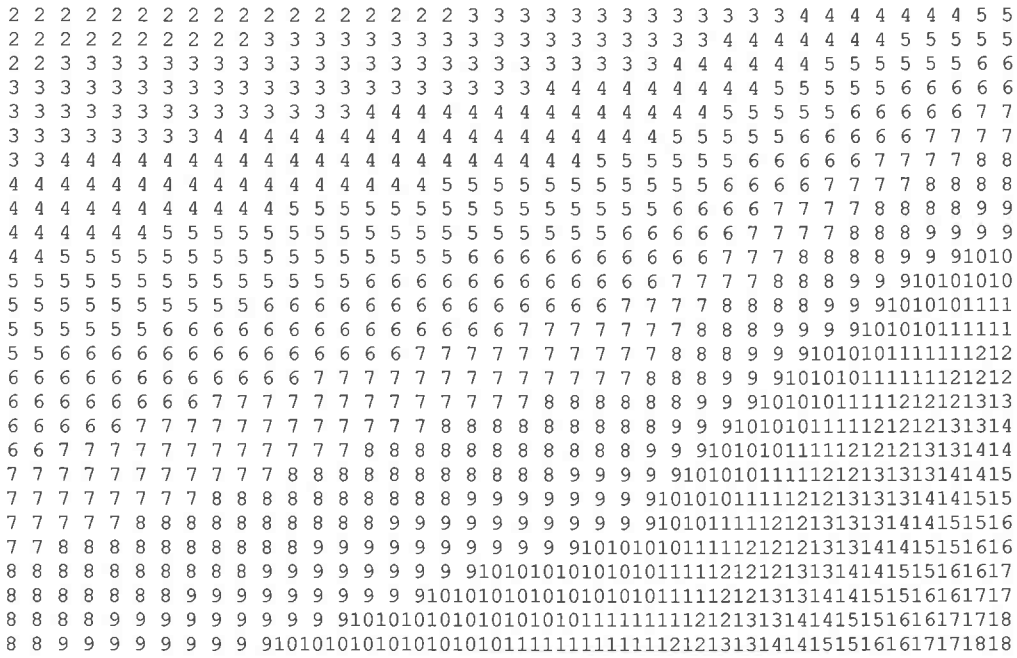

Figure 469: Response surface showing integerized surge values in feet as a function of row from top to bottom (ΔP from 53 to 133 millibars in increments of 3 millibars) and column from left to right (R_p from 1 nautical mile to 40 nautical miles in increments of 1 nautical mile).

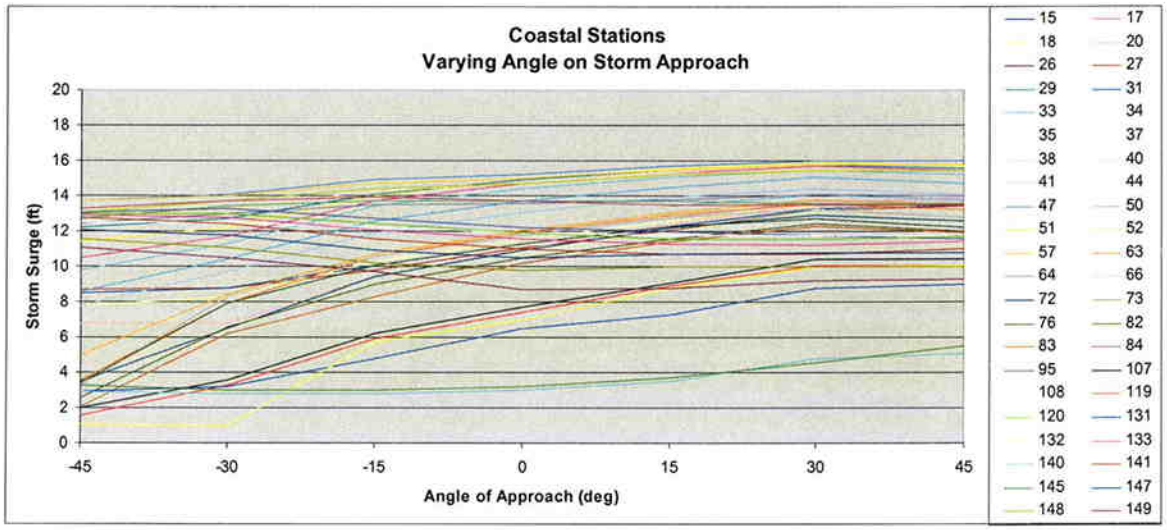

Figure 470: Surge levels (feet) at coastal stations (Station numbers denoted on right hand side of chart) along Mississippi coast as a function of angle of storm approach to land.

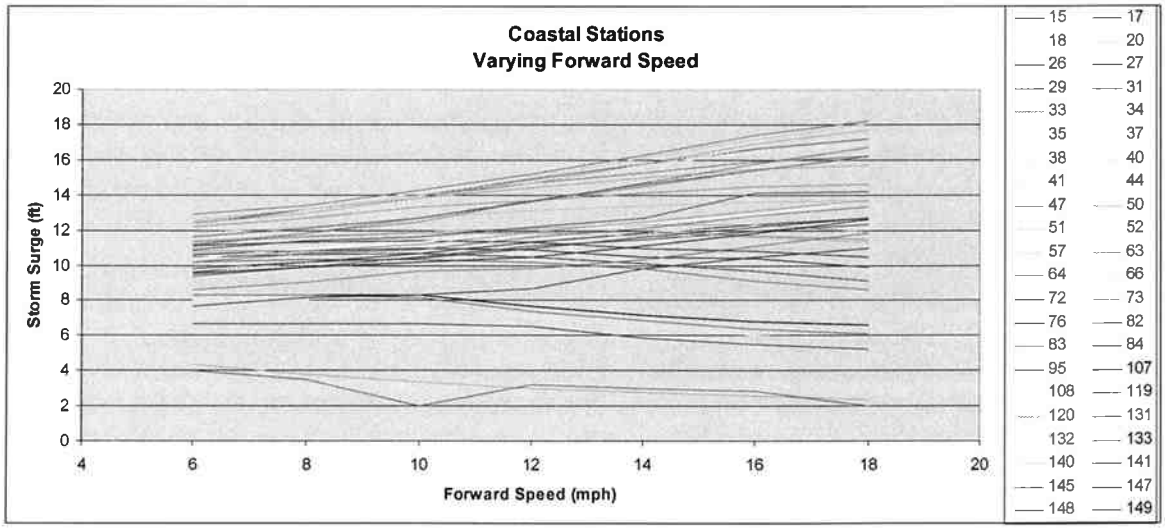

Figure 471: Surge levels (feet) at coastal stations (Station numbers denoted on right hand side of chart) along Mississippi coast as a function of forward speed of storm (mph).

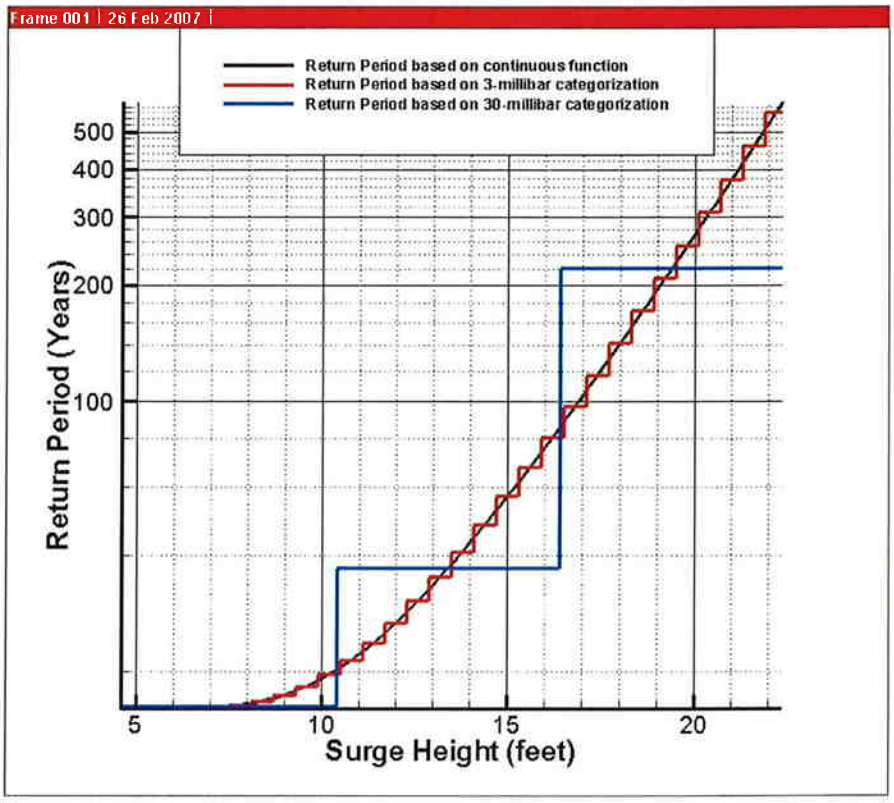

Figure 472: Comparison of Return Periods for surges estimated from 3-millibar and 30-millibar categories compared to a continuous function.

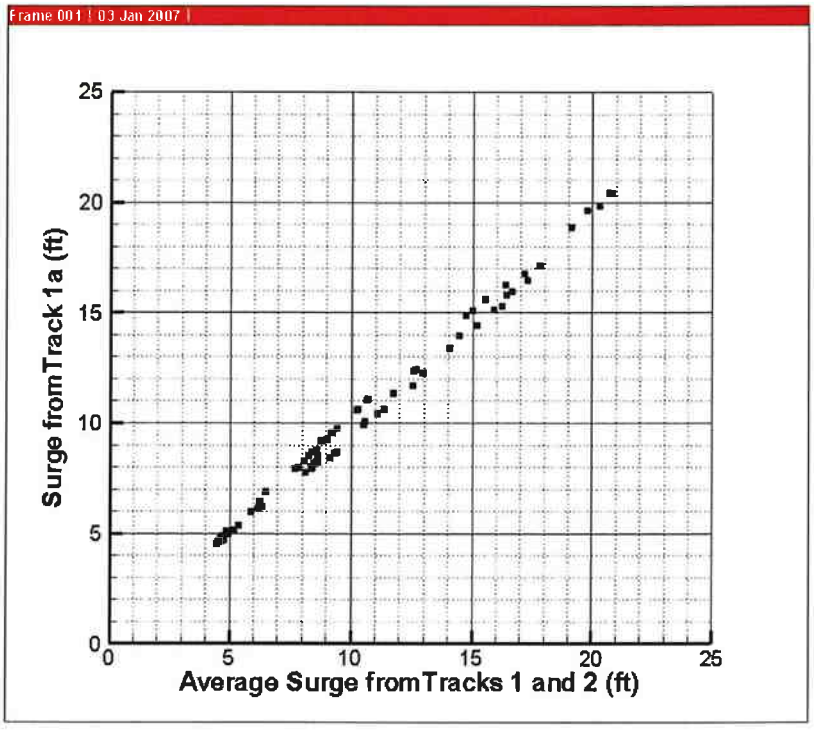

Figure 473: Comparison of results from Track 1a (midway between Tracks 1 and 2) to interpolated values using information from Tracks 1 and 2 for a set of points spread throughout the entire New Orleans region.

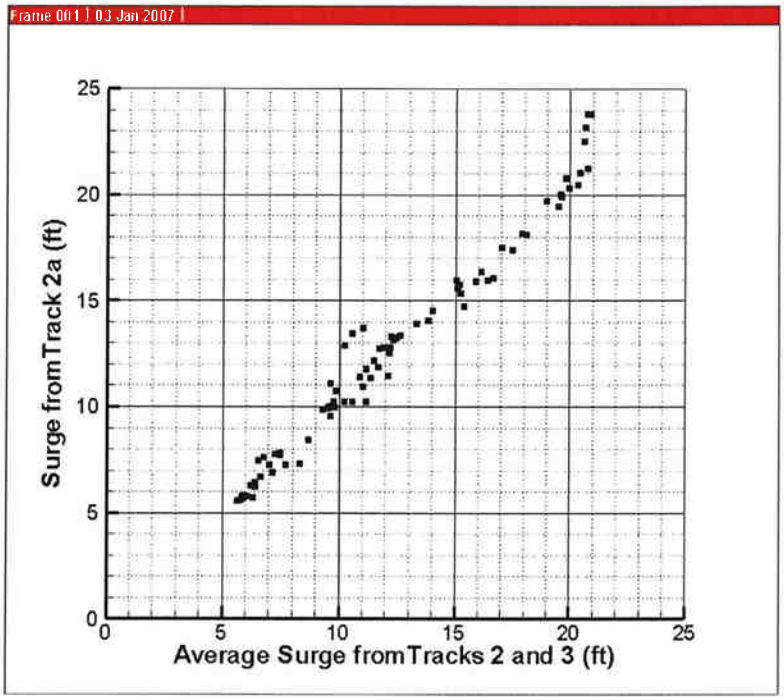

Figure 474: Comparison of results from Track 2a (midway between Tracks 2 and 3) to interpolated values using information from Tracks 2 and 3 for a set of points spread throughout the entire New Orleans region.

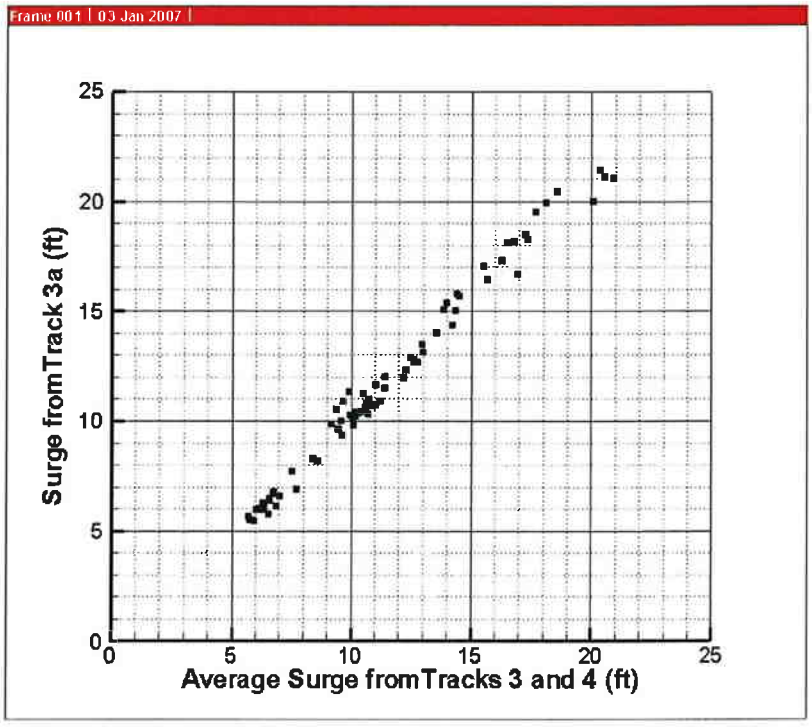

Figure 475: Comparison of results from Track 3a (midway between Tracks 3 and 4) to interpolated values using information from Tracks 3 and 4 for a set of points spread throughout the entire New Orleans region.

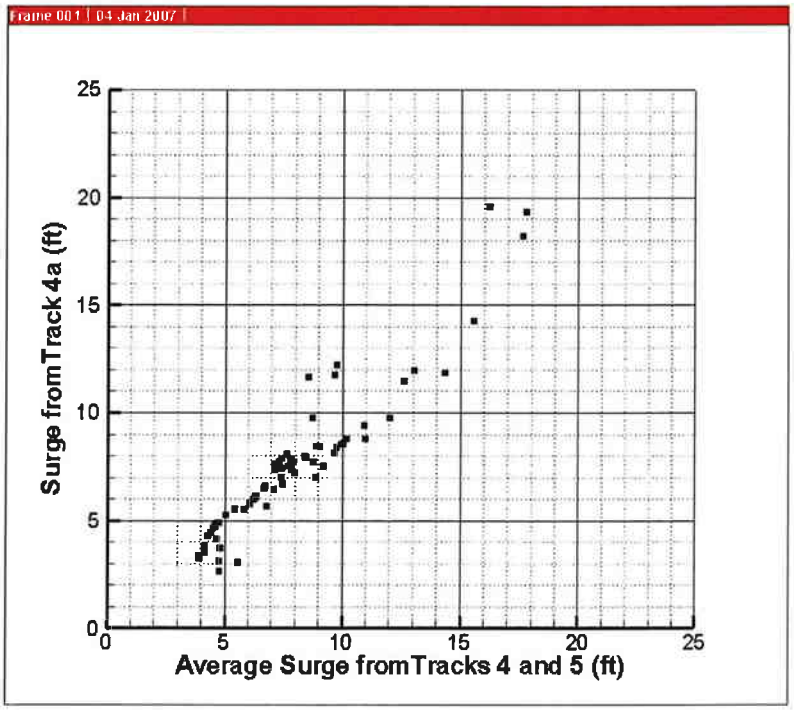

Figure 476: Comparison of results from Track 4a (midway between Tracks 4 and 5) to interpolated values using information from Tracks 4 and 5 for a set of points spread throughout the entire New Orleans region.